Quantum decoherence effects on electronic transport in molecular wires and nanodevices.

por

Carlos José Cattena

Presentado ante la Facultad de Matemática, Astronomía y Física
como parte de los requerimientos para la obtención del grado de

Doctor en Física

de la

UNIVERSIDAD NACIONAL DE CORDOBA

Marzo, 2012

Director: Dr. Horacio M. Pastawski
Co-Director: Dr. Gustavo A. Monti

Agradecimientos

Este trabajo no hubiera sido posible sin la voluntad, la dedicación y el apoyo de muchas personas, que en diferentes circunstancias y a través de diversos mecanismos han realizado aportes invaluables.

En primer lugar debo agradecer a los directores de este trabajo, **Horacio M. Pastawski** y **Gustavo A. Monti**, por su esfuerzo, dedicación y paciencia. No sólo se han brindado amplia y desinteresadamente en lo académico impulsando en mi una forma distinta de ver la física, sino también se han preocupado especialmente por los diferentes aspectos relacionados con la formación humana y científica integral.

Agradezco a **Raúl A. Bustos Marún**, cuya impronta es ampliamente manifiesta en todos los tópicos cubiertos por este trabajo. Mi gratitud también con **Lucas Fernandez**, con quien tuve el enorme gusto de trabajar en transporte magnético, y con todo el **capital humano del LANAIS de RMS**, por su simpatía y cordialidad.

Agradezco al jurado de esta tesis: **Cristián Sanchez**, **Gonzalo Usaj** y **Pablo Serra**, por haber leído el trabajo y aportado comentarios muy interesantes.

Agradezco a **los amigos**, que son muchos, porque cada uno de ellos, en mayor o menor medida, ha facilitado y endulzado mis días, haciendo más propicia mi labor. En especial, mi reconocimiento a **Eduardo O. Schmidt** y a **Leo Bianco** cuya invalorable compañía ha hecho mucho más amena mi jornada de trabajo.

A mis **hermanos de PyU**, con quienes tengo el orgullo de compartir profusas y prodigiosas discusiones y puntos de vista que han enriquecido enormemente mis perspectivas y horizonte intelectual.

Agradezco a **mi padre**, a quien admiro en su generosidad y fuerza de corazón, y **mis hermanos**, por su apoyo constante y disposición sincera en todo momento. El incansable apoyo de mi familia en los momentos más difíciles ha sido para mi el más preciado de los tesoros. En especial quiero agradecer a **mi madre**, a quien le debo mi forma de entender y de desenvolverme en el mundo. Muy tristemente no ha podido ver el fruto de este trabajo, dejando recientemente un vacío desgarrador en mi vida. Su recuerdo, que ha dejado en mi una impronta profunda e indeleble, ha sido y seguirá siendo fuente de inspiración y fortaleza.

Finalmente y tal vez el más importante, mi enorme agracecimiento a **Vanesa**, mi mujer, compañera y sostén de mi vida. Su apoyo y comprensión constante, el resguardo que me brindó en los tiempos de duda, el empeño y el sacrificio

personal desinteresados en favor de mi bienestar y de este trabajo en particular son algunas de las razones por las que le estoy plenamente agradecido. Este trabajo es, en buena parte, de ella.

Abstract

Keywords: Electronic transport, decoherence, conductive polymers, polyaniline, carbon nanotubes, magneto-transport.
PACS: 72.80.Le, 72.10.d, 73.20.Jc, 72.15.Rn

Quantum transport at the nanoscale is a blooming field where we can explore the properties of matter in a realm where quantum effects become crucial. The control of quantum interference phenomena and their interplay with the electronic structure offers fascinating opportunities for escaping from the usual constraints of the classical world. However, environmental degrees of freedom might also play a crucial role at the nanoscale, where the presence of both, classical *and* quantum behavior is expected. Therefore, a proper approach to decoherence in these kind of systems is a matter of fundamental importance with practical applications of recent interest. Generally, the effect of decoherence on quantum transport is expected to be negative, with inhibitory effect on constructive interference of quantum waves propagation. Although electronic coherent quantum transport in disordered materials leads to destructive interference of electron wave function, the role of decoherence in disordered systems might be crucial, since decoherent events are able to suppress interferences, which in this kind of systems are destructive. In this case, this is reflected as an increased quantum transport efficiency due to system-environment interactions.

The present work is devoted to the impact of decoherence effects in electronic transport, with particular interest in multi-terminal devices. The modeling of decoherence and its computational approach is presented with special emphasis in the use of efficient algorithms. With this methodology, the case of conductive polymers is analyzed through one of the paradigmatic examples: *polyaniline* (PAni). In spite of the important experimental results that in the XXI century led to adjudicate the Nobel prize to the field of conductive polymers, there is still an absence of consensus in the scientific community on a conceptual description with predictive capacity of the physical processes involved. With the use of realistic parameters electronic transport is computed for the disordered lattice model of PAni, which represents its stable structure at room temperature, and we show that it becomes highly conductive when the effects of decoherence are properly accounted. Furthermore, this results prove to be robust, not depending critically on variations in the polymer preparation. Also, results for transport in carbon nanotubes, a discussion on electron-phonon in-

teractions, transport under the influence of periodic time-dependent potentials and magneto-transport are presented.

Resúmen

Palabras clave: Transporte electrnico, decoherencia, polímeros conductores, polianilina, nanotubos de carbono, transporte magnético.
PACS: 72.80.Le, 72.10.Xd, 73.20.Jc, 72.15.Rn

El transporte electrónico a escalas nanométricas es un campo floreciente, en el que pueden ser exploradas las propiedades de la materia en un ámbito en el cual los efectos cuánticos resultan cruciales. El control de los fenómenos de interferencia y su papel en la estructura electrónica ofrece oportunidades novedosas que permiten escapar de las restricciones usuales del dominio de la física clásica. Sin embargo, los grados de libertad del ambiente también pueden jugar un rol sustancial en los sistemas de dimensiones nanométricas, donde se espera la presencia de comportamientos tanto clásicos como cuánticos. Por ello, abordar el impacto de la decoherencia en este tipo de sistemas es una cuestión de importancia fundamental con aplicaciones prácticas de interés reciente. Generalmente los efectos de la decoherencia en el transporte cuántico se suponen negativos, con resultados inhibitorios en la interferencia cuántica constructiva sobre la función de onda electrónica. Sin embargo, debido a que en los sistemas desordenados predominan las interferencias destructivas, el rol de la decoherencia en estos sistemas puede ser crucial, ya que los eventos decoherentes son capaces de suprimir las interferencias cuánticas (en este caso destructivas) lo cual se ve reflejado como un incremento en la eficiencia del transporte debido a la asistencia del ambiente.

En el presente trabajo se plantea el impacto de los efectos de la decoherencia sobre el transporte electrónico, con interés particular en sistemas con múltiples terminales. El modelado de la decoherencia y su abordaje computacional se presenta con especial hincapié en la utilización de algoritmos eficientes. De acuerdo con esta metodología, se analizó el caso de los polímeros conductores a través de uno de los ejemplos paradigmáticos: las *polianilina* (PAni). A pesar de los importantes resultados experimentales que a principios del siglo XXI llevaron a adjudicar el premio Nobel al campo de los Polímeros Conductores, se carece aún de consenso en la comunidad científica sobre una descripción conceptual con capacidad predictiva de los procesos físicos involucrados. Utilizando parámetros realistas para el cálculo del transporte electrónico se muestra que la estructura desordenada de PAni, que es la más estable a temperatura ambiente, se vuelve altamente conductora cuando los efectos de la decoherencia son incluidos en la forma apropiada. Más aún, estos resultados para la conductancia prueban ser robustos, ya que no dependen críticamente de variaciones

en la preparación del polímero. También se presentan resultados para el transporte en nanotubos de carbono y se incluye una discusión sobre la interacción electrón-fonón, el transporte sujeto a potenciales dependientes del tiempo en forma periódica y el transporte magnético en modelos simples.

Contents

1 Introduction

1.1 Overview

The study of the electronic transport properties of solids is one of the cornerstones of condensed matter physics. Over the last decades, astounding technological advances have made possible the realization of electronic devices whose fundamental properties lie in the nanoscale, determined by collections of single molecules. Recent progress in the measurement of electron transport in molecular junctions is significant but its modeling often stands behind. The ability to manipulate objects at nanoscopic scales has been one of the driving forces of the science of our time, the nanotechnology. In particular, the development of the field of *molecular electronics* offers a unique opportunity to lift the veil of the quantum realm, engaging its surprising features to the design of novel devices. This interdisciplinary field grows at the boundaries of applied chemistry and physics, not only with the promise of a wide variety of immediate technological applications, but also offering important intellectual challenges for fundamental science.

Because of their small dimensions, nanodevices constitute a playground to study the behavior of coherent electron states under the influence of several distinctive quantum interactions. Understanding their basic transport properties is of fundamental importance for future applications. In 1957, Rolf Landauer

proposed that the problem of electronic conductivity can be approached as a quantum transmission probability problem. The conductance is determined by the coherent transmission probability of incident carriers across the sample, computed between two one-dimensional electrodes acting respectively as current source and drain. Yet, calculations of conductance of specific samples from their quantum transmission probabilities only became fashionable following the work of Philip W. Anderson, David Thouless and others in the late 1970's, where the concept appears as a key ingredient for the scaling theory of quantum localization [KM93]. Discussions of localization and subsequently its ramifications led to a renewed interest and more rigorous derivations of the Landauer formula. However, early discrepancies caused confusion and controversy in the physical community by the time. Throughout the 1980's a general framework for the treatment of mesoscopic conductance was maturated providing a concise and final form of Landauer's picture. This is known as *Landauer-Büttiker formalism* and its development was led by the work of Rolf Landauer, Markus Büttiker and Yoseph Imry [IL99]. Nowadays, Landauer's picture of electronic transport has almost no rival in the evaluation of quantum coherent electronic transport at the nanoscale [HR03]. The simplicity of Landauer's picture and the ease of its computational approach allowed a remarkable expansion of the implementation of these methods for the calculation of conductance in many freely distributed computational codes which are used in wide range of materials. However, perhaps its limitations are not always well understood and nowadays there are many examples in which there is an attempt to apply this simpler coherent treatment improperly, beyond its range of validity.

A first hint emerged from the work of Markus Büttiker who address the problem of multiprobe measurements within a scattering matrix formalism. He soon came out with the original idea that a voltage probe acts as a sort of inelastic scatterer. As an actual voltmeter, it should not extract net particles from the system, so it returns a particle for each one collected. Hence, for every process of "escape" from the coherent beam due to the interaction with the environment, a fresh incoherent particle must be re-injected into the system. However, when inelastic events are allowed to take out electrons from one energy channel and re-inject them at any other energy, the equations that

govern the behavior of Büttiker probes require a self-consistent evaluation of the chemical potentials at the voltmeters. The insight for the proper treatment of decoherence in electron transport as described by Hamiltonian models was developed by Jorge D'Amato and Horacio Pastawski (DP) [DP90]. The underlying idea of this approach is that, in several important systems, complex many-body interactions result in the loss of the simple interferences of a one-body description which is described by the rate obtained from the Fermi golden rule. Because of charge conservation, this rate should be formally equivalent to the coupling with a voltmeter. The consequence of this assumption is that after having evaluated a matrix with transmission amplitudes among every site in a sample, one still would need to evaluate its inverse. Despite of its recognized conceptual value, the DP strategy was rarely implemented, probably because of its seemingly computational cost. Thus the main majority of the work to date ignored the role of inelasticity and decoherence even for those applications, such as room temperature transport in polymers [Hee01a], where coherent transport should be safely ruled out. Therefore, in this work we intend to develop the DP model to a degree where its efficiency is beyond doubt and implement clear algorithms that could enable its widespread implementation in the great variety of systems that require it.

1.2 Our contribution

We present an alternative derivation of the effective transmission probability in the D'Amato-Pastawski model, specially suited for the computational implementation. A new compact matricial notation is introduced allowing simple expressions for the local chemical potentials and transmission functions. In this sense, basic strategies for the computational are presented, with a new model which constitutes an approximation for the introduction of decoherence into electronic transport, the coarse-grained D'Amato-Pastawski model.

The field of intrinsically conducting polymers is extensively reviewed through the paradigmatic case of polyanilines, and we show the crucial role of decoherence for electronic transport in these systems. A dramatic increase in its conductance is explained in terms of the D'Amato-Pastawski model, where the relevant sources of decoherent events are reveled.

Practical applications of the D'Amato-Pastawski model remained reduced to one-dimensional problems where it was originally formulated. Having a more efficient method would greatly improve the prospects for better simulations at the nanoscale in the presence of dephasing, a field of much current interest. In this spirit we provide a generalization for the general multi-terminal case, presenting efficient algorithms for the calculation of the self-consistent local chemical potentials. An exemplary approach to electron-phonon interactions, periodic time-dependent Hamiltonians and carbon nanotubes is presented in this context.

Finally, we show that the DP model provides all the ingredients for a generalized Landauer-Büttiker approach of magneto-transport in nanowires. A generalized version of this model that can be fairly applied to account for all the basic characteristics involved in giant magnetoresistance effect, a phenomenon that was previously described in terms of the self-consistent solutions of the phenomenological Boltzmann equation. This DP implementation should open the possibility to evaluate more complex quantum interference effects at the interface which have not been addressed yet in enough detail [Fer08].

1.3 Organization of this thesis

The introduction of the basic theory in the field of molecular electronics is presented in **Chapter 2**, covering the relevant analytical tools on the basis of which the following chapters are build. As the starting point, the fundamental ideas behind Rolf Landauer's picture of electronic transport are briefly reviewed. The real space renormalization group approach provides a quantitative framework that allows systematic investigation of the changes of a physical system as viewed at different scales. Tight-binding models usually provide convenient approximations of the Schrödinger equation which proved very useful to describe the relevant band structures of solids. In this way, the Green's function formalism becomes a powerful concept which provides an invaluable method for the computation of transmission functions provided by the Fisher-Lee relation. Since real solids always contain a certain amount of disorder with their underlying lattice structure never perfectly regular, we reviewed the basic features of transport in these kind of systems. Anderson localization and Mott's

variable range hopping constitute the center of our brief discussion. The final section of the chapter is dedicated Floquet theory applied to periodic driven quantum transport.

The question regarding the problem of decoherence and its role in one-particle quantum transport is deemed in **Chapter 3**. D'Amato-Pastawski model provides a general framework for the study of decoherene in one-electron transport problems and is discussed in detail. We also provide the basic strategies for the computational approach and a brief discussion of the coarse-grained version of the DP model which provides a natural approximation for weakly coupled molecular chains.

The role of decoherence in electronic transport is shown to be crucial in **Chapter 4**, where the physics involved in the electronic properties of intrinsically conducting polymers is approached. For many years, it has been assumed that conduction of polyanilines is inseparably linked to the existence of a polaronic crystalline structure. However, although our main intention is qualitative, we showed that decoherent processes are able to give appreciable metallic conduction in the more entropically favorable bipolaronic lattice. For this system, the uncertainty of energy associated with thermal processes cannot be neglected in the study of conductance. Based in our simulations we can estimate bulk conductivity for these chains and arrive to a remarkably good value as compared with experimental data.

In many problems, there are certain many-body interactions suffered by carriers in electronic devices that can not be treated within the simple Fermi golden rule approximation, providing extra degrees of freedom that must be accounted explicitly. Fortunately many times, in some approximation, this extra degrees of freedom can be mapped into the one-electron picture as extended topological spaces, transferring the complexity of the many-body interactions to the geometry of the one-electron transport problem. The extension of Landauer's picture of transport for the study of decoherence effects in multi-terminal devices, in this sense, provides a starting point. **Chapter 5** is devoted to the discussion of electronic transport on multi-terminal molecular devices, in the presence of decoherent events, in terms of a simple generalization of the D'Amato-Pastawski model. The review of the computational approach is also presented with particular emphasis on efficient recursive algorithms for solving

this kind of problems. Some meaningful physical examples of its application are also presented and discussed: the case of electron-phonon interactions and Floquet theory applied to simple periodic time-dependent Hamiltonians. An important application that deserved a separate chapter, magneto-transport in nanowires and the giant magnetoresistance effect is discussed on **Chapter 6**.

Finally, important remarks and conclusion of this work is stated on **Chapter 7**.

2

A primer on molecular electronics

Early quantum theories conceived to explain the relevant aspects of electron transport phenomena were semi-classical. Electrons were accelerated according to the Bloch theorem and this was partly balanced by back scattering due to phonons and several kinds of impurities. Although scattering cross sections and band structures were calculated according to quantum mechanics, the balancing process were carried out in terms of occupation probabilities and purely coherent processes were ruled out [IL99]. Kubo's theory represents the first effort widely accepted of a purely quantum mechanical transport formalism. In this theory non-equilibrium irreversible processes are connected, by the assumption of linear response, with the equilibrium properties of the system under study. Until the scaling theory of localization, the complicated microscopic Kubo formulation for transport in disordered conductors was mostly used loosely to justify the purely intuitive semi-classical Bloch-Boltzmann approach. Moreover, the advent of mesoscopic physics led to a revision of the most important ideas associated with the electron transport phenomena [Nac01].

The fact that the conductance of a single localized tunneling barrier, with very small transmission probability, is proportional to that probability was well understood in the early 1930's [Fre30]. However, Landauer [Lan88] related the linear response conductance to the transmission probability and draw attention

to the subtle questions that arise when we apply this relation to conductors having transmission probabilities close to unity.

2.1 Conductance from transmission probability

The approach in which the current through a conductor is expressed in terms of 'the probability that an electron can transmit through it' is often referred to as the *Landauer approach* to electronic transport. A key ingredient in *Landauer's picture* is that, besides the "sample" or device one must explicitly incorporate the electrodes or contacts in the transport description. An ideal conducting channel with no irregularities or scattering mechanisms along its length is shown in Fig. 2.1. The conductor is tied to a couple of large electron reservoirs via adiabatically tapered reflectionless large contact pads. In this context and for the remainder of the discussion, by *reflectionless* contacts we mean carriers that approaching a reservoir from the conductor pass into that reservoir with certainty. Going the other way, from the contact to the conductor, the reflections can be quite large [IL99].

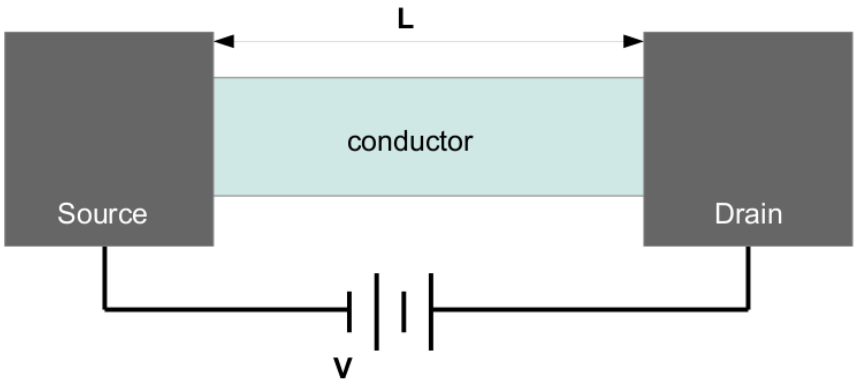

Figure 2.1: *A conductor between two large reservoirs via large contact pads.*

The electrons coming out of a reservoir are occupied according to the *local* Fermi distribution function that characterizes the reservoir itself. For the sake of simplicity we assume, initially, that the conductor is narrow enough so that only the lowest of the (discrete) transverse eigenstates in the channel

has its energy below the Fermi level. That makes the channel effectively one-dimensional. We consider the left-hand reservoir be filled up to level μ_1, higher than that of the right-hand reservoir, μ_2. We also assume 'zero temperature', so that there is current flow only in the energy range $\mu_1 > E > \mu_2$. In this simplified case, the current flow is just [IL99]:

$$I = -(\mu_1 - \mu_2)ev\frac{dn}{d\mu} \tag{2.1}$$

where $dn/d\mu$ is the density of states and v is the velocity component along the conductor at the Fermi surface. It was essential in Landauer's reasoning to note that in a propagating channel the density of states is inversely proportional to the corresponding group velocity [Pas92]:

$$\frac{dn}{d\mu} = \frac{2}{\pi\hbar v} \tag{2.2}$$

and the conductance of an ideal one-dimensional conductor is simply:

$$G = \frac{I}{\Delta V} = 2e^2/h \tag{2.3}$$

where ΔV is the voltage difference between the leads, $V_1 - V_2 = -(\mu_1 - \mu_2)/e$. As stressed emphatically by Landauer [IL99], the voltage specification deep inside the reservoir and the geometrical spreading are essential aspects of the derivation of Eq. 2.3. If the conductor is not ideal, there is an *average* transmission probability T that an electron injected at one end of the conductor will transmit to the other end. The current will be reduced accordingly, and we find

$$G = (2e^2/h)T \tag{2.4}$$

This is one of the most celebrated relations, in which the linear response conductance is expressed in terms of the transmission probability of electrons through one channel across conductor.

2.1.1 Multichannel two-probe conductance

The generalization of the preceding discussion for the case of leads that involve more than one transverse eigenstates with energy below the Fermi level is straightforward [MGM86]. In leads of finite cross section we have to consider both the motion of carriers transverse to the lead and the motion along the lead

[B̈86a]. Motion in the transverse direction is quantized and characterized by a set of discrete energies, E_n. For each of these energies smaller than the Fermi level, E_F, we obtain two states at the Fermi energy (i.e. a 'quantum channel'). In general, transverse states can be considered orthogonal and the linear response current is given by summing over all the channels, that we assume that are connected with the same reservoirs,

$$I_i = \frac{2e}{h} \sum_{ij} (T_{ij}\delta\mu_1 - T_{ji}\delta\mu_2) \tag{2.5}$$

Just be highlighted that in the particular case where we have M perfectly transmitting channels the conductance simply becomes:

$$G = M(2e^2/h) \tag{2.6}$$

One of the earliest and most significant experimental verifications of this approach was reported independently by two groups in 1988 [vWvHB$^+$88, DAWJ88]. Studying narrow two-dimensional channels connecting wide reservoirs, where the channel width were controlled by externally applied gate voltages, it was shown that as the width W of the constriction was reduced the conductance went down in discrete steps each of height $2e^2/h$. This is shown in Fig. 2.2.

2.1.2 More than two reservoirs

One step forward in the generalization of the Landauer formula is easily obtained by considering the case of a multi-probe setup explicitly. Büttiker found a simple and elegant solution noting that, since there is no qualitative difference between the current and voltages terminals, they must be treated on an equal footing [B̈86a]. This results from the application of the Kirchhoff law using Landauer's conductance formula. For the current in the n transverse mode of the i-th probe, we have:

$$I_{in} = \frac{2e}{h} \sum_{m,j} (T_{ni,mj}\delta\mu_j - T_{mj,ni}\delta\mu_i) \tag{2.7}$$

In order to simplify the notation we can treat the all transverse modes and probes in the same footing, loosing track in the notation of which are the

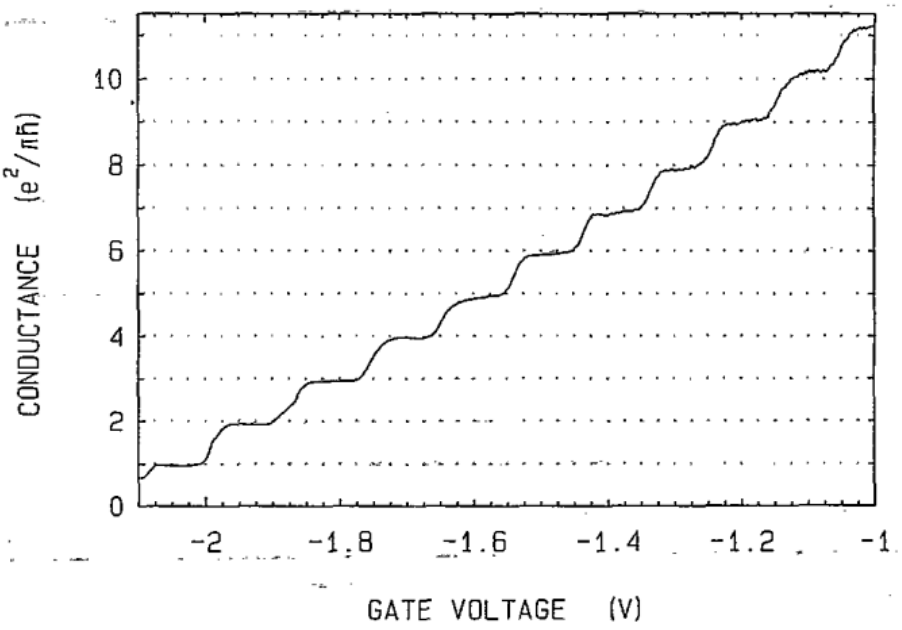

Figure 2.2: *Quantized conductance on a ballistic wave guide. First experimental point-contact conductance measurement report as a function of the gate voltage, by B. J. van Wees et al. [vWvHB+88].*

channels that share the same chemical potential,

$$I_i = \frac{2e}{h} \sum_j \left(T_{i,j} \delta\mu_j - T_{j,i} \delta\mu_i \right) \tag{2.8}$$

2.1.3 Non-zero temperature and bias

So far our discussion was simplified by the assumption of zero temperature so that we did not have to write explicitly how the Fermi distribution functions enter in Landauer's approach. In general, transport takes place through multiple energy channels in the energy range [Dat97]

$$\mu_i + (a\ few\ k_B T) > \varepsilon > \mu_j - (a\ few\ k_B T) \tag{2.9}$$

and the transmission probability is a function of the energy ε. Each reservoir i emits electrons with an energy availability controlled by a local distribution function:

$$f_i(\varepsilon) = \frac{1}{e^{(\varepsilon - \mu_i)/k_B T} + 1} \tag{2.10}$$

and the net current for a system composed by many channels (and in the spirit of the last section we include all probes and transverse modes in the same

footing) is [PM01]:

$$I_i = \int i(\varepsilon) d\varepsilon = \frac{2e}{h} \sum_j \int \left[T_{ji}(\varepsilon) f_i(\varepsilon) - T_{ij}(\varepsilon) f_j(\varepsilon) \right] d\varepsilon \tag{2.11}$$

This equation reduces easily to Eq. 2.8 when linear response is invoked.

2.2 Real space renormalization group procedures

The renormalization group (RG) is a quantitative framework that allows systematic investigation of the changes of a physical system as viewed at different scales. Basically, it consist of a decimation procedure that involves drawing a few parameters representatives of the physics at a given length scale which are used as basic input to obtain the physics at a next length scale [KGH$^+$67]. At the beginning of the 1970s, Kenneth Wilson [Wil83, Wil79] devised a specific version of the renormalization group formalism for statistical systems for which he was awarded the Nobel Prize in 1982. The basic scaling idea was soon applied by Thouless and Licciardello as a strategy to evaluate the localization of quantum eigenstates in disordered discrete systems [DT74]. Their idea was to obtain a sort of coarse-grain description of the wave function. The RG concept was central in the Abrahams, Anderson, Licciardello and Ramakrishnan solution of the quantum localization problem in terms of the scaling properties of the conductance [AALR79]. Crucial to the description of the localized regime was the use of the Landauer's formula which in turn was clearly connected to Thouless criterion for localization. For a review we refer to the article by MacKinnon and Kramer [KM93], who developed the first practical algorithm for calculation of scaling functions [MK81].

2.2.1 Tight-binding models

With a long history and applied in several different contexts, the *tight-binding model* can be regarded as an approach to the calculation of the electronic structure of solids. As developed by Bloch in his doctoral dissertation in 1928 under the tutoring of Heisenberg, the idea lies in the expansion of the extended crystal states by means of linear combinations of atomic orbitals (LCAO) of the composing atoms [Sla75]. This method generally provides a reasonable description

of the occupied states in solids and often also of the lowest lying conduction states whose advantage for the calculation of electronic structure was discussed by Slater and Koster [SK54]. From our point of view [PM01], it is enough to see it as a convenient conceptual approximation to the Schrödinger equation. It starts with a discretization of the Schrödinger equation at a subatomic scale, which is followed by the application of one step of the renormalization group procedure to achieve the relevant parameters at the atomic scale [Pas86]. This is eventually follow up by subsequent renormalization or decimation procedure. See Fig. 2.3.

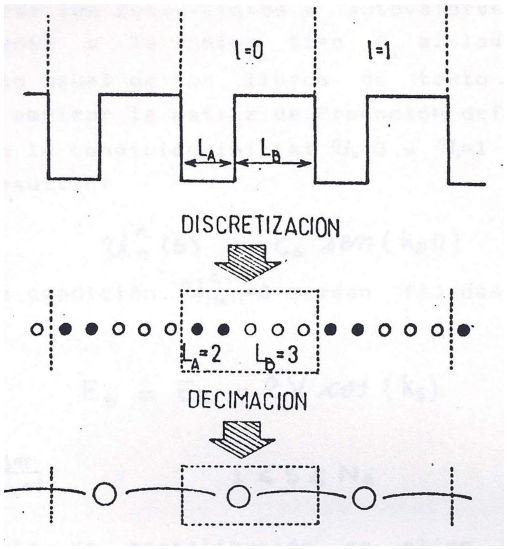

Figure 2.3: *Progressive decimation procedure to achieve the relevant parameters at the scale of interest. Extracted from Ref. [Pas86].*

Thus, to fix ideas we consider a one-dimensional case, in which the probability amplitude $\psi(x)$ to find a particle in a given position x is obtained as,

$$\frac{-\hbar^2}{2m}\nabla^2\psi(x) + U(x)\psi(x) = \varepsilon\psi(x) \tag{2.12}$$

We can discretized this equation obtaining a finite differences approach,

$$\nabla^2\psi(x) = \frac{\frac{\psi(x+\Delta x)-\psi(x)}{\Delta x} - \frac{\psi(x)-\psi(x-\Delta x)}{\Delta x}}{\Delta x} \tag{2.13}$$

where Δx is the lattice constant, namely the minimum distance between two possible positions. The last expression can be simplified using the following

substitutions, $\Delta x = a$, $x = na$, $u_n = \psi(na)$, $E_n = U(na)$ and $V = \hbar^2/2ma^2$, and we obtain:

$$(\varepsilon - E_n)u_n - Vu_{n+1} - Vu_{n-1} = 0 \tag{2.14}$$

Therefore, one is left with a discrete equation where the off-diagonal interaction is provided by the *kinetic energy* terms V, and the *local potential energy* terms are given by E_n, which in the LCAO description can be identified with the energy of atomic orbitals. Although here V appears as a constant value, a more general expression is often very useful (to take account, for example, of a discretized Schrödinger equation in which Δx is not a constant value). The one-dimensional Hamiltonian operator in a general tight-binding representation can be expressed as,

$$\hat{H} = \sum_n \left(E_n \hat{c}_n^\dagger \hat{c}_n - V_{n,n+1} \hat{c}_n^\dagger \hat{c}_{n+1} - V_{n+1,n} \hat{c}_{n+1}^\dagger \hat{c}_n \right) \tag{2.15}$$

and the single particle Schrödinger equation in this discrete basis can be written in term of the probability amplitudes u_n for the creation operator at each "site" n,

$$\left(\varepsilon \hat{I} - \hat{H} \right) |\psi\rangle = 0 \tag{2.16}$$

where

$$|\psi\rangle = \sum_n u_n \hat{c}_n |\emptyset\rangle \tag{2.17}$$

And Eq. 2.16 can be expressed in the matrix form:

$$\varepsilon \begin{bmatrix} \vdots \\ u_{n-1} \\ u_n \\ u_{n+1} \\ \vdots \end{bmatrix} - \begin{bmatrix} \ddots & & & & \\ & E_{n-1} & V_{n-1,n} & 0 & \\ & V_{n,n-1} & E_n & V_{n,n+1} & \\ & 0 & V_{n+1,n} & E_{n+1} & \\ & & & & \ddots \end{bmatrix} \begin{bmatrix} \vdots \\ u_{n-1} \\ u_n \\ u_{n+1} \\ \vdots \end{bmatrix} = 0 \tag{2.18}$$

When the *site energies* are taken from a random distribution in the range $[-W/2, W/2]$, the Hamiltonian is referred to as the Anderson model and it is the standard model to represent disordered systems. This is discussed in section 2.3.1.

2.2.2 Decimations and continued fractions

Most problems in solid state physics involve complex underlying structures with a huge number of available degrees of freedom and its study can not be carried out without the insight of proper simplifications designed so that the original significant physical properties are not altered. Real complex systems need to be mapped in simpler ones with equivalent properties. This can be accomplished with the help of renormalization procedures. In a convenient way, it allows the decimation of the degrees of freedom that are not *directly* relevant to the problem under study and then to calculate the physical quantities of interest of the remaining *effective* system.

The basis of the decimation strategy consists in the progressive reduction of the number of available variables initially provided by a discrete Schrödinger equation represented by a matrix Hamiltonian $\mathbb{H}$. Consider a small finite system of three sites. The Schrödinger equation takes the form:

$$\begin{bmatrix} \varepsilon - E_1 & -V_{1,i} & -V_{1,2} \\ -V_{i,1} & \varepsilon - E_i & -V_{i,2} \\ -V_{2,1} & -V_{2,i} & \varepsilon - E_2 \end{bmatrix} \begin{bmatrix} u_1 \\ u_i \\ u_2 \end{bmatrix} = [\varepsilon \mathbb{I} - \mathbb{H}] \overrightarrow{u} \equiv 0 \tag{2.19}$$

obtaining u_i from the second row and replacing in the first and the third equation one gets a *reduced* system of equations,

$$\begin{bmatrix} \varepsilon - \overline{E}_1 & -\overline{V}_{1,2} \\ -\overline{V}_{2,1} & \varepsilon - \overline{E}_2 \end{bmatrix} \begin{bmatrix} u_1 \\ u_2 \end{bmatrix} = 0, \tag{2.20}$$

where

$$\begin{aligned} \overline{E}_1 &= E_1 + \Sigma_1(\varepsilon) = E_1 + V_{1,i} \tfrac{1}{\varepsilon - E_i} V_{i,1} \\ \overline{E}_2 &= E_2 + \Sigma_2(\varepsilon) = E_1 + V_{2,i} \tfrac{1}{\varepsilon - E_i} V_{i,2} \\ \overline{V}_{1,2} &= V_{1,2} + V_{1,i} \tfrac{1}{\varepsilon - E_i} V_{i,2} \end{aligned} \tag{2.21}$$

Here, $\Sigma_1(\varepsilon)$ and $\Sigma_2(\varepsilon)$ are real numbers accounting for the energy shift or "self-energy" produced by the interaction of states 1 and 2 with the *eliminated* state, i. With this procedure, states 1 and 2 were *renormalized* or *dressed* by the presence of the eliminated state. Notice that as long as one conserves the analytical dependence of Σ_1 on ε, the actual secular equation is still cubic in ε and provides the exact spectrum of the whole system. However, in most cases one can obtain a good approximation to the corrected site energies by performing the evaluation at the "old" eigenvalue [PM01]:

$$\overline{E}_1 \approx E_1 + \Sigma_1(E_1) \tag{2.22}$$

$$\overline{E}_2 \approx E_2 + \Sigma_2(E_2) \tag{2.23}$$

which becomes equivalent to the second order Rayleigh-Schrödinger perturbation theory. That is, we have gone from the three orbital problem to a two-orbital effective system. The procedure of decimation of variables is very simple and easily generalized, providing a systematic way to reduce the dimension of the Hamiltonian. This is done at the cost of transforming the linear set of equations into a non-linear smaller set. Although this procedure is exact, the smaller set of equations can often be linearized in the region of interest as in Eqs. 2.22 and 2.22.

The general recipe remains very simple for the special case of a system with a Hamiltonian that can be represented with a tridiagonal matrix. Thankfully, this kind of situations (together with the generalization to block tridiagonal Hamiltonians, which are dealt with some detail in chapter 5) are commonly encountered in many physical examples. Any tight-binding chain of nearest-neighbors interacting atoms meet this condition. If $i < j$, the self-energy for site i due to the decimation of all the sites between i and j is simply [PM01]:

$$\Sigma_{i,j}(\varepsilon) = V_{i,i+1}\frac{1}{\varepsilon - E_{i+1} - \Sigma_{i+1,j}(\varepsilon)}V_{i+1,i} \tag{2.24}$$

and for the self-energy of site j we have, analogously,

$$\Sigma_{j,i}(\varepsilon) = V_{j,j-1}\frac{1}{\varepsilon - E_{j-1} - \Sigma_{j-1,i}(\varepsilon)}V_{j-1,j} \tag{2.25}$$

If the chain in consideration has N sites and all of them were decimated, except for i and j, one gets an effective two-level system, with a Schrödinger equation completely equivalent to Eq. 2.20, but with the renormalized energies,

$$\overline{E}_i(\varepsilon) \quad = E_i + \Sigma_{i,1}(\varepsilon) + \Sigma_{i,j}(\varepsilon) \tag{2.26}$$

$$\overline{E}_j(\varepsilon) \quad = E_j + \Sigma_{j,i}(\varepsilon) + \Sigma_{j,N}(\varepsilon) \tag{2.27}$$

and the effective hopping,

$$\overline{V}_{i,j} = V_{i,j-1}\frac{1}{\varepsilon - E_j - \Sigma_{j,i}(\varepsilon)}V_{j-1,j} \tag{2.28}$$

The algebraic decimation procedure is closely related with matrix inversion. This is specially shown in section 2.2.4.

2.2.3 Self-energies for the leads

A very important example involves the computation of the self-energy of an ordered semi-infinite one-dimensional chain. Drawing on the example below, we assume $V_{j,j+1} = V$ and $E_j = E$ ($\forall_{j>0}$) and we take $i = 0$ and $N \to \infty$ in order to obtain the renormalized energy of the site $i = 0$ due to the decimation of the entire semi-infinite chain. In this case, we have that for any site $j > 0$ on the chain,

$$\Sigma_{j,\infty}(\varepsilon) = V \frac{1}{\varepsilon - E - \Sigma_{j+1,\infty}(\varepsilon)} V \tag{2.29}$$

However, the fact that every site $j > 0$ sees to the right the "same" semi-infinite chain implies that $\Sigma_{j,\infty} = \Sigma$ ($\forall_{j>0}$). Inserting this into Eq. 2.29 results:

$$\Sigma(\varepsilon) = V \frac{1}{\varepsilon - E - \Sigma(\varepsilon)} V = \Delta \mp i\Gamma \tag{2.30}$$

The striking fact is that even when we are working with real quantities the solution of this equation may lay in the complex plane [PM01, WP84]. The solution of this second order equation gives:

$$\Delta = \begin{cases} \frac{(\varepsilon - E)}{2} - \sqrt{\left(\frac{\varepsilon - E}{2}\right)^2 - V^2} & \text{if } \varepsilon - E > 2|V| \\ \frac{(\varepsilon - E)}{2} & \text{if } |\varepsilon - E| \leq 2|V| \\ \frac{(\varepsilon - E)}{2} + \sqrt{\left(\frac{\varepsilon - E}{2}\right)^2 - V^2} & \text{if } \varepsilon - E < -2|V| \end{cases} \tag{2.31}$$

and,

$$\Gamma = \begin{cases} 0 & \text{if } |\varepsilon - E| > 2|V| \\ \sqrt{V^2 - \left(\frac{\varepsilon - E}{2}\right)^2} & \text{if } |\varepsilon - E| \leq 2|V| \end{cases} \tag{2.32}$$

This expressions are particularly important when dealing with the electrodes in systems such as the one depicted in Fig. 2.1. In this way, one can include the effects of a whole lead in a Hamiltonian description through an complex correction to the energy of the site connected to the lead.

2.2.4 Green's function formalism

The Green's function method is a powerful concept which provides an alternative framework to discuss the solutions of the Schrödinger equation. Besides the intuitive structure of the perturbative calculations, the use of the Green's function has the additional advantage of a clearer connection to transport properties and a special role in quantum field theory which allows a definitive treatment of

the many-body problems. The Green's function gives the response at any point due to an excitation at any other. For the case of non-interacting transport the only relevant excitations are those due to plain waves incident from the leads. As mentioned in section 2.2.5, the transmission probability of the Landauer formula (Eq. 2.4) can be computed with the help of the Green's function matrix evaluated at the sites the leads are attached. However, the real power of the Green's functions becomes evident when there is a need to include in the transport description the effect of interactions, such as electron-electron or electron-phonon couplings. This is dealt with in some detail throughout chapter 2, doomed to establish how to include of decoherent events in the transport description.

Green's functions are named after the British mathematician George Green, who first developed the concept in the 1830's. The construct of Green's functions appears in many physical contexts, specially in quantum field theory, electrodynamics and statistical field theory. It is a common practice to define two different Green's functions (retarded and advanced) that satisfy two different boundary conditions. For the Schrödinger equation, the retarded (advanced) Green's function is defined as a function of the real variable ε,

$$\hat{G}^{R(A)}(\varepsilon) = \left[\varepsilon\hat{I} - \hat{H} \pm i\eta\hat{I}\right]^{-1} \quad (\eta \to 0^+) \tag{2.33}$$

where $\hat{H}$ is the complete Hamiltonian of the system and $i\eta$ is an infinitesimal imaginary part with the purpose of the incorporation of the boundary conditions into the equation itself.

Consider the Green's function matrix of the 3x3 Hamiltonian matrix given in Eq. 2.19. It is given just by the inverse $[\varepsilon\mathbb{I} - \mathbb{H}]^{-1}$. After some algebra, it is straightforward to show that:

$$\begin{aligned} G_{11} &= \left[\varepsilon - \overline{E}_1 - \overline{V}_{12}\tfrac{1}{\varepsilon - \overline{\overline{E}}_2}\overline{V}_{21}\right]^{-1} = \left[\varepsilon - \overline{\overline{E}}_1\right]^{-1} \\ G_{12} &= \overline{V}_{12}\left[\left(\varepsilon - \overline{E}_1\right)\left(\varepsilon - \overline{E}_2\right) - \overline{V}_{12}\overline{V}_{21}\right]^{-1} \end{aligned} \tag{2.34}$$

That is, the elements of the Green's function matrix of Eq. 2.19 are easily obtained from the reduced Eq. 2.20, where the intermediate site i was decimated. This, which seems a simple triviality, is a reflection of the fact that the decimation procedure is exact if the dependence on ε is held in renormalized

sites. Also, it shows the close connexion between decimations procedures and a related matrix inversion algorithm. No matter how large is the matrix Hamiltonian, the elements of the Green's function matrix can always be expressed in the form:

$$\begin{aligned} G_{nn} &= \left[\varepsilon - \overline{E}_n - \overline{V}_{nm}\tfrac{1}{\varepsilon-\overline{E}_m}\overline{V}_{mn}\right]^{-1} = \left[\varepsilon - \overline{\overline{E}}_n\right]^{-1} \\ G_{nm} &= \overline{V}_{nm}\left[\left(\varepsilon - \overline{E}_n\right)\left(\varepsilon - \overline{E}_m\right) - \overline{V}_{nm}\overline{V}_{mn}\right]^{-1} \end{aligned} \tag{2.35}$$

where the over-line in every quantity means the decimation of all the elements $i \neq n, m$ into the elements n and m. The decimation procedures give not only a natural way to reduce the degrees of freedom of the system when an approximation is needed, but also provide a simple and exact algorithm to compute the elements of the Green's function (and, by extension, for the computation of the elements of the inverse of any matrix).

The local density of states represents the weight of the eigenenergies of the system on the basis states. The definition of the Green's function, given by Eq. 2.33, implies that its poles coincide with the eigenenergies of the system and, as a consequence, the local density of states N_i at the site i of the system is obtained from the retarded Green's function matrix simply by [PM01]:

$$N_i(\varepsilon) = -\frac{1}{\pi}\lim_{\eta\to 0}\ \mathrm{Im}\ G^R_{ii}(\varepsilon - \mathrm{i}\eta) \tag{2.36}$$

2.2.5 The Fisher-Lee formula

Although the entire discussion of sections 2.1-2.1.3 is devoted to elucidate how the conductance of a quantum system can be understood in terms of its quantum transmission probability, the question of a handy formula to deal with this transmission probability is left aside. It is clear that there is a close relation between the electronic structure of a given system, described by its Hamiltonian and the associated Green's function, and its electron transport properties that are reflected in the transmission function. The original demonstration of the connection between the transmission probability and the Green's function, by Fisher and Lee [FL81], is based on the properties of the scattering matrix in a continuum model. This demonstration is reviewed in a tight-binding approach by H. Pastawski and E. Medina [PM01].

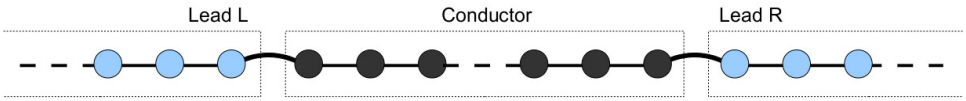

Figure 2.4: *Sketch of the tight-binding model for a conductor attached to two contact pads.*

Consider the tight-binding model of a conductor attached to the leads as shown in Fig. 2.4. The Landauer formulation requires to calculate the transmission of the system between the sites where the leads are connecting to the electrodes. Assuming that the sample's Hamiltonian is known one must incorporate explicitly the leads. Although they are modeled as semi-infinite ordered chains, they must be decimated and included as self-energies (computed as in Eq. 2.30) that shift the sites energies,

$$\overline{E}_1 = E_1 + \Sigma_L(\varepsilon) \tag{2.37}$$

$$\overline{E}_N = E_N + \Sigma_R(\varepsilon) \tag{2.38}$$

Thus, to an original molecular orbital tight-binding Hamiltonian with N orbitals,

$$\hat{H}_S = \sum_{i=1}^{N} \left(E_i \hat{c}_i^{+} \hat{c}_i + \sum_{j>i}^{N} \left[V_{i,j} \hat{c}_i^{+} \hat{c}_j + V_{j,i} \hat{c}_j^{+} \hat{c}_i \right] \right) \tag{2.39}$$

we complete the entire *effective* Hamiltonian adding the self-energies of the leads that renormalize the sites attached to them,

$$\hat{H}_{eff.} = \hat{H}_S + \hat{\Sigma}_L + \hat{\Sigma}_R \tag{2.40}$$

where $\hat{\Sigma}_L = \Sigma_L \hat{c}_1^{\dagger} \hat{c}_1$ and $\hat{\Sigma}_R = \Sigma_R \hat{c}_N^{\dagger} \hat{c}_N$ are the operators describing the escape to the left and right leads respectively. This effective Hamiltonian accounts for the entire system and allows the evaluation of the associated Green's function.

The Fisher-Lee formula for the transmission probability for this case reads:

$$T_{RL}(\varepsilon) = \left[2\Gamma_R(\varepsilon) \right] G^R_{N1}(\varepsilon) \left[2\Gamma_L(\varepsilon) \right] G^A_{1N}(\varepsilon) \tag{2.41}$$

Note that the only elements of the Green's function involved in the Fisher-Lee transmission formula are the ones associated with the sites directly connected to the leads. More complicated setups may involve more than two probes or

even several leads connected to the same site. In general, whenever a site i is connected to a lead α and a site j is connected to a lead β, the related transmission probability between them given by the Fisher-Lee formula takes the form:

$$T_{(\alpha,i),(\beta j)}(\varepsilon) = [2\Gamma_\beta(\varepsilon)]\, G^R_{ji}(\varepsilon)\, [2\Gamma_\alpha(\varepsilon)]\, G^A_{ij}(\varepsilon) \tag{2.42}$$

2.3 Transport properties of disordered solids

Real solids always contain a certain amount of disorder since their underlying lattice structure is never perfectly regular. Physically, the disorder can be thought to be related with the presence of impurities, vacancies and dislocations in otherwise ideal crystal lattices. In fact, strong disorder can be achieved if the concentration of impurities is sufficiently large and a completely disordered assembly of atoms will be one in which the atoms or molecules are distributed completely independent and randomly. Many physical properties are either influenced or even mainly determined by this randomness. The understanding of the consequences of disorder in the properties of solids is of enormous practical importance and took a cardinal role in condensed matter physics in the last half century.

Clearly, the common belief is that disorder prevents the electrons in a semiconductor to move freely. In a first approach to the problem of the disorder effects on electronic conductivity, electrons can be imagined to be multiply scattered by impurities and diffusing through the solid. The central concept in the description of the diffusion is the mean free path of the electron, the average length it travels before suffering a collision. The appearance of strong multiple scattering correlates with a very short mean free path. The classical Ohmic law dictates that the electronic conductivity is directly proportional to this mean free path. However, the increase of the degree of disorder may not just lead to a decrease of the conductivity but also may trigger profound effects in its behavior. This issue was raised as the problem of "localization". Being in principle a property of the states in a random quantum mechanical systems, it presents its most striking experimental manifestation in the transport properties of condensed matter physics [KM93].

2.3.1 Anderson localization

In 1958, P. W. Anderson published an article [And58] where he conceived the idea of electron localization analyzing, in a tight-binding model, the behavior of electrons in a crystal with site impurities. In this simple model, transport is considered in a random lattice, where diffusion is expected to take place via quantum jumps between localized sites. The essential randomness is introduced by requiring the energy to vary randomly from site to site. In this early work, he established the conditions for the absence of quantum diffusion: Beyond a critical amount of impurity scattering the diffusive motion of the electron will freeze. It was later showed that the transition occurs when the electrons mean free path becomes smaller than its wavelength. This mobility halt or "localization" has dramatic consequences for the conductivity, the material turns into an insulator. P. W. Anderson, jointly to N. F. Mott and J. H. van Vleck received the Nobel prize in physics in 1977 "*for their fundamental theoretical investigations of the electronic structure of magnetic and disordered systems*".

The simplest model for Anderson localization, which contains only the essentials, is a linearized, random tight-binding model of non-interacting particles [And78],

$$\hat{H} = \sum_n E_n \hat{c}_n^\dagger \hat{c}_n + V \sum_{<n,m>} \hat{c}_n^\dagger \hat{c}_m \tag{2.43}$$

where V are the hopping elements, considered only between nearest neighbors $< n, m >$, and the site energies E_n are taken from a random probability distribution of width W, $[-W/2, W/2]$. The Hamiltonian model given by Eq. 2.43 leads to a linear equation of motion of the form:

$$i\hbar\dot{\hat{c}}_n^\dagger = E_n \hat{c}_n^\dagger + \sum_m V \hat{c}_m^\dagger \tag{2.44}$$

If $W = 0$, all the site energies have the same value and this equation describes a conventional band of extended Bloch states, with energies:

$$E_k^0 = \sum_{nm} V \cos[\mathbf{k}\cdot(\mathbf{R}_i - \mathbf{R}_j)] \tag{2.45}$$

In the case of $W \ll V$, a possible way to investigate the solutions of the diagonal-disordered Hamiltonian of Eq. 2.43 is by a *perturbative treatment*

of disorder. The starting point is, therefore, the energy of the unperturbed k states of Eq. 2.45. Thus, we assume that the presence of the impurities can be accounted by a self-energy that renormalizes the unperturbed energies, $E_k^0 + \Sigma_k(\varepsilon)$. The diagonal elements of the retarded Green's function of these states are,

$$G_{k,k}(\varepsilon) = \frac{1}{\varepsilon - E_k^0 - \Sigma_k(\varepsilon)} \tag{2.46}$$

The perturbative expansion of the introduced self-energy is [Pas10],

$$\Sigma_k(\varepsilon) = \sum_{k' \neq k} V_{k,k'} G_{k'}^0 V_{k',k} + \sum_{k'',k' \neq k} V_{k,k'} G_{k'}^0 V_{k',k''} G_{k''}^0 V_{k'',k} + ... \tag{2.47}$$

That is, of course, k states are mixed due to the perturbation. Evaluating the perturbative expansion to first order, $\Sigma_k(E_k^0)$, the finite lifetime of k states can be obtained with the Fermi Golden Rule.

In the case of $W \gg V$ we are faced with the failure of the perturbative treatment of k states. Anderson proposed to analyze this problem starting on the opposite side of the perturbative expansion with local, impurity states as the unperturbed ones. Thus, the diagonal elements of the retarded Green's function in this basis, is:

$$G_{ii}(\varepsilon) = \frac{1}{\varepsilon - E_i - \Sigma_i(\varepsilon)} \tag{2.48}$$

and the perturbative expansion of the impurity states is given by [Pas10],

$$\Sigma_i(\varepsilon) = \sum_{j \neq i} V_{i,j} G_j^0 V_{j,i} + \sum_{j,k \neq i} V_{i,j} G_j^0 V_{j,k} G_k^0 V_{k,i} + ... \tag{2.49}$$

This expansion diverges if the states are extended, and converges otherwise.This expression constitutes a geometric series with terms of the form,

$$T^L = \underbrace{VG^0\ VG^0\ ...\ VG^0}_{L\ times} \tag{2.50}$$

for which we can take [Pas10],

$$\ln T^L \simeq L \left\langle \ln |VG^0| \right\rangle \tag{2.51}$$

and if z denotes the coordination number of the lattice, the perturbative expansion involves the terms,

$$z^L T^L \simeq z^L V^L \exp\left[L \ln \left\langle |G^0| \right\rangle\right] \tag{2.52}$$

The criterion for convergence for the series is therefore given by [Pas10],

$$zV \exp\left[\ln\left\langle|G^0|\right\rangle\right] < 1 \tag{2.53}$$

The analysis of the convergence of this series is complex and exceeds the purpose of this introductory approach. What emerges from this criterion is that in a 3D system there is a critical value W_c at which a band of delocalized states begin to appear, and at its ends a series of localized states. The greatest achievement of Anderson was the formulation of the extended-localized transition. Non-interacting electronic or vibrational eigenstates in solids would transform from Bloch plane waves into exponentially localized functions whenever the strength of a homogeneous disorder exceeds a critical value. In 1D and 2D cases the states are localized at any disorder. A very significant result for the field of polymeric conductors is that localization guaranties an absence of transport for any degree of randomness in one dimension.

2.3.2 Mott's variable range hopping

The variable range hopping theory was introduced by Mott [Mot69] to describe the low temperature behavior of the resistivity in strongly disordered systems where states are localized. The energies of these localized states is assumed to be distributed statistically over a finite energy range. The hopping probability between two arbitrary states depend on two fundamental parameters, the spacial separation r, and the energy difference ΔE of the sites. Since the states are localized, it is natural to assume exponential decaying associated wave functions and the tunneling probability will be proportional to a term of the form $\exp(-2r/\xi)$, where ξ is the localization length [Mad96]. Also, in any of these transitions between localized states the energy difference must be provided by phonons. The number of phonons of energy ΔE in thermal equilibrium, for sufficiently low temperatures, is given by the Boltzmann factor $\exp(-\Delta E/k_B T)$. Therefore, the probability of hopping between two states has the form:

$$P \propto \exp\left(-\frac{2r}{\xi} - \frac{\Delta E}{k_B T}\right) = e^{-\mathcal{R}} \tag{2.54}$$

The quantity $\mathcal{R} = \frac{2r}{\xi} + \frac{\Delta E}{k_B T}$ is usually called *range* of the hopping probability. Since with longer hops, there is a better probability of reducing the activation

energy $e^{-\Delta E/k_BT}$, this *range* is determined by the competition of the overlap term, which favors short hops, and the energy activation, which favors long hops. The maximal value for the range $\overline{\mathcal{R}}$ will determine the final conductivity of the disordered solid, proportional to a probability of the form 2.54, that is

$$\sigma \propto e^{-\overline{\mathcal{R}}} \tag{2.55}$$

If we assume the density of states, g, to be constant over the range of energies considered, the number of states between E_i and $E_i + \Delta E$ in a sphere of radius r is equal to $(4\pi/3)r^3 g\Delta E$. Therefore we can estimate [Mad96],

$$\Delta E = \frac{3}{4\pi r^3 g} \tag{2.56}$$

and the range will have the form,

$$\mathcal{R} = \frac{2r}{\xi} + \frac{3}{4\pi r^3 g k_B T} \tag{2.57}$$

which is maximal for $r^4 = 9\xi/(8\pi g k_B T)$. Hence, evaluating Eq. 2.55 for this value we obtain [Mad96],

$$\sigma \approx \exp\left[-\left(\frac{T_0}{T}\right)^{\frac{1}{4}}\right] \qquad T_0 = \frac{5/2}{9\pi\xi^3 k_B g} \tag{2.58}$$

The last expression is the famous Mott's variable range hopping law. It is experimentally observed in doped semiconductors at low temperatures.

2.3.3 Correlations and metal-insulator transition in 1D

As stated in section 2.3.1, the theory of Anderson localization predicts the vanishing of the diffusion constant for an electron moving in a one-dimensional lattice even for infinitesimal amount of disorder. The disordered site energies were strictly statistical independent values, taken from a random distribution. However, over the last twenty years analytical and numerical studies revealed that current-carrying states can exist in a one-dimensional disordered lattice with short and long range *correlations*.

A very interesting example, in which a simple correlation among the distribution of disordered energies has profound effects in the transport properties of the system, is the Random Dimer Model (RDM) [DWP90]. In this section we focus on this instructive example that presents important implications for

the field of conductive polymers [WP91]. RDM is a special case of the *random binary alloy*, in which two different energies, E_a and E_b, are assigned at random to the sites of a one-dimensional nearest-neighbor tight-binding Hamiltonian. All states in the random binary alloy model are localized [Phi03]. The RDM emerge from the random binary alloy replacing all clusters containing and odd number of sites with energies E_b with the same number of sites of energy E_a. That is, in the RDM, sites with energies E_b, although selected at random, are forced to appear in clusters containing an even number of sites. Another way to obtain the RDM is to consider an initial perfect chain of site energies E_a in which *pairs* of randomly distributed defects with site energies E_b are produced. The surprising result of the correlation induced in this disordered model (where defects are forced to appear in pairs) is that $\sqrt{N}$ states of this system are extended over the entire sample, provided that $-1 \leq W \leq 1$, where [Phi03]:

$$W = \frac{E_a - E_b}{2V} \tag{2.59}$$

Is easy to show [DWP90] that the reflexion coefficient of a k state through a single dimer in an otherwise perfect chain is given by:

$$R = \frac{(W + \cos k)^2}{(W + \cos k)^2 + \sin^2 k} \tag{2.60}$$

and this implies that the reflection vanishes when $W = -\cos k$. Then, because the transmission through a single dimer in this range is perfect, the particular random distribution of dimers should not affect the overall transmission probability [Phi03]. Since the time τ between scattering states is inversely proportional to the reflection probability, then the mean free path can be approximated by

$$\ell = v_F \tau \propto |R|^{-2} \approx \frac{1}{(k - k_0)^2} \tag{2.61}$$

where we expanded R around $k_0 = \cos^{-1} W$. Taking $(k - k_0) = \Delta N / 2\pi N$, assuming N sites in the chain and equating ℓ to the length of the system, it is possible to predict the total number of extended states scales as $\sqrt{N}$.

2.4 Periodic time-dependent transport: Floquet theory

Consider a one-dimensional quantum system, subject to a time dependent periodic potential, so that the system Hamiltonian satisfies $H(t) = H(t+T)$ for all arbitrary times t, where T is the period. This peculiar symmetry of the Hamiltonian under discrete temporal translations, $t \to t+T$, allows the use of the Floquet methodology, which simplifies enormously the description of the behavior of the system.

The interest of this section is to introduce the Floquet method for the study of periodic time dependent driven transport. The system under study will not be isolated, in general, because of the presence of the contacts that connect the sample with particle reservoirs. The quantum dynamics of this system will be governed by a Schrödinger equation of the type:

$$i\hbar\frac{\partial}{\partial t}\left|\Psi(t)\right\rangle = \left[H(t) - i\Sigma\right]\left|\Psi(t)\right\rangle \tag{2.62}$$

where the Hermitian term Σ, or "self-energy" comes from the decimation of the degrees of freedom of the environment (in this case constituted by the leads) and implies that the time evolution of a given initial state of this system will not be unitary since the full Hamiltonian is no longer Hermitian.

Notice that, due to the explicit time-dependence of the Hamiltonian, the energy is not a constant of motion and therefore the usual separation of the type $\left|\Psi(t)\right\rangle = \exp\left(-iEt/\hbar\right)\left|\phi\right\rangle$, where E is the (complex) energy of the state $\left|\phi\right\rangle$, is no longer possible. However, the periodic time dependence of the Hamiltonian allows the use of the Floquet theory to obtain a *similar* description to that resulting from the time independent Schrödinger equation [GH98].

Floquet theory states that when a Hamiltonian has a periodic dependence on time, $H(t) = H(t+T)$, there is a complete set of solutions $\{\left|\Psi_\alpha(t)\right\rangle\}$ of the form:

$$\left|\Psi_\alpha(t)\right\rangle = e^{-(i\varepsilon_\alpha+\gamma_\alpha)t/\hbar}\left|\phi_\alpha(t)\right\rangle \tag{2.63}$$

where the functions $\left|\phi_\alpha(t)\right\rangle$, called *Floquet modes* (and also *Floquet states*), have a periodic dependence on time, with the same period T as the Hamiltonian:

$$\left|\phi_\alpha(t)\right\rangle = \left|\phi_\alpha(t+T)\right\rangle \tag{2.64}$$

The quantities $E = (\varepsilon_\alpha - i\gamma_\alpha)$ are often referred to as *quasienergies*, due to the formal analogy to the quasimoments that characterize the Bloch states in a system with spatial periodicity. Inserting the solutions 2.63 into Eq. 2.62, it is immediately verified that Floquet modes satisfy:

$$\mathcal{H}_F \left|\phi_\alpha(t)\right\rangle = (\varepsilon_\alpha - i\gamma_\alpha) \left|\phi_\alpha(t)\right\rangle \tag{2.65}$$

where the operator $\mathcal{H}_F = H(t) - i\Sigma - i\hbar\partial/\partial t$, is called *Floquet Hamiltonian*. The formal analogy between the last expression and the time-independent Schrödinger equation is evident. It should be stressed that the conceptual importance of the Floquet theory lies in the fact that it allows to separate the long time dynamics, governed by the eigenvalues $\varepsilon_\alpha - i\gamma_\alpha$, from the dynamics within a single period, determined by the Floquet modes $|\phi_\alpha(t)\rangle$.

Floquet modes and quasienergies are not uniquely defined, since

$$|\phi_{\alpha'}(t)\rangle = e^{ik\omega t} |\phi_\alpha(t)\rangle \equiv |\phi_{\alpha k}(t)\rangle \tag{2.66}$$

where k is an integer number $k = 0, \pm 1, \pm 2, ...$ and $\omega = 2\pi/T$, gives identical solutions to the equation 2.63 but with quasienergies shifted as:

$$\varepsilon_\alpha \to \varepsilon_{\alpha'} = \varepsilon_\alpha + k\hbar\omega \equiv \varepsilon_{\alpha k} \tag{2.67}$$

Hence, the label α corresponds to a complete set of solutions indexed by $\alpha' = (\alpha k)$, for $k = 0, \pm 1, \pm 2, ...$ In other words, Floquet modes and quasienergies appear in *clases* from which we can select a representative one usually inside of the "Brillouin zone" $E - \hbar\omega/2 \leq \varepsilon_\alpha \leq E + \hbar\omega/2$, where E is an arbitrary, but fixed, energy.

2.4.1 Extended Hilbert space

According to the basic postulates of quantum mechanics, the state of a system is described by a vector $|\Psi\rangle$ in a Hilbert space $\mathbb{R}$ with the internal product $\langle\Psi'|\Psi\rangle_R$. Without loosing generality, can be assumed that there is a complete numerable set $\{|\alpha\rangle\}$ of orthonormal states in $\mathbb{R}$:

$$\langle\alpha|\beta\rangle_R = \delta_{\alpha\beta}, \quad \sum_\alpha |\alpha\rangle \langle\alpha| = 1 \tag{2.68}$$

The Hilbert space $\mathbb{T}$ of all complex functions periodic in T have the internal product,

$$\langle\phi|\varphi\rangle_T = \frac{1}{T}\int_0^T dt\phi^*(t)\varphi(t) \tag{2.69}$$

and the functions $\exp(ik\omega t)$ with $k = 0, \pm1, \pm2, ...$ constitute the corresponding complete orthonormal set. The decomposition of an arbitrary complex function with periodicity in T, in this basis, is identical to the decomposition into the standard Fourier series.

Hideo Sambe [Sam73] was the first who suggested that due to the time periodicity of Floquet modes, they can be treated in a composed Hilbert space of the form $\mathbb{R}\otimes\mathbb{T}$. Its elements, denoted by $|\phi(t)\rangle$, are all T-periodic vectors $|\phi(t)\rangle = |\phi(t+T)\rangle$. The internal product is defined in the canonical way:

$$\langle\phi^{'}|\phi\rangle = \frac{1}{T}\int_0^T dt\langle\phi^{'}(t)|\phi(t)\rangle \tag{2.70}$$

An orthonormal basis for the extended Hilbert space $\mathbb{R}\otimes\mathbb{T}$ is given by the set of states $\{|\alpha k\rangle\}$, defined by

$$|\alpha k\rangle = e^{ik\omega t}|\alpha\rangle. \tag{2.71}$$

since it is clear that,

$$\langle\beta m|\alpha n\rangle = \frac{1}{T}\int_0^T dt e^{i(n-m)\omega t}\langle\beta|\alpha\rangle = \delta_{m,n}\delta_{\beta,\alpha} \tag{2.72}$$

and they constitute a complete set in $\mathbb{R}\otimes\mathbb{T}$.

The decomposition of a state $|\phi_\alpha(t)\rangle$ in this basis is given by:

$$|\phi_\alpha(t)\rangle = \sum_k e^{-ik\omega t}|\phi_{\alpha,k}\rangle \tag{2.73}$$

$$|\phi_{\alpha,k}\rangle = \tfrac{1}{T}\int_0^T dt e^{ik\omega t}|\phi_\alpha(t)\rangle \tag{2.74}$$

When using the extended Hilbert space formalism it should be noticed that the solution $|\Psi(t)\rangle$ of Eq. 2.62 is not T-periodic in general and then it is not an element of the extended Hilbert space. Also, Floquet modes are orthonormal only at equal times.

With the introduction of the extended Hilbert space to deal with the periodic time dependence, a mapping was performed between the computation of the Floquet modes and a time-independent Hamiltonian with an additional degree of freedom.

2.4.2 Green-Floquet functions

With the introduction of the Floquet methodology for the resolution of the time dependent Schrödinger equation, in a system subject to a potential with periodic time dependence, the problem is simplified to a *time-independent* eigenvalue equation, but in a space of higher dimensionality. According to the sections below, the fundamental problem is reduced to find the Floquet modes and the quasienergies

$$\mathcal{H}_F \left|\phi_\alpha(t)\right\rangle = \varepsilon_\alpha \left|\phi_\alpha(t)\right\rangle \tag{2.75}$$

From this equation and hereafter the notation is slightly changed, since ε_α stands for a complex value (includes the imaginary part $i\gamma_\alpha$, compare to Eq. 2.65). In terms of the basis introduced in the last section (Eq. 2.71), the matrix elements of the Floquet Hamiltonian are obtained straightforwardly,

$$\langle \beta m|\mathcal{H}_F|\alpha n\rangle = \frac{1}{T}\int_0^T e^{-im\omega t}\left[H_{\beta\alpha}(t) - i\hbar\delta_{\beta\alpha}\frac{\partial}{\partial t}\right] e^{in\omega t}dt \tag{2.76}$$

$$= \frac{1}{T}\int_0^T e^{i(n-m)\omega t}H_{\beta\alpha}(t)dt + n\hbar\omega\delta_{\beta\alpha}\delta_{nm} \tag{2.77}$$

Introducing the Fourier decomposition of the matrix elements of the system Hamiltonian, $H_{\beta\alpha}(t)$,

$$H_{\beta\alpha}(t) = \sum_{k=-\infty}^{\infty} H_{\beta\alpha}^{(k)} e^{ik\omega t} \tag{2.78}$$

one finally arrives to:

$$\langle \beta m|\mathcal{H}_F|\alpha n\rangle = H_{\beta\alpha}^{(n-m)} + n\hbar\omega\delta_{\beta\alpha}\delta_{nm} \tag{2.79}$$

Although there are several methods to solve the eigenvalue equation 2.75, the most direct consists of a diagonalization of the Floquet Hamiltonian matrix in the basis 2.71, whose elements are given by 2.79, in terms of the Fourier components $H_{\beta\alpha}^{(k)}$ of the original periodic Hamiltonian of the problem. It is important to stress here that $\mathcal{H}_F$ is of infinite dimensionality and thus it must be truncated in some value k.

The natural strategy for the solution of the Floquet equations in the context of transport problems is based on the computation of the Green's functions. Starting from the fundamental equation 2.75, the retarded Green's function can be defined as usual,

$$G_F = \left[\varepsilon_\alpha \hat{I} - \hat{H}_F\right]^{-1} \tag{2.80}$$

Some useful relations for the retarded Green's function of the system can be obtained from the formal definition

$$G(t,t') = -\frac{i}{\hbar} U(t,t')\Theta(t-t') \tag{2.81}$$

in which $U(t,t')$ is the time evolution operator of the system, defined by:

$$|\Psi(t)\rangle = U(t,t')|\Psi(t')\rangle, \quad U(t',t') = 1 \tag{2.82}$$

where $|\Psi(t)\rangle$ is the entire wave function of the system, given by the solution of Eq. 2.62. On the other hand, since the Floquet modes constitute (at equal times) an orthonormal basis,

$$\langle \phi_\alpha^\dagger(t)|\phi_\beta(t)\rangle = \delta_{\alpha,\beta}, \quad \sum_\alpha |\phi_\alpha(t)\rangle\langle\phi_\alpha^\dagger(t)| = 1 \tag{2.83}$$

the evolution operator can be written as:

$$U(t,t') = \sum_\alpha e^{-i\varepsilon_\alpha(t-t')}|\phi_\alpha(t)\rangle\langle\phi_\alpha(t')| \tag{2.84}$$

This last equation can be verified immediately noting that, due to the equation 2.63, the right hand side term of this expression satisfies the original differential equation in 2.62. Using this, we have

$$U_{\beta\alpha}(t,t_0) = \sum_m \sum_\alpha \langle \beta m|\phi_\alpha(t)\rangle e^{-i\varepsilon_\alpha(t-t_0)}\langle\phi_\alpha(t)|\alpha n\rangle e^{i(n-m)\omega t} \tag{2.85}$$

$$= \sum_m \langle \beta m|e^{-i\mathcal{H}_F(t-t_0)}|\alpha n\rangle e^{i(m-n)\omega t} \tag{2.86}$$

Therefore, and following J. Shirley [Shi65], $U_{\beta\alpha}(t,t_0)$ represents the amplitude for the evolution of the system under the influence of a periodic Hamiltonian $H(t)$ from the initial state $|\alpha\rangle$ at time t_0 to a state $|\beta\rangle$ at time t. This can be also interpreted as the amplitude for the evolution of an initial Floquet state $|\alpha n\rangle$ at time t_0 to a final Floquet state $|\beta m\rangle$ at time t due to a *time-independent Floquet Hamiltonian* $\mathcal{H}_F$, summing over m with weighting factors $e^{i(m-n)\omega t}$.

The essence of Floquet theory, thus, is that with the last interpretation of Eq. 2.86, problems involving time-dependent periodic Hamiltonians can be resolved using methods applicable to time-independent Hamiltonians.

With the relation 2.81, in terms of the basis 2.68 in the Hilbert space $\mathbb{R}$,

$$G_{\beta\alpha}(t,\varepsilon) = -\frac{i}{\hbar}\int_{o}^{\infty} d\tau e^{i\varepsilon\tau/\hbar} U_{\beta\alpha}(t,t-\tau) \tag{2.87}$$

using the expression 2.86 for $U_{\beta\alpha}(t-\tau)$, and integrating over τ one obtains [Tor05]:

$$G_{\beta\alpha}(t,\varepsilon) = \sum_{k=-\infty}^{\infty} \langle \beta k | \left[\varepsilon \hat{I} - \hat{\mathcal{H}}_F\right]^{-1} |\alpha 0\rangle e^{ik\omega t}. \tag{2.88}$$

his expression shows the relation between the Floquet Green's function and the Green's functions of the original problem. The coefficients of the exponential factors can be interpreted as the Fourier coefficients in the expansion of $G_{\beta\alpha}(t,\varepsilon)$,

$$G_{\beta\alpha}(t,\varepsilon) = \sum_{k=-\infty}^{\infty} G^{(k)}_{\beta\alpha} e^{ik\omega t} \tag{2.89}$$

$$G^{(k)}_{\beta\alpha}(\varepsilon) = \tfrac{1}{T}\int_{0}^{T} dt e^{-ik\omega t} G_{\beta\alpha}(t,\varepsilon) \tag{2.90}$$

2.4.3 Average DC currents in Floquet systems

Finally, for the sake of simplicity, we consider a one-dimensional molecular system under the influence of a periodic time-dependent potential. The fundamental aspects of the physics involved can be accounted, as in the other sections of this chapter, in a one-electron picture where transport is considered as a coherent processes and, influences such as electron-electron interaction, dissipation, etc, are neglected [KLH05b]. The system Hamiltonian is described, as usual, in the form:

$$\hat{H}(t) = \hat{H}_s(t) + \hat{H}_{leads} + \hat{H}_{contactos} \tag{2.91}$$

where different terms on the right hand side of the last equation correspond, respectively, to the leads (L and R) and the coupling to this leads. In terms of the creation and destruction operators, the tight-binding formulation for a

one-dimensional molecular system with N sites can be written as:

$$\hat{H}_s(t) = \sum_{\alpha=1,\beta=1}^{N} H_{\alpha\beta}(t)\hat{c}_\beta^\dagger \hat{c}_\alpha \tag{2.92}$$

Note that in the absence of the periodic potential, the direct diagonalization of the Hamiltonian leads to the stationary eigenvalues, energy levels, of the molecular wire. The influence of an AC applied external field with frequency $\omega = 2\pi/T$ results in a periodic time-dependence of the Hamiltonian: $H_{\beta\alpha}(t + T) = H_{\beta\alpha}(t)$.

Contributions of the leads to the complete Hamiltonian and its couplings with the system are given by:

$$\hat{H}_{leads} = \sum_m E_m \left(\hat{c}_{Lm}^\dagger \hat{c}_{Lm} + \hat{c}_{Rm}^\dagger \hat{c}_{Rm}\right) \tag{2.93}$$

$$\hat{H}_{contactos} = \sum_m E_m \left(\hat{c}_{Lm}^\dagger \hat{c}_1 + \hat{c}_{Rm}^\dagger \hat{c}_N\right) + h.c. \tag{2.94}$$

where the operators $\hat{c}_{Lq}^\dagger$ ($\hat{c}_{Rq}^\dagger$) create an electron in the state $|Lm\rangle$ ($|Lm\rangle$) in the lead L (R). Contacts to the L and R leads are attached at the sites 1 and N respectively.

If the leads L and R are characterized, respectively, by the occupations f_L and f_R, it can be proved that the average current over a period is given by [KLH05b]:

$$\overline{I} = \frac{e}{h} \sum_{k=-\infty}^{\infty} \int d\varepsilon \left\{T_{LR}^{(k)}(\varepsilon) f_R(\varepsilon) - T_{RL}^{(k)}(\varepsilon) f_L(\varepsilon)\right\} \tag{2.95}$$

where Floquet transmission functions are given in terms of the Green-Floquet functions of Eq. 2.89, as:

$$T_{LR}^{(k)}(\varepsilon) = \Gamma_L(\varepsilon + k\hbar\omega)\Gamma_R(\varepsilon) \left|G_{1N}^{(k)}(\varepsilon)\right|^2 \tag{2.96}$$

$$T_{RL}^{(k)}(\varepsilon) = \Gamma_R(\varepsilon + k\hbar\omega)\Gamma_L(\varepsilon) \left|G_{N1}^{(k)}(\varepsilon)\right|^2 \tag{2.97}$$

The transmission functions $T_{LR}^{(k)}$ and $T_{RL}^{(k)}$ represent the probabilities that an electron can be transmitted from one lead to the other, absorbing (emitting) $|k|$ photons if $k > 0$ ($k < 0$).

In a static situation, the transmission probabilities $T_{LR}^{(k)}$ and $T_{RL}^{(k)}$ are identical and the contributions with $k \neq 0$ vanish. For this case, is possible to write Eq. 2.95 as the product of a unique transmission function $T(\varepsilon)$, independent

of the direction of the electron path, and the difference between the Fermi distribution functions $f_R(\epsilon) - f_L(\varepsilon)$. In tis way, the best known expression for the current is obtained.

3

Decoherence in quantum transport

Environmental degrees of freedom might play a crucial role in the nanoscale, where the presence of both, classical and quantum behavior is expected [PH08, RMK+09]. The interaction of a quantum system with its environment is reflected as a change in its dynamical behavior. Common system-environment interactions appear similarly to an indirect measure on the open system, leading to a collapse of the system wave function. Generally, the effect of decoherence on quantum transport is expected to be negative, with inhibitory effect on constructive interference of quantum waves propagation. Although electronic coherent quantum transport in disordered materials leads to destructive interference of electron wave function, and therefore to its localization, the role of decoherence in disordered systems might be crucial [CBMP10], since decoherent events are able to suppress interferences, which in this kind of systems are destructive. In this case, this can be reflected as increased quantum transport efficiency due to system-environment interactions. Destruction of quantum coherence due to dephasing effects of the interaction with the environment might lead to an enhancement of transport excitations.

Nowadays the term *decoherence* is mostly used in connection with quantum information theory, where it denotes the (full or partial) collapse of a pure quantum state due to usually unspecified interactions with the environment. This might seem different from the usual language of electronic transport in

the solid state. There, it is common to deal with specific interactions, such as those with phonons, magnetic impurities or other electrons, which may involve transitions with given selection rules, e.g. $|k\rangle \rightarrow |k+q\rangle$. These transition probabilities are evaluated within a Fermi Golden Rule (FGR). In this approximation, the coupling with the extra degrees of freedom, the environment, prevents the interference among the component remaining in $|k\rangle$ with that in $|k+q\rangle$. Thus, with some probability the environment "measures" an electron in the state $|k\rangle$ and "re-injects" it incoherently in $|k+q\rangle$. These processes, which usually involve some inelasticity, are inherently different from the elastic scattering with imperfections and impurities that produce the interferences leading to localization [And78]. Quite often one realizes that, regardless of the specific selection rule, the relevant role of interactions is just to provide for decoherence, a mechanism that competes with the coherent scattering that results in localization. This is precisely the spirit of the "local phonon" bath or the fictitious voltage probes that lead to the imaginary site energies introduced in the D'Amato-Pastawski model [Pas91, Pas92]. Thus, the idea is that decoherence from the system-environment interaction might provide a knob that sweeps transport between a Mott's variable range hopping regime and a typical metal [Pas91, BAA06].

3.1 Environment-induced decoherence

The quantum world is described by essentially arbitrary linear superpositions of states. Schrödinger's cats can be thought of being in a superposition of alive and dead "states" at the same time before the "measurement" is accomplished. However, our perception of "classical" states in the macroscopic world is a comparatively small subset of the states allowed by the quantum mechanical superposition principle. A cat in the limbo is a bizarre concept from the point of view of the "classical" intuition. The question of why and how our experience of a classical world emerges from quantum mechanics thus lies at the heart of the foundational problems of quantum theory [Sch05]. Decoherence provides an explanation for this quantum-to-classical transition. The key insight of decoherence is that realistic quantum systems are never isolated, but are immersed in a surrounding environment and interact continuously with it.

The decoherence problem involves the study, within the standard quantum formalism, of the resulting formation of quantum correlations between the states of the system and its environment. Often, surprising effects result of these system-environment interactions [Sch05]. Decoherence, therefore, is the natural mechanism by which the classical world emerges out of the quantum world. It somehow determines a sort of quantum-classical boundary, as illustrated by the catching picture (shown below as Fig. 3.1) in a work by W. Zurek [Zur03].

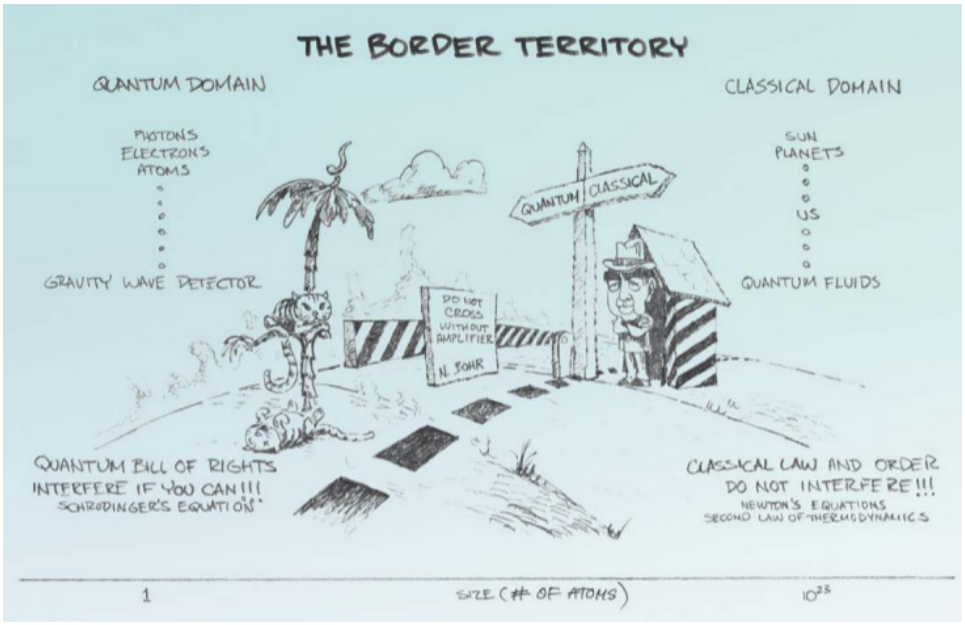

Figure 3.1: *"The border territory", a catching illustration of the boundary between the quantum and the classical world, in a work by W. Zurek [Zur03].*

The assumption of the possibility of a division into "systems" and "environment" is implied in the approach to the study of quantum decoherence [Sch05]. The environmental component of the problem can be usually understood as composed by the degrees of freedom that are typically not controlled and are not *directly* relevant to the observation under consideration. The presence of a quantum environment, requires the solution of the dynamics of open systems. In the previous chapter, specially in sections 2.2.3-2.2.5, the discussion of the transport problem involves a general system where a sample conductor is attached with two semi-infinite ordered chains that represent the leads. The topology involved, therefore, corresponds to an infinite array of discrete linked

sites, each of which being associated to an orbital electron state within the tight-binding approximation. However, by virtue of the decimation procedures discussed there, this infinite system was *reduced* to an *effective* finite system, where the site energies of the sample conductor were renormalized by the presence of the leads. A crucial characteristic is that due to the infinite nature of the leads, we obtained an effective energy with an *imaginary* component. In the dynamics, this should manifest as a progressive decay of an initial state within the reduced system. This means that the probability escapes towards the semi-infinite chains. Hence, an electron originally localized in the conductor should eventually escape or decay toward the lead, leaving the sample. The ordered nature and the infiniteness of the tight-binding chain representing the lead, ensures that an electron escaping toward it can not go back into the sample. The physical meaning of the imaginary part that we introduced as the self-energy is now evident: it represents the interaction with an environment [Pas07].

Although the role of the environment is played by usually unspecified interactions, sometimes the most relevant sources of dephasing events for the transport problem can be properly identified, as electron-phonon couplings, electron-electron interactions, inter-chain couplings, etc, and an explicit form for the imaginary energy shift is evaluated through the FGR. The key insight was given by D'Amato and Pastawski [DP90] who, extending an idea of Büttiker [B$\ddot{8}$6b], realized that the escape to an environment is equivalent to a escape to a chain which could act as a voltmeter. As an actual voltmeter, however, it should not extract net particles from the system, so it returns a particle for each one collected. Hence, for every process of "escape" from the coherent beam due to the interaction with the environment, a fresh incoherent particle must be re-injected into the system [Pas07]. This physical picture finds its formal justification when the system-environment interactions are local and the environment spectrum is so broad that it becomes instantaneous and energy independent [Pas07].

3.2 Phenomenology of decoherent events

Because of the restrictions of the *coherent* electronic transport, many experimental situations present important departures from the predictions made throughout the previous introductory chapter. In spite of this, the simplicity of Landauer's picture and the ease of its computational implementation allowed a remarkable expansion of the use of these methods for the calculation of conductance in a wide range of materials. However, perhaps its limitations are not always well understood and nowadays there are many examples in which there is an attempt to apply this simpler coherent treatment improperly. In part this is due to the fact that a proper generalized treatment of non-coherent transport requires a more general framework with increased conceptual complexity which, in most cases limits a straightforward applicability.

There are, however, certain wide applicable conditions under which the Landauer-Büttiker approach can be readily extended to treat non-coherent quantum transport, keeping intact the ease of implementation that characterizes this approach. This section is devoted to elucidate this fundamental conditions by means of a simple phenomenological insight to the problem of decoherence in quantum transport.

3.2.1 Büttiker probes.

While accepting a quantum description of their spectra and their ability to propagate excitations, the leads are the ultimate source of irreversibly and decoherence [PM01]. Electrons leaving the leads toward the sample are completely incoherent with the electrons coming from the other leads. As observed by Büttiker [B$\ddot{8}$6b, B$\ddot{8}$8], a voltage probe, which detects electron density without absorbing of emitting any, acts as a phase-breaking scatterer, as any other quantum measurement apparatus, and provides a natural source of decoherence. Such a voltage probe can be readily described in the Landauer's picture if one uses the Kirchhoff balance equations and ensures that no net current flows towards it. This can be easily understood by considering the current flow from terminal L to R in a device having a voltage probe (or voltmeter) in between, as the one depicted in Fig. 3.2. In this structure, the net current flows with two components. In the coherent one, electrons go directly from L

to R bypassing the voltage probe entirely. The other component to the net current involves electrons that go from L to the probe ϕ and have their phases randomized before they are re-injected incoherently into the device.

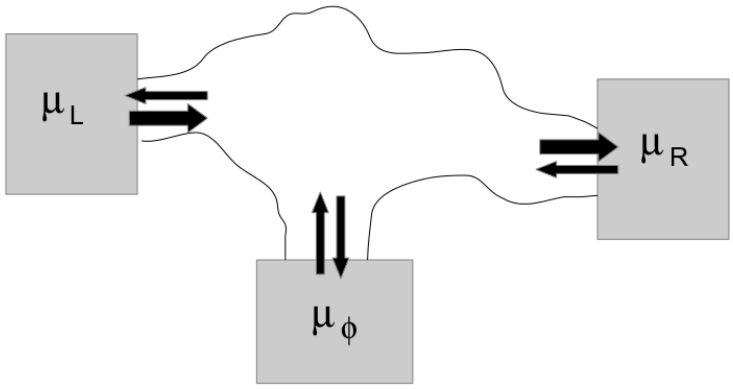

Figure 3.2: *Representation of a three probe measurement. A voltage probe in between floats to an appropriate potential ensuring no net current through it.*

The presence of a voltage probe thus introduces an incoherent component to the overall current flow from L to R, acting as a phase-scatterer. Therefore, phase-braking scatterers can be modeled by *fictitious* voltage probes. There are, however, some important considerations that follow from the simple example considered. The current in such a structure follows from Eq. 2.11, and can be described in the from [Dat97]:

$$i_R(\varepsilon) = \frac{2e}{h} T_{RL}(\varepsilon)\left[f_R(\varepsilon) - f_L(\varepsilon)\right] + \frac{2e}{h} T_{R\phi}\left[f_R(\varepsilon) - f_\phi(\varepsilon)\right] \tag{3.1}$$

and the current at the fictitious probe is given by:

$$i_\phi(\varepsilon) = \frac{2e}{h} \sum_{n=R,L} T_{\phi n}(\varepsilon)\left[f_\phi(\varepsilon) - f_n(\varepsilon)\right] \tag{3.2}$$

Using the last equation, the distribution function at the fictitious probe is easily isolated,

$$f_\phi(\varepsilon) = \frac{1}{T_{\phi R} + T_{\phi L}} \left[i_\phi \frac{h}{2e} + \sum_{n=R,L} T_{\phi n}(\varepsilon) f_n(\varepsilon) \right] \tag{3.3}$$

Substituting this expression into Eq. 3.1 we obtain an expression for the current in the structure in terms of an *effective* transmission where the phase-braking

probe have been *decimated*,

$$i_R(\varepsilon) = \frac{2e}{h}\tilde{T}_{RL}(\varepsilon)\left[f_R(\varepsilon) - f_L(\varepsilon)\right] - \frac{2e}{h}\left[\frac{T_{R\phi}}{T_{\phi R} + T_{\phi L}}\right] i_\phi(\varepsilon) \tag{3.4}$$

and the effective transmission between terminals L and R is given by:

$$\tilde{T}_{RL} = T_{RL} + \frac{T_{R\phi}T_{\phi L}}{T_{R\phi} + T_{\phi L}} \tag{3.5}$$

The next step, therefore, is to apply the *voltmeter* condition on the Büttiker probe ensuring that no net current flows through it, $\int i_\phi(\varepsilon)d\varepsilon = 0$, and we get a *generalized* Landauer-Büttiker equation for the current which looks just like the original,

$$I = \frac{2e}{h}\int \tilde{T}_{RL}(\varepsilon)\left[f_R(\varepsilon) - f_L(\varepsilon)\right] d\varepsilon \tag{3.6}$$

except for the *effective* transmission that comes from the decimation of the voltage probe.

In this approach the Landauer's picture is nicely extended to account for decoherence in a very intuitive manner, but it has some drawbacks. To understand it properly we shall look closer at the Büttiker condition:

$$0 = \int i_\phi(\varepsilon)d\varepsilon = \frac{2e}{h}\sum_{n=R,L}\int T_{\phi n}(\varepsilon)\left[f_\phi(\varepsilon) - f_n(\varepsilon)\right] d\varepsilon \tag{3.7}$$

Note that the chemical potential at real leads are given while the chemical potentials at the probes must be evaluated self-consistently through the functions f_ϕ which depend on i_ϕ itself. The integral expression complicates enormously the computational approach to this self-consistent equation in which every energy ε participates in all relevant available energy channels. Also, this current per unit energy $i_\phi(\varepsilon)$ of the voltage probes may depend on the Fermi functions in the real contacts in a complicated manner due to the *exclusion principle*.

3.2.2 Decoherence and the exclusion principle

Throughout the first chapter, the question regarding how the Pauli exclusion principle affects the reviewed current expressions was not considered in the discussion. As suggested by Landauer [Lan92], the absence of the Pauli blocking factors $(1 - f)$ can be understood recurring to a simple thought. A typical transition from a *local state* 1 to another *local state* 2 involves a term which is proportional to the exclusion principle factors $f_1(1 - f_2)$, where f_1 and f_2

represent respective occupation probabilities. In the usual assumption, back and forth transitions are independent, and then the net transition rate between these states becomes proportional to:

$$f_1(1-f_2) - f_2(1-f_1) = f_1 - f_2 \tag{3.8}$$

That is, as stated by Landauer [Lan92], *the attention given to the Pauli principle disappears in the end.* However, the essence of Landauer's picture is that it is build in term of *scattering states.* Within a given reservoir, say L, only the occupation of the *outgoing states* (those with momentum k or simply "OUT") is fixed by temperature through f_L. The occupation of *ingoing states* (those with momentum -k or "IN"), are fixed by the occupations in the other reservoirs and the scattering process. This picture, shown in Fig. 3.3 remains valid in a multichannel and multiterminal description. The electronic current is carried by electrons that occupy single-particle transverse scattering states that extend across the conductor. Due that these scattering states are orthogonal

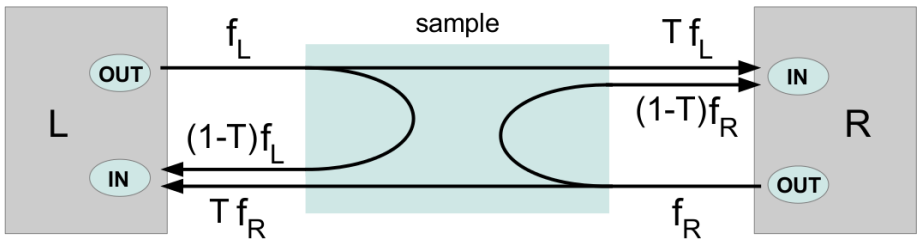

Figure 3.3: *A sketch for single-particle scattering states in Landauer's picture.*

to each other, an electron in one of these states does not compete with any of the other occupied scattering states. Thus, the Pauli exclusion principle for the final states in the scattering processes does not play a role in the determination of the electronic current even in the multi-channel scheme. With a little more attention this picture applies to situations where also vertical process are included [EK00].

Since the Büttiker insight for the introduction of inelastic events into the Landauer's picture of transport can be regarded as an extension of the coherent multi-terminal problem allowing, therefore, the treatment of decoherent transport in the same footing of coherent transport, at first glance it may seem that

we do not need any additional regard for the Pauli principle when dephasing is introduced. However, a closer look at the Büttiker's voltmeter condition,

$$0 = \int i_\phi(\varepsilon) d\varepsilon \tag{3.9}$$

shows that scattering processes introduced by the fictitious probes are allowed to take out electrons from one energy channel and re-inject them at any other energy. In these incoherent re-injections, the destination states can be occupied producing an "overflow" inconsistent with the exclusion principle. As pointed out by Datta [Dat97], the effect of the Pauli principle in these cases cannot be accounted for with a simple ad-hoc insertion of the blocking factors $(1-f)$, and a detailed microscopic theory is needed to compute the "vertical flow" of carriers between different energy channels. This is a limitation of the one-electron picture in which all the discussion so far was based. A proper description requires an advanced many-body formalism. When transport in a many-electron system is described in terms of one-electron scattering processes, the Pauli exclusion principle needs to be considered since in general electrons involved in different transitions may compete to occupy the same final state [EK00].

Although the Keldysh formalism provides a general and successful framework to deal with many-body interactions it is desirable to reduce it into a simple model where the role of decoherence results more evident. The key was provided by the D'Amato-Pastawski model, which is discussed in the following section. Here, we notice that, if all the multiple outgoing channels associated with "vertical flow" are consistently transformed into an energy conserving flow, the Pauli principle problem does not appear at all. It needs to be stressed that circumventing vertical flows explicitly might be somewhat restrictive for certain inelastic transport problems, but it is a valid strategy to deal with decoherence in electron states. The underlying idea of this approach is that, in several important systems, complex many-body interactions result in the loss of the simple interferences of a one-body description.

3.3 D'Amato-Pastawski model

The key insight of Büttiker proposal [B̈86b] that a voltage probe can be used to model *local* dephasing events within Landauer's picture was taken to a new level

by J. D'Amato and H. Pastawski [DP90]. They presented an alternative way to model the strength of dephasing events in order to examine the conductance of a one-dimensional system. A nearest neighbor tight-binding Hamiltonian is employed to simulate semi-infinite perfect wires attached to the sample. The idea is that these perfect lateral leads represent local couplings of environmental degrees of freedom with the sample, that can be treated within the Fermi Golden Rule approximation. In this way, the effect of local dephasing events is to introduce an imaginary part to the energy levels at the associated *sample sites*.

An important assumption, which is one of the keys of the powerful of the computational approach that this model involves, implies that local dephasing events at different Fermi energies are independent. Electrons "measured" by fictitious voltage probes randomize its phases but do not alter its energies. Decoherent events introduce energy uncertainties associated with imaginary shifts that only modify the site energies of the tight-binding Hamiltonian that is used to model the sample. In other words, after the decimation of the environmental degrees of freedom one is left with an *effective*, non-Hermitian, Hamiltonian with which Landauer conductances are computed and the restriction that no net current flows towards the fictitious voltages probes is imposed at every energy, $i_\phi(\varepsilon) = 0$. While this last condition is far more restrictive than Büttiker's, it has successfully proven to be sufficiently general and wide applicable for the introduction of decoherence into Landauer's picture of electronic transport.

3.3.1 Layout of the model

Consider a one-dimensional sample connected to two large contacts through the leads L and R. The D'Amato-Pastawski (DP) model refers to a simple way to account for the infinite degrees of freedom of the thermal bath or the electron reservoirs. The sample's Hamiltonian is described in a tight-binding approach,

$$\hat{H}_S = \sum_{i=1}^{N} \left(E_i \hat{c}_i^+ \hat{c}_i + \sum_{j>i}^{N} \left[V_{i,j} \hat{c}_i^+ \hat{c}_j + V_{j,i} \hat{c}_j^+ \hat{c}_i \right] \right) \tag{3.10}$$

where the labels i and j indicate sites on a lattice and N is the total number of sites. Notice that interactions are not restricted to nearest neighbors, however, for the usual short range interactions the Hamiltonian matrix has the advantage

of being sparse. As in Eq. 2.40, the leads are included as complex self-energies introduced at the sites in which they are attached to the sample,

$$\hat{\Sigma}_L = [\Delta_L(\varepsilon) - i\Gamma_L(\varepsilon)]\,\hat{c}_1^\dagger \hat{c}_1 \tag{3.11}$$

$$\hat{\Sigma}_R = [\Delta_R(\varepsilon) - i\Gamma_R(\varepsilon)]\,\hat{c}_N^\dagger \hat{c}_N \tag{3.12}$$

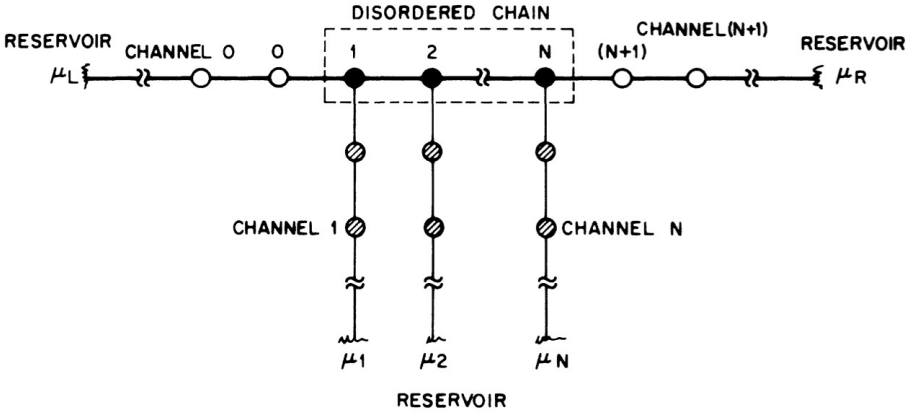

Figure 3.4: *A one-dimensional system attached to the L and R leads and later perfect chains that are used to simulate fictitious voltage probes. This figure was extracted from Ref. [DP90].*

Lateral leads are used to model fictitious voltage probes as semi-infinite ordered tight-binding chains attached to several sites on the sample. This is shown in Fig. 3.4. As in the case of the real leads, DP probes are included into the system Hamiltonian as self-energies that renormalize the energy of the sites to which they are attached. Denoting with E_ϕ and Γ_ϕ the site energies and hopping parameters of this lateral chains, and using Eqs. 2.31 and 2.32 we have

$$\Sigma_\phi = \frac{\varepsilon - E_\phi}{2} - i\sqrt{\Gamma_\phi^2 - \left(\frac{\varepsilon - E_\phi}{2}\right)^2} \tag{3.13}$$

where the sign of the imaginary part corresponds to the retarded Green's function. Looking this last equation one immediately sees that, adopting E_ϕ equal to the Fermi energy ε under study, the self energy becomes purely imaginary:

$$\Sigma_\phi = -i\Gamma_\phi \tag{3.14}$$

This is equivalent to requiring that the band center of the lateral leads should coincide with the Fermi energy of the system. By neglecting arbitrary real

corrections at every energy ε considered, the overall effect of these DP probes is controlled by one *real* parameter, Γ_ϕ. *However, notice the generality of the model in the sense that it can represent any interaction with the environment provided that it gives a finite lifetime to the electron state at a given site.*

Therefore, we include the effects of the incoherent processes in the Hamiltonian, e.g. electron-phonon or through space electron-electron interactions, simply through an imaginary correction to selected site energies. In this way, all local dephasing fields are represented by the terms

$$\hat{\Sigma}_\phi = \sum_l -\mathrm{i}\Gamma_\phi \hat{c}_l^+ \hat{c}_l. \tag{3.15}$$

The effective Hamiltonian of the system, thus, incorporates the self-energies associated with the leads and the interactions with the environment,

$$\hat{H}_{\text{eff.}} = \hat{H}_S + \hat{\Sigma}_L + \hat{\Sigma}_R + \hat{\Sigma}_\phi \tag{3.16}$$

The amount Γ_ϕ represents an energy uncertainty associated to a decay rate of the local state at site l described by the Fermi Golden Rule. An electron originally localized in the site l should eventually escape or decay toward the fictitious probe, since there is a escape rate associated with the finite lifetime introduced by the imaginary shift in the site, $\tau_l^{-1} = 2\Gamma_\phi/\hbar$. The on-site chemical potentials will ensure that no net current flows through fictitious channels and this is shown in the next section.

3.3.2 Solution for decoherent transport

We adopt the notation $\Gamma_L \equiv \Gamma_{L1}$, $\Gamma_R \equiv \Gamma_{RN}$, $\Gamma_\phi \equiv \Gamma_{\phi i}$, to emphasize that each site can decay through different processes, e.g. $\alpha, \beta \,\epsilon\, \{L, R, \phi\}$ are the possible decay processes taking place at sites $i, j \,\epsilon\, \{1, ..., N\}$. With this notation the generalized Fisher-Lee transmission probability can be expressed (as in Eq. 2.42):

$$T_{\alpha i,\beta j}(\varepsilon) = 2\Gamma_{\beta j}(\varepsilon) G^R_{j,i}(\varepsilon) 2\Gamma_{\alpha i}(\varepsilon) G^A_{i,j}(\varepsilon). \tag{3.17}$$

These transmission probabilities between fictitious and real leads can be computed in terms of the Green's function of the effective Hamiltonian, as discussed in section 2.2.4. Within the DP model current conservation is imposed at each

probe and energy ε. This requires an incoherent re-injection of every electron that has decayed due to the finite lifetimes introduced by the terms $\Gamma_{\phi i}$.

If linear response is invoked, the adimensional conductances are just the transmission probabilities. Thus, the electronic current associated with a process α on site i is given straightforward by the balance between in and out flow:

$$I_{\alpha i} = \frac{2e}{h} \sum_{\beta=L,\phi,R} \sum_{i,j=1}^{N} \left(T_{\alpha i \beta j} \mu_{\beta j} - T_{\beta j, \alpha i} \mu_{\alpha i} \right) \tag{3.18}$$

Defining the total transmission from each process as

$$(1/g_{\alpha i}) = \sum_{\beta=L,\phi,R} \sum_{i,j} T_{\beta j, \alpha i} \tag{3.19}$$

the balance equations for the currents become:

$$I_{\alpha i} = \frac{2e}{h} \left[-(1/g_{\alpha i}) \mu_{\alpha i} + \sum_{\beta=L,\phi,R} \sum_{i,j=1}^{N} T_{\alpha i \beta j} \mu_{\beta j} \right] \tag{3.20}$$

This set of equations can be written in a compact matrix notation:

$$\overrightarrow{I} = \frac{2e}{h} \mathbb{T} \overrightarrow{\mu} \tag{3.21}$$

where the matrix $\mathbb{T}$ is composed by all the relevant transmission (and reflexion) probabilities of the entire system, and is given by:

$$\mathbb{T} = \begin{pmatrix} T_{L1,L1} - 1/g_{L1} & T_{L1,RN} & T_{L1,\phi 1} & \dots & T_{L1,\phi N} \\ T_{RN,L1} & T_{RN,RN} - 1/g_{RN} & T_{RN,\phi 1} & \dots & T_{RN,\phi N} \\ \vdots & & & \dots & \\ T_{\phi N,L1} & T_{\phi N,RN} & T_{\phi N,\phi 1} & \dots & T_{\phi N,\phi N} - 1/g_{\phi N} \end{pmatrix}$$

The net current must be identically zero at any dephasing channel, $I_{\phi j} = 0 \ \ \forall_j$, and for the real leads we have $I = I_{RN} = -I_{L1}$. Since the net current only flows between real leads L and R, there must be an effective transmission amplitude between them that relates this net current I with the voltage drop $\mu_{L1} - \mu_{RN}$ in the usual form:

$$I = \frac{2e}{h} \tilde{T}_{RL} \left(\mu_{L1} - \mu_{RN} \right) \tag{3.22}$$

Notice that the last expression *defines* the effective transmission probability in this context. We solve the problem of finding an appropriate expression for

$\tilde{T}_{RL}$ in terms of the direct transmission probabilities $T_{\alpha i,\beta j}$ in two meaningful complementary ways.

To obtain the first expression for the effective transmission, we refer all voltages to the one on the right lead, $\delta\mu_{\beta j} = \mu_{\beta j} - \mu_{RN}$ so $\delta\mu_{RN} = 0$. The Eq. 3.20 can be written in matrix notation, and after taking $\delta\mu_{RN} = 0$ the relevant equation looks like:

$$\begin{pmatrix} -I \\ 0 \\ \vdots \\ 0 \end{pmatrix} = \frac{2e}{h}\overline{\mathbb{T}} \begin{pmatrix} \delta\mu_{L1} \\ \delta\mu_{\phi 1} \\ \vdots \\ \delta\mu_{\phi N} \end{pmatrix} \tag{3.23}$$

where the over-line in $\overline{\mathbb{T}}$ is a reminder that this is not the complete transmissions matrix, since we eliminate the row and the column related to $\alpha = R, i = N$ when $\delta\mu_{RN} = 0$ in Eq. 3.20. The effective transmission is easy to obtain after the last expression, since

$$\overline{\mathbb{T}}^{-1} \begin{pmatrix} -I \\ 0 \\ \vdots \\ 0 \end{pmatrix} = \frac{2e}{h} \begin{pmatrix} \delta\mu_{L1} \\ \delta\mu_{\phi 1} \\ \vdots \\ \delta\mu_{\phi N} \end{pmatrix} \tag{3.24}$$

and this implies:

$$-\left[\overline{\mathbb{T}}^{-1}\right]_{L1,L1} I = \frac{2e}{h}\delta\mu_{L1} \tag{3.25}$$

which finally leads to a solution to the effective transmission probability through the sample:

$$\tilde{T}_{RL} = \frac{-1}{\left[\overline{\mathbb{T}}^{-1}\right]_{L1,L1}} \tag{3.26}$$

The last equation shows that the effective transmission probability is directly related to only one element of the inverse of the matrix $\overline{\mathbb{T}}$. This expression for the effective transmission is better suited for the computational approach (as discussed in section 3.3.3) but the following gives a better insight of its nature.

To obtain the second expression for $\tilde{T}_{RL}$, consider Eq. 3.21 in terms of the complete matrix $\mathbb{T}$ in the form:

$$\begin{pmatrix} -I \\ I \\ 0 \end{pmatrix} = \frac{2e}{h} \begin{pmatrix} T_{L1,L1} - 1/g_{L1} & T_{L1,RN} & \overrightarrow{T}_{L1,\phi} \\ T_{RN,L1} & T_{RN,RN} - 1/g_{RN} & \overrightarrow{T}_{RN,\phi} \\ \overrightarrow{T}_{\phi,L1} & \overrightarrow{T}_{\phi,RN} & \mathbb{T}_{\phi\phi} \end{pmatrix} \begin{pmatrix} \delta\mu_{L1} \\ 0 \\ \delta\overrightarrow{\mu}_{\phi} \end{pmatrix} \tag{3.27}$$

In this matrix representation of $\mathbb{T}$ we have separated explicitly the contributions that involve real leads from the contributions that only relate fictitious probes: the block $\mathbb{T}_{\phi\phi}$. This sub-matrix has the same structure of $\mathbb{T}$ but only includes transmission probabilities between fictitious leads. The equations associated to the second and third rows of the last matrix expression are:

$$\frac{h}{2e}I = T_{RN,L1}\delta\mu_{L1} + \overrightarrow{T}_{RN,\phi}\cdot\delta\overrightarrow{\mu}_{\phi} \tag{3.28}$$

$$0 = \overrightarrow{T}_{\phi,L1}\delta\mu_{L1} + \mathbb{T}_{\phi,\phi}\delta\overrightarrow{\mu}_{\phi} \tag{3.29}$$

From the last one we have

$$\delta\overrightarrow{\mu}_{\phi} = \mathbb{T}^{-1}_{\phi\phi}\overrightarrow{T}_{\phi,L1}\delta\mu_{L1} \tag{3.30}$$

using this equation to replace $\overrightarrow{\mu}_{\phi}$ on Eq. 3.28, we arrive to:

$$I = \frac{2e}{h}\left(T_{RN,L1} + \overrightarrow{T}_{RN,\phi}\mathbb{T}^{-1}_{\phi\phi}\overrightarrow{T}_{\phi,L1}\right)\delta\mu_{L1} \tag{3.31}$$

Therefore, the effective transmission can be finally expressed as:

$$\tilde{T}_{RL} = T_{RN,L1} + \sum_{i,j=1}^{N} T_{RN,\phi i}\left[\mathbb{T}^{-1}_{\phi\phi}\right]_{i,j} T_{\phi j,L1} \tag{3.32}$$

The right hand side of Eq. 3.32 contains two contributions: the first one represents electrons that propagate coherently through the sample, the second term contains the incoherent contributions due to electrons that suffer their first collision at site i and their last collision at site j.

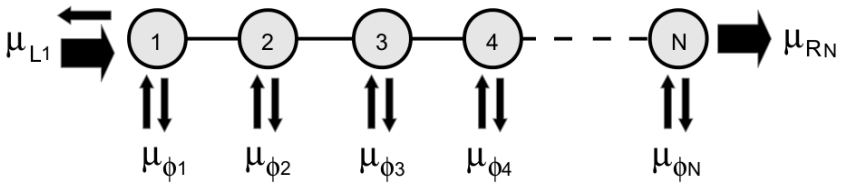

Figure 3.5: *Final layout of the D'Amato-Pastawski model in the case of a linear chain.*

The final layout of the DP model is depicted on Fig. 3.5. This model was designed as a simple analytical solution for various situations ranging from tunneling to ballistic transport. The procedure introduced in the DP model can be summarized as follows:

- The self-energies after the decimation of the environmental degrees of freedom are accounted by the introduction of imaginary shifts to the site energies of the tight-binding representation of the sample. An *effective* Hamiltonian is obtained.

- The matrix elements of the retarded Green's function (associated to the effective Hamiltonian of the system) between sites connected to real and fictitious probes are calculated.

- By means of the Fisher-Lee formula, the direct transmission probabilities between all sites attached to real or fictitious probes are computed.

- The effective transmission probability $\tilde{T}_{RL}$ is obtained in terms of the direct transmission probabilities using Eq. 3.26 or Eq. 3.32.

Finally, since $\widetilde{T}(\varepsilon)$ piles up all vertical processes into the energy ε, one can approximate the net current through the sample by:

$$\mathrm{I} = \frac{2e}{h}\int \widetilde{T}_{RL}(\varepsilon)[f_L(\varepsilon) - f_R(\varepsilon)]\mathrm{d}\varepsilon \tag{3.33}$$

$$\simeq \frac{2e^2}{h}\widetilde{T}_{RL}(\varepsilon_F)\mathrm{V} \equiv \mathrm{GV}, \tag{3.34}$$

where $f_{R(L)}$ is the Fermi distribution function at the right (left) lead and the factor 2 accounts for spin degeneracy. Here, we assumed that an electron with energy ε coming from the left lead arrives to the right lead with the same energy, which is only true for very small Γ_ϕ. The second line is the linear approximation for infinitesimal voltage `V` and temperature, where G accounts for conductance.

3.3.3 Basic strategies for the computational approach

The two-probe Landauer conductance requires the computation of only one element of the Green's function matrix of the effective Hamiltonian of the system, the element that connect the sites to which the leads are attached. In the most frequent case, the element G_{1N} (where N is the number of sites of the system). However, the DP model adds up to the problem a given number of fictitious probes and the extra amount of elements of the Green's function matrix that need to be computed scales roughly as $M(M-1)/2$, where $M \leq$

N is the number of phase-breaking probes. Furthermore, once that all the transmission functions between every pair of leads is obtained, the computation of the effective transmission requires the inversion of a $M \times M$ matrix, $\mathbb{T}_{\phi\phi}$, since it is usually expressed as in Eq. 3.32. The computational approach to the DP model, thus, must be based in efficient algorithms and the aim of this section is to give some guidelines.

As mentioned in section 2.2.4, any element G_{ij} of the Green's function matrix can be obtained from decimation procedures as:

$$\begin{aligned} G_{ii} &= \frac{1}{[\varepsilon - E_i - \Sigma_{i,1} - \Sigma_{i,j}]} \\ G_{ij} &= \frac{\overline{V}_{ij}}{\left[(\varepsilon - E_i - \Sigma_{1,i} - \Sigma_{i,j})\,(\varepsilon - E_i - \Sigma_{j,i} - \Sigma_{j,N}) - \overline{V}_{ij}\overline{V}_{ij}\right]} \end{aligned} \tag{3.35}$$

where it is assumed that $i < j$. There are, hence, four self-energies that must be computed for every non-diagonal element: $\Sigma_{1,i}$, $\Sigma_{i,j}$, $\Sigma_{j,i}$ and $\Sigma_{j,N}$. For the diagonal elements of the Green's function matrix, there are only two self-energies needed. We recall that these terms are obtained by the recursion equations given in section 2.2.2. The situation is illustrated on Fig. 3.6 for a 1D chain. As consequence, the computation of all the elements of the Green's

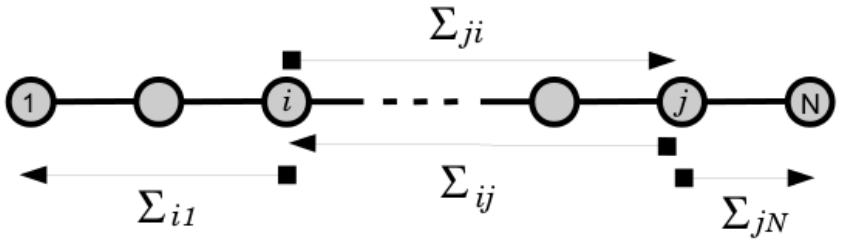

Figure 3.6: *Self-energies involved in the computation of the elements of the Green's function matrix.*

function matrix in the general case involves, roughly, $\sim N^2$ terms Σ's, assuming that $G_{ij} = G_{ji}$. However, there is a handy expression that involves $\sim 2N$ terms, which appeared for the first time in the context of transport (to our known) in an article by Thouless and Kirkpatrick [TK81], and applies when the Hamiltonian of the system can be expressed as a tridiagonal matrix. That is, in the case of a one-dimensional system with nearest neighbors interactions.

A generalization for quasi 1D systems is given on chapter 5. The elements of the Green's function can be written:

$$G_{ij} = G_{ii} \prod_{k=i}^{j-1} \Sigma_{k,N} V_{k+1,k}^{-1} \tag{3.36}$$

Notice that, in this way, non-diagonal are obtained through diagonal elements, and the only self-energy terms that appear in this equation are already needed for the computation of the diagonal terms, that is, Σ_{1i}'s and Σ_{iN}'s. Also, in this way it is no necessary to compute any effective hopping $\overline{V}_{ij}$. For tridiagonal Hamiltonians, therefore, the expression in Eq. 3.36 constitute the most efficient way to go for the computation of the Green's function matrix.

The other neuralgic point is the computation of the effective transmission probability function. Consider the diagonal elements of the matrix $\mathbb{T}$ defined in Eq. 3.21. These elements are not transmission, but reflexion probabilities. As shown in appendix A,

$$(1/g_{\alpha i}) = \sum_{\beta=L,R,\phi} \sum_{j=1}^{N} T_{\alpha i,\beta j} = 4\pi N_i \Gamma_{\alpha i} \tag{3.37}$$

where N_i is the local density of states at the site i. Therefore, using this expression we can write

$$\begin{aligned}
[\mathbb{T}]_{\alpha i,\alpha i} &= T_{\alpha i,\alpha i} - \sum_{\beta=L,R,\phi} \sum_{j=1}^{N} T_{\alpha i,\beta j} \\
&= 4\Gamma_{\alpha i,\alpha i}^2 |G_{ii}^R|^2 - 4\pi \Gamma_{\alpha i} N_i \\
&= 4\Gamma_{\alpha i,\alpha i}^2 |G_{ii}^R|^2 + 4\Gamma_{\alpha i} \mathrm{Im} G_{ii}^R \\
&= 4\Gamma_{\alpha i,\alpha i}^2 \left(\mathrm{Re} G_{ii}^R + \mathrm{Im} G_{ii}^R \right) + 4\Gamma_{\alpha i} \mathrm{Im} G_{ii}^R
\end{aligned} \tag{3.38}$$

and is easy to see that this finally leads to:

$$[\mathbb{T}]_{\alpha i,\alpha i} = |\mathrm{i}2\Gamma_{\alpha i} G_{ii}^R - 1|^2 - 1 \tag{3.39}$$

This expression relates each diagonal element of the transmission matrix with only one element of the Green's function.

In the previous section it is mentioned that the expression of Eq. 3.26 for the effective transmission is better suited for the computational approach. This equation relates the effective transmission with one element of the matrix

$\left[\overline{\mathbb{T}}\right]^{-1}$. With the help of the decimation procedures discussed in section 2.2.2, is possible to construct a recursion algorithm to obtain any element of a matrix inverse. In this case, we have

$$\overline{\overset{\sim}{\mathbb{T}}}^{(k)}_{ij} = \overline{\overset{\sim}{\mathbb{T}}}^{(k-1)}_{ij} - \frac{\overline{\overset{\sim}{\mathbb{T}}}^{(k-1)}_{i,k}\overline{\overset{\sim}{\mathbb{T}}}^{(k-1)}_{k,j}}{\overline{\overset{\sim}{\mathbb{T}}}^{(k-1)}_{k,k}} \tag{3.40}$$

where k runs over incoherent channels, $k \,\epsilon\, \{\phi 1 ... \phi N\}$ and $\overline{\overset{\sim}{\mathbb{T}}}^{(k)}_{ij}$ stands for the matrix element $i, j \,\epsilon\, \{L1...(k-1)\}$ of matrix $\overline{\mathbb{T}}$ after the decimation of k incoherent channels. If M is the number of fictitious probes, then all incoherent channels are decimated after M steps of this recursion and we have

$$\left[\overline{\mathbb{T}}^{-1}\right]_{L1,L1} = \left[\overline{\overset{\sim}{\mathbb{T}}}^{(M)}_{L1,L1}\right]^{-1} \tag{3.41}$$

and therefore the effective transmission $\tilde{T}_{RL}$ is given by,

$$\tilde{T}_{RL} = -\overline{\overset{\sim}{\mathbb{T}}}^{(M)}_{L1,L1} \tag{3.42}$$

Although the negative sign in the last expression might seem odd, we recall that in the $\mathbb{T}$ matrix sums over rows as well as over columns must be zero. Since all non diagonal elements are of the same sign, diagonal elements must have the opposite sign and this is reflected in the last expression. In this way, the effective transmission probability of the DP model can be understood as the coherent transmission T_{RL} renormalized by the presence of the fictitious leads.

We mention one final computational aspect that is described in much more detail in Ref. [PM01]. The idea is to expand the inverse matrix $\mathbb{T}^{-1}_{\phi\phi}$ of Eq. 3.32 in series in the dephasing collisions,

$$\tilde{T}_{RL} = T_{RN,L1} + \sum_i T_{RN,i\phi} g_{\phi i} T_{\phi i,L1} + \sum_i \sum_j T_{RN,i\phi} g_{\phi i} T_{\phi i,\phi j} g_{\phi j} T_{\phi j,L1} + ... \tag{3.43}$$

This expression constitutes the basis for a perturbative method of calculating the effective transmission probability.

3.3.4 Coarse-grained D'Amato-Pastawski model

As discussed in section 3.3.2, in order to obtain the decoherent transmission probability, the DP model requires the computation of all the direct transmissions $T_{\alpha i,\beta j}$ that involve every pair of (fictitious or real) leads. Furthermore, the block matrix $\mathbb{T}_{\phi\phi}$ that incorporates all the incoherent contributions, which is not sparse, must be inverted at the full computational cost. For large systems, this process requires large computational time since the dimension of this matrix can grow considerably. For overcoming this difficulty, a *coarse grained* version of DP model, the CGDP model, has been proposed by Daijiro Nozaki [NBMC$^+$].

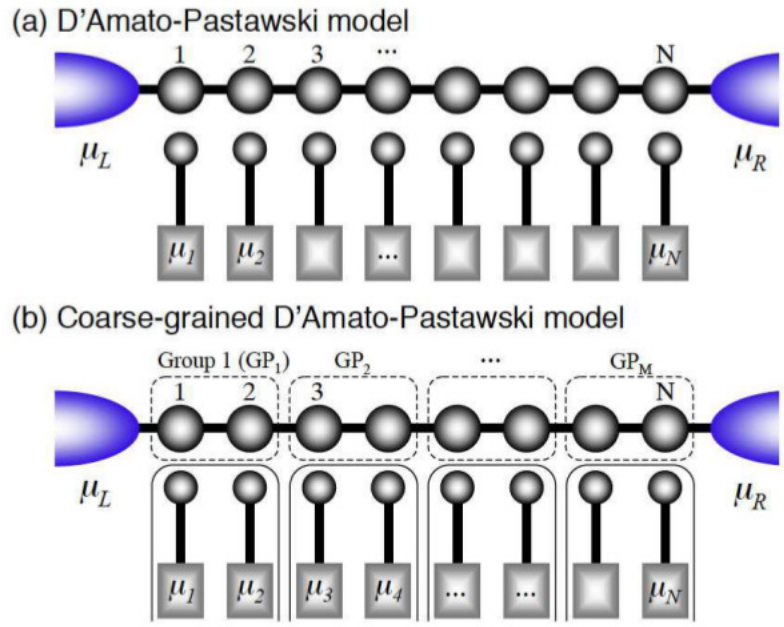

Figure 3.7: *Schematic representations of (a) D'Amato-Pastawski and (b) Coarse-Grained D'Amato-Pastawski models.*

In the CGDP approach, the fictitious leads of the DP model are considered by groups. Probes within the same group must share the chemical potential and the imposition of zero net current at fictitious probes is somehow relaxed. This condition can be bypassed by *single* dephasing probes, but must be satisfied by each group. The idea behind this "coarse grained" vision of the original DP model is to reduce the number of available incoherent channels forcing

contiguous sites to share them. A schematic representation of the CGDP and the DP models is shown in Fig. 3.7.

In the CGDP model, N fictitious probes are divided into M groups. Each of this groups is labeled as GP_X for $X = 1, ..., M$. Then, the condition of no net current at groups of fictitious probes can be expressed as:

$$0 = I_{GP_X} = \sum_{i \in GP_X} \left[-(1/g_{\phi i})\delta\mu_{\phi i} + \sum_{\beta j} T_{\phi i,\beta j}\delta\mu_{\beta j} \right] \tag{3.44}$$

and we have also the condition that each group share the chemical potential:

$$\delta\mu_{\phi i} = \delta\mu_{GP_X} \quad for \quad i \in GP_X \quad with \quad X = 1, ..., M \tag{3.45}$$

Although at first sight the notation may seem a little confusing, we are only adding summations over probes that share group. Therefore, the equivalent of the current balance equation of the DP model (Eq. 3.24), adopts the form:

$$\begin{pmatrix} -I \\ 0 \\ \vdots \\ 0 \end{pmatrix} = \frac{2e}{h}\widehat{\mathbb{T}} \begin{pmatrix} \delta\mu_{L1} \\ \delta\mu_{GP_1} \\ \vdots \\ \delta\mu_{GP_M} \end{pmatrix} \tag{3.46}$$

where we have chosen $\widehat{\mathbb{T}}$ for the notation of the transmission probabilities matrix of the CGDP model. The procedure used to obtain the decoherent transmission is exactly the same as the one discussed in section 3.3.2, through Eqs. 3.26 and 3.32, except that the elements of $\mathbb{T}$ are related to those of $\widehat{\mathbb{T}}$ by

$$\left[\widehat{\mathbb{T}}\right]_{XY} = \sum_{i \in GP_X} \sum_{j \in GP_Y} [\mathbb{T}]_{ij} \tag{3.47}$$

We can write, for example, the analogous of Eq. 3.32 for the CGDP model as:

$$\tilde{T}_{RL} = T_{RN,L1} + \sum_{i,j=1}^{N} T_{RN,\phi i} \left[\widehat{\mathbb{T}}_{\phi\phi}^{-1}\right]_{i,j} T_{\phi j,L1} \tag{3.48}$$

where $\widehat{\mathbb{T}}_{\phi\phi}$ represents the transmission probability matrix between groups of probes. This is the coarse-grained version of $\mathbb{T}_{\phi\phi}$ of Eq. 3.32. The advantage of this approximation, of course, is the reduction of the dimension of the matrix $\mathbb{T}_{\phi\phi}$ (from $N \times N$ to $M \times M$, $N > M$), which is the one that needs to be inverted.

The CGDP model can be an efficient estimate for the calculation of decoherent transport in weakly-coupled 1D systems. There are, as explained above,

two approximations involved in the CGDP model. On one hand, probes within the same group must share the same chemical potential. This is depicted in Fig. 3.8, for two tight-binding chains of 1000 sites, one ordered and the other with Anderson disorder, where the CGDP is obtained by grouping fictitious probes every 100 sites. The resulting chemical potential at each site is shown there. Since the overall potential drop does not change, the net linear response

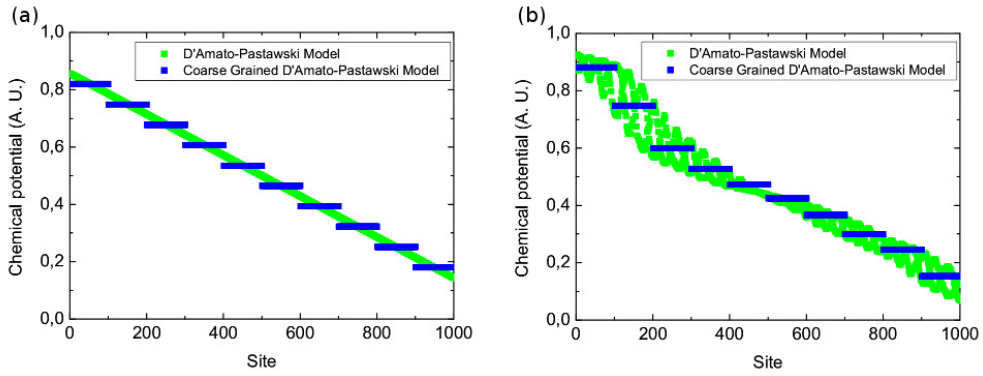

Figure 3.8: *Local chemical potentials for DP and CGDP models in a 1D chain of 1000 sites: (a) Ordered chain, (b) Chain with diagonal disorder,* $E_i \in [0, 1]$. *In both cases, CGDP is constructed with groups of 100 contiguous probes.*

current obtained should be exactly the same as the one given by the DP model. On the other hand, the condition of zero net current *by groups* of probes grant additional processes, and this is illustrated on Fig. 3.9. By allowing additional paths in this one-electron picture, the resulting total transmission probability in the CGDP scheme is higher. However, it should be noted that the magnitude of the hopping parameter toward the fictitious probes in most cases is not greater than $k_B T \sim 0.0258$eV, compared with $\sim$ 1eV of a typical coupling between two sites in a tight-binding chain.

The CGDP model provides and interesting alternative to the original DP model which under certain conditions gives an efficient approach to study of electron decoherent transport through large molecules. The effective conductance could be calculated efficiently reducing computational time considerably. This model would give an opportunity to investigate the fundamental charge transporting process through the nanostructures such as organic semiconducting devices and DNAs, where system dimensions are very large and

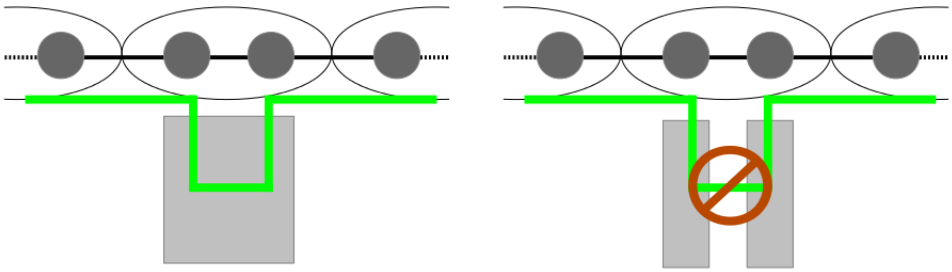

Figure 3.9: *The electron traveling process in (a) entering into external reservoir from one scattering probe and returning back to the molecular system from another probe is not allowed in the conventional DP model.*

dephasing effects play an important role. Anyway, the CGDP scheme grant processes not allowed in the original DP model, where the phase-breaking probes are *local*, and therefore can be thought as a different approach to the problem of decoherence in electronic transport.

3.4 Summary

Quantum ballistic transport can be experimentally observed in metallic molecular wires of nanometer lengths. Landauer's picture of electronic transport provides an elegant and accurate framework to understand and predict the nature of this behavior. However, there are important departures from these predictions which are the natural consequences of the limits of the coherent description. Phase breaking processes are, of course, increasingly important as the size of the system increases. In this way, environmental degrees of freedom might play a crucial role. The interaction of a quantum system with its environment is reflected as a change in its dynamical behavior. The effect of decoherence on quantum transport is usually expected to be negative, with inhibitory effect on constructive interference of quantum waves propagation. Although electronic coherent quantum transport in disordered materials leads to destructive interference of electron wave function, and therefore to its localization, the role of decoherence in disordered systems might be dramatic, since decoherent events are able to suppress interferences, which in this kind of systems are destructive. In this case, this is reflected as increased quantum transport efficiency due to system-environment interactions. Destruction

of quantum coherence due to dephasing effects of the interaction with the environment might lead to an enhancement of transport excitations. Therefore, the fundamentals of decoherent processes in transport and their consequences are currently of intense interest.

While accepting a quantum description of their spectra and their ability to propagate excitations, the leads are the ultimate source of irreversibly and decoherence in a typical transport problem. Electrons leaving the leads toward the sample are completely incoherent with the electrons coming from the other leads. The key insight of Büttiker proposal that a voltage probe can be used to model *local* dephasing events within Landauer's picture was taken to a new level by J. D'Amato and H. Pastawski. They presented an alternative way to model the strength of dephasing events in order to examine the conductance of a one-dimensional system. A nearest neighbor tight-binding Hamiltonian is employed to simulate semi-infinite perfect wires attached to the sample. The idea is that these perfect lateral leads represent local couplings of environmental degrees of freedom with the sample, that can be treated within the Fermi Golden Rule approximation. In this way, *the effect of local dephasing events is to introduce an imaginary part to the energy levels at the associated sample sites.* As an actual voltmeter, however, it should not extract net particles from the system, so it returns a particle for each one collected. Hence, for every process of "escape" from the coherent beam due to the interaction with the environment, a fresh incoherent particle must be re-injected into the system. This physical picture finds its formal justification when the system-environment interactions are local and the environment spectrum is so broad that it becomes instantaneous and energy independent.

The underlying idea of this approach is that, in several important systems, complex many-body interactions result in the loss of the simple interferences of a one-body description which is described by rate obtained from Fermi golden rule. Because of charge conservation, this rate should be formally equivalent to the coupling with a voltmeter. The consequence of this assumption is that after having evaluated a matrix with transmission amplitudes among every site in a sample, one still would need to evaluate its inverse. Despite of its recognized conceptual value, the DP strategy was rarely implemented, probably because of its seemingly computational cost. Thus the main majority

of the work to date ignored the role of inelasticity and decoherence even for those applications where coherent transport should be safely ruled out. In this Chapter, we developed the DP model to a degree where its efficiency is beyond doubt and implement clear algorithms that could enable its widespread implementation in the great variety of systems that require it. In this way, a new compact matricial notation was introduced allowing simple expressions for the quantities of interest, and the strategies for the computational implementation were discussed in extent. Furthermore, a new model which constitutes an approximation for the introduction of decoherence into electronic transport, the coarse-grained D'Amato-Pastawski model, was introduced.

4

On the nature of electronic transport in intrinsically conducting polymers: Polyaniline as a case study.

From the point of view of electronic materials, polymers are often considered uninteresting, since they are typically insulators. Although this might be true for saturated polymers, in which all the four carbon valence electrons are tied up in covalent bonds, in conjugated polymers the situation is completely different. In the latter case, the sp2p_z hybridization usually leads to one unpaired electron per carbon site. As a consequence the electronic structure is determined by the chain symmetry, from which the result is that in such polymers, electronic transport can be expected to exhibit semi-conducting or even metallic properties [HKSS88]. The electronic structure of polymers and molecules with conjugated orbitals can be conveniently described in terms of σ bonds formed by overlap of hybrid sp2 orbitals and p_z orbitals in adjacent carbons. This description allows an useful parametrization of the electronic properties in which the σ electrons provide the tight force for carbon bonds and the π electrons are described by tight-binding methods.

In the late 1970's, Alan MacDiarmid, Alan Heeger and Hideki Shirakawa led the investigations which put conducting polymers at the center stage by unraveling the transition from insulator to metal upon doping of polyacetylene

[Hee01a]. The following decades, these materials encountered numerous technological applications [FSWL07, Con85]. As stressed by MacDiarmid at the beginning of its Nobel lecture,

> 'An organic polymer that possesses the electrical, magnetic, and optical properties of a metal while retaining the mechanical properties, processability, etc. commonly associated with a conventional polymer, is termed an "intrinsically conducting polymer" (ICP), more commonly known as a "synthetic metal". Its properties are intrinsic to a doped form of the polymer. This class of polymer is completely different from "conducting polymers" which are merely a physical mixture of a non-conductive polymer with a conducting material such as a metal or carbon powder distributed throughout the material.'

Polyacetylene is a particularly important example, for, in this case, the π band is half-filled, implying the possibility of metallic conductivity. Because of the strong intra-chain bonding and weak inter-chain interactions, characteristic of such polymers, the π electrons are delocalized principally along the polymer chain. These systems are therefore electronically essentially one dimensional. The most successful model for this system was developed by Su, Schrieffer and Heeger (SSH) and involves a tight-binding scheme for the polymeric chain with cyclic boundary conditions and neglecting electron-electron interactions [SSH79]. The polymer chain is represented as a series of atom carbons, with σ bonds represented as an effective spring constant between neighbor atoms. The novelty of polyacetilene's physical properties, e.g. transport through solitonic excitations [SSH79], made it the most intensively studied conductive polymer. However, the interest then shifted to polyanilines [Hee01b] and related compounds because they are inexpensive, stable and easy to made.

The development of the field of conducting polymers has presented a strong fundamental scientific challenge, and a the variety of conducting polymers and their derivatives that have been discovered is huge. This field has been taken up by a diverse community of scientists, with importance to a cross-disciplinary section of researchers, chemists, electro-chemists, biochemists, experimental and theoretical physicists, and electronic and electrical engineers and to important technological emerging applications of these materials [Mac01].

4.1 Doping of conductive polymers

As emphatically remarked in their Nobel lectures by both, A. Heeger [Hee01a] and A. MacDiarmid [Mac01], the process of charge injection onto conjugated, semi-conducting macromolecular chains, commonly referred as "doping" by analogy with the doping of inorganic semiconductors, is the responsible for the wide variety of interesting and important features which distinguishes conducting polymers from all other types of polymers. This is an underlying central concept with an unifying role for the field of conductive polymers. During the doping process, an organic polymer, either an insulator or a semiconductor with small electrical conductivity, is taken to a "metallic" or conducting regime. There are dramatic changes in its electronic, magnetic, optical, and structural properties which are accomplished by the controlled addition of known, usually small non-stoichiometric quantities of chemical species. By adjusting arbitrarily the doping level, it is possible to control the electrical conductivity of polymers over the range from insulating (non-doped) to a highly conducting metallic state (fully doped).

Reversible charge injection by "doping" can be introduced in several of ways, among them by redox and acid-base chemistry. The redox doping involves the partial addition (reduction) or removal (oxidation) of electrons to or from the π system of the polymer backbone. Before the discovery of the protonation doping by acid-base chemistry of polyaniline, during which the number of electrons associated with the polymer chain does not change, the doping of all conducting polymers had previously been accomplished by redox doping [Mac01]. In the non redox doping of polyaniline, protonation by acid-base chemistry leads to an internal redox reaction and the conversion from semiconductor (the emeraldine base) to metal (the emeraldine salt).

The general hypothesis is that, in the doped state, the backbone of a conducting polymer consists of a delocalized π system. On the other hand, in the undoped state, the polymer may have a conjugated or a non-conjugated backbone. An example of the latter is polyaniline in its leuco-emeraldine base form, which becomes truly conjugated only after oxidation doping. In the emeraldine base form of polyaniline a non-conjugated structure becomes conjugated only after protonic acid doping.

4.2 Conjugated polymers and charged defects

The simplest conjugated polymer is trans-polyacetylene. Trans-polyacetylene band structure was modeled in early 1980's [Ric79, HKSS88]. The simplified structure of this compound is shown schematically on Fig. 4.1. Due to the fact that it has two geometric structures corresponding exactly to the same total energy, given by the two possible directions of bond alternations, it is known as a *degenerate ground state conjugated polymer*. In this case the carbon atoms are equidistant and form a perfect one dimensional array, with strong intra-chain bonding and weak inter-chain interactions. The π band, with one unpaired electron per carbon site, is half-filled. This implies that this material should behave as a 1D metal, with the π electrons principally delocalized along the polymer chain.

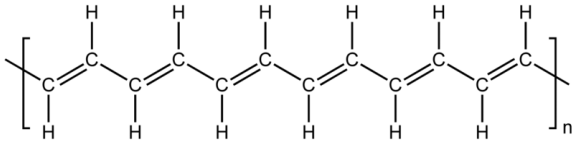

Figure 4.1: *Structure of trans-polyacetylene shown schematically.*

A theoretical observation due to Peierls [Pei55] states that a one dimensional equally spaced chain with one electron per ion is unstable. Atomic positions change so that the perfect order of the crystal lattice is broken. In other words, quasi-one dimensional metals tend to distort spontaneously and become semiconductors. When the band is half-filled, the tendency towards spontaneous symmetric breaking is particularly strong, and the distortion leads to a pairing of successive sites along the chain. This site pairing is known as "dimerization", and opens a gap in the Fermi surface lowering the energy of the occupied states and stabilizing the lattice distortion. The fundamental excitations of the polymer chain with a Peierls distortion and a half filled energy band are known as phase kinks, or solitons, in the bond alternation pattern of the polymer, as shown in Fig. 4.2. By adding electrons along the polymer backbone, by reduction doping, these soliton defects are formed modifying its optical properties, with new allowed optical transitions. The existence of solitons is closely related with the electronic ground state degeneration, since they allow the polymer to

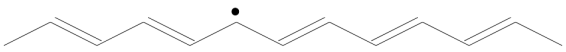

Figure 4.2: *Soliton defect of a trans-polyacetylene chain.*

conserve the minimum energy state at both sides of the defect. Solitons are not localized on one, but spread over several carbons.

In polymers with non degenerated ground state, as polyaniline (see Fig. 4.3), the two possible bond alternation directions do not have equivalent energy. In this kind of materials, a soliton can not be a stable fundamental excitation of the system. Charge excitations in polymers with non degenerate ground state are "polarons" and "bipolarons". Polarons are localized electronic states coupled with lattice distortions and bipolarons consists of two confined localized electrons also coupled with phonons. The bipolarons are thus spin-less. The formation of a bipolaron implies that the energy gained by the interaction with the lattice is larger than the Coulomb repulsion between the two confined charges of same sign.

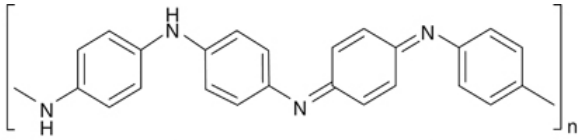

Figure 4.3: *The emeraldine base form of PAni is a non degenerate ground state polymer.*

The high conductivity increase observed upon doping organic polymers is not simply the result of electrons removed from the top of the valence band or added to the bottom of the conduction band, in analogy to the mechanism of generation of charge carriers in doped inorganic semiconductors. Charge defect states are placed inside the initial band gaps, where the valence band remains full while the conduction band empty [BS85]. In simplified picture, the interaction of polymer defects with all its neighbors leads to the formation of new electronic bands that are placed inside the initial gap. In this way, solitonic states in polyacetylene typically have energies of order of the band gap center [SSH79]. Since polarons can be thought as a pair of confined solitons (so that

there is no extra bond alternation after the formation of the defect), their energies can be pictured as a result from a level splitting

The nature of the defect band formed inside the gap is of enormous importance, since these materials are rather amorphous and inhomogeneous. The effect of disorder (the importance of which can be determined from experiments) need therefore to be properly taken into account. Strong disorder among defect formation is a natural side effect of the polymerization and doping processes, and as a consequence it should lead to a localized regime in which charge defects form pseudo bands of confined states. Within this localized regime, metallic transport properties of conductive polymers can not be properly explained, since this leads to an exponential decay of the conductance (as discussed in section 2.3.1). As a result, numerous modern theoretical studies of the electrical properties of conductive polymers, inspired in the Landauer picture, have to resort to lattice models with exaggerated symmetries to account for the high conductivity properties of these kind of materials. As we will attempt to show in the following sections, the coherent picture of electron transport in conductive polymers is unjustified, since quantum decoherence, through the effects of dephasing events, is of crucial importance and might lead to a dramatic change in the expected conductance and other related properties.

4.3 Polyanilines

The monomer aniline was obtained for the first time in 1826 by Otto Unverdorben from a dry and destructive distillation of natural vegetable indigo and was called *Krystallin* because it produced well formed crystalline salts with acids [Ngu07]. In 1836 it was rediscovered by F. Runge but named *kyanol* because of the appearance of a bright blue color whenever it was mixed with a bleaching powder [Ngu07]. Only a few years later, in 1840, Carl Fritzsche obtained a colorless oil from indigo, called it *aniline* (from the Arabic *al-nil*, which means indigo), and oxidized it to polyaniline (PAni). Although it is believed that this was the oldest *paper* of polyaniline, the first definitive report did not occur until 1862, by Henry Letheby (see Fig. 4.4). From the early 20th century on, occasional reports about the structure of PAni appeared in the literature. By the 1960s, it was recognized that the oxidation product of aniline was a linear

XXIX.—*On the Production of a Blue Substance by the Electrolysis of Sulphate of Aniline.*

By H. Letheby, M.B., M.A., Ph.D., &c.

[Professor of Chemistry in the College of the London Hospital.]

Having had to investigate two cases of fatal poisoning by nitrobenzol, and finding that this compound is changed in the living stomach into aniline, I was led to enquire into the chemical reactions of this alkali, in the hope of discovering a delicate and certain test for it. That which first commanded my attention was the fact, that a salt of aniline, under the influence of nascent oxygen, from any source, acquired a blue or purple colour. But the reactions were not in all cases equally delicate, a $\frac{1}{1000}$ of a grain of aniline in half a drop of dilute sulphuric acid (1 to 1) gradually became blue when treated with a little peroxide of lead, or red prussiate of potash, but it required about double this quantity of aniline to show the blue or purple reaction with peroxide of manganese or bichromate of potash; and it was

Figure 4.4: *First definitive report of polyaniline, in 1862, by Henry Letheby.* "On the production of a blue substance by the electrolysis of sulphate of aniline" *(Journal of the Chemical Society Volume 15, pgs. 161-163).*

oligomer or polymer, and the effect of acid on its conductivity had been discovered [Sco10]. Polyaniline is one of the oldest artificial conducting polymers and it stands out among organic compounds due to its high electrical conductivity.

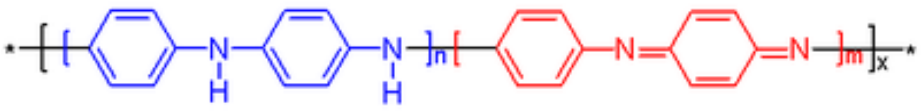

Figure 4.5: *Main polyaniline structures n+m = 1, x = degree of polymerization.*

Polymerized from the aniline monomer, polyaniline, can be found in one of three idealized oxidation states, represented in Fig. 4.5: *Leucoemeraldine*, with n = 1, m = 0 is the fully reduced state. *Pernigraniline* is the fully oxidized state, with n = 0, m = 1, and *emeraldine*, with n = m = 0.5, often referred to as emeraldine base (EB). Emeraldine base is regarded as the most useful form of polyaniline due to its high stability at room temperature and the fact

that, upon doping with acid, the resulting emeraldine salt form of polyaniline is electrically conducting.

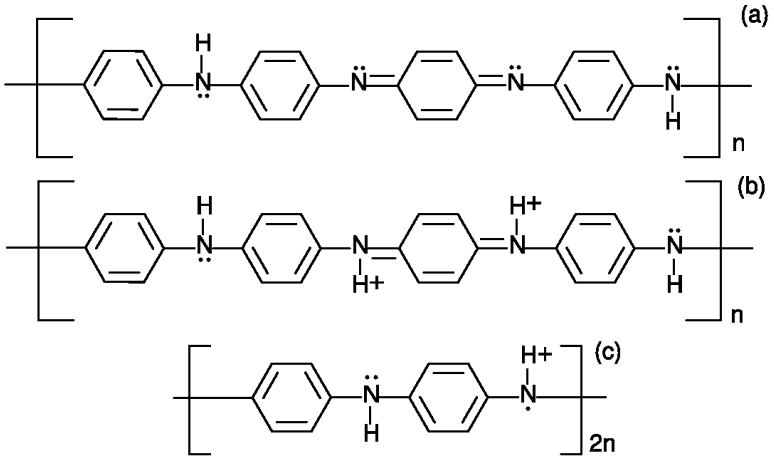

Figure 4.6: *Three different forms of PAni: (a) Emeraldine base, and two lattice models after a doping process, (b) Bipolaron, (c) Polaron*

In spite of its long history, PAni became a new paradigm for polymeric conductors as it shows a dramatic increase in conductivity either by acidic treatment or by electrochemical oxidation. However, the physical basis of its transport mechanism and of the insulator-metal transition proved more elusive. Starting from a semi-conducting PAni in an emeraldine base form (Fig. 4.6-a), protonation leads to an internal redox reaction that converts it into a metal (emeraldine salt). In order to account for the highly conducting nature of this doped polymer there are two well established models that imply two different lattice arrangements. These are associated to the appearance of two possible charged defects upon protonation. On one hand, the polaronic lattice (PL), which describes a lattice of Nitrogen bridged benzene rings that becomes fully periodic in the case of 100% of protonation. Even when one of every two Nitrogens is in the form N^+ supporting a polaron, the corresponding p_z electrons form a collective band of Bloch extended states which, being half-filled, behaves as a metal (Fig. 4.6-c). On the other hand, in a crystalline bipolaronic lattice (BL) the protonated quinoid units ($NH^+ = Q = NH^+$) are bridged by three benzene rings. The electron tunneling between neighbor NH^+ units, leads to a bonding basic unit that justifies a bipolaronic description. Natural disorder appears through the fluctuation of the bridge length

(Fig. 4.6-b). Hence, while further tunneling between units could be possible, within the standard wisdom, disorder ensures localized eigenstates that prevent propagation[And78, KM93]. Galvão *et al.* [GdSL$^+$89] concluded that disorder should be an essential ingredient in these systems. They made molecular orbitals calculations of the electronic structure of PAni chains which showed that disorder pulls the Fermi energy down through the localized states of the valence band. Later on, Wu and Phillips [WP91] agreed with Galvão in the role of the protonation, further showing that induced disorder can be identified with a Random Dimer Model (RDM) [DWP90, Phi03]. By adopting Landauer's view that "conductance is transmission" [IL99], the current *motto* of molecular electronics [JGA00, NR03], it was proved that the short range order of the RDM produces a set of delocalized or propagating states [DWP90, SGC91, Phi03]. This opened the possibility that Fermi energy might lie in a delocalized region. However, Farchioni *et al.* [FVG99], by using an *ab initio* parametrization, made a detailed tight-binding based study of PAni-HCl comparing the BL and PL models [VFG01]. They showed that even when the BL model exhibits extended states, its Fermi energy is far from the high transmission regions. These ideas seemed to support the PL as the only PAni emeraldine salt capable of metallic behavior. Indeed, the observation of Pauli susceptibility on conducting samples was attributed to extended states in a polaronic lattice [SHC94]. However, first-principle energy stability calculations point into the opposite direction. A BL is by far the more stable energy configuration when compared to a PL [CCFG02] or its variants [VS08]. A picture that could unify these conclusions is that of segregated metallic (PL) regions and insulating (BL) domains. Transport would be mediated by hopping between metallic fibers in the polymer backbone [GRME87, EGZ$^+$87]. However, it is not clear that such structures could give a lower free energy than a pure BL one. Besides, in this model disordered islands would constitute the conductance bottle-neck for which a microscopic description is lacking. Further emphasizing the role of BL, it was recently suggested that susceptibility experiments could not be used to rule out the bipolaronic structure from conducting samples. This is because an internal chemical redox equilibrium between bipolaronic structures and a number of polaronic defects with Curie susceptibility, should manifest as an overall susceptibility whose temperature dependence would be indistinguishable from

the Pauli paramagnetism [PND05]. In summary, the early works associate the conducting state of PAni with periodic order because the existence of extended Bloch eigenstates is a condition for coherent propagation.

In order to account for the surprising frequency dependence of the dielectric constant and of the conductivity observed on conjugated polymers [SBE$^+$87], Prigodin and Epstein [PE01, PE03] suggested a new mechanism of charge transport. They argued that the metallic state of polymers like PAni is sustained by a granular picture of transport where metallic islands, separated by amorphous material, interact through intra-chain resonant tunneling events in a quasi 1-D variable range hopping theory. However, after an energy scale analysis, Martens *et al.* [MB04, Mar06] arrived to the conclusion that intra-chain charge carrier delocalization should extend over several grains. In consequence, there is some critical mechanism that governs the formation of truly delocalized states. They propose a quasi 1-D model of weakly coupled disordered chains with phase-breaking events that are modeled in the Landauer-Büttiker framework. In this case the 1-D Schrödinger wave function picture for a single chain remains essentially correct with the additions of a finite lifetime, i.e. decoherence, due to dephasing events. Their source can be multiple, ranging from electron-phonon coupling [PFM02, FTPM01] to through-space electron-electron interactions between charge fluctuations [DÁLP07], or even a weak inter-chain coupling [PU98]. Increasing the inter-chain coupling eventually will give rise to a transition from a quasi 1-D to a fully 3-D behavior as demonstrated by numerical simulations [Sta95, MRSU00]. However, for conjugated polymers such as PAni, the inter-chain charge transfer is weak and a 1-D model that includes decoherence should be a good approximation. Within this framework, Martens *et al.* invoke dimensional arguments that explain the anomalous frequency dependence of the dielectric constant and conductivity of several polymers. However, their conclusions are based on estimations of the relevant system quantities.

4.4 Preliminary NMR experiments

We have performed preliminary Nuclear Magnetic Resonance (NMR) experiments on several PAni samples. Basic theoretical aspects of NMR are sum-

marized on appendix B. Polyanilines used in this study were synthesized by conventional methods at the chemical physics department at Facultad de Ciencias Químicas, Universidad Nacional de Córdoba, in the group of Rodrigo Iglesias. PAni emeraldine base, which is a semiconductor, exhibits a green/copper-colored appearance. After protonation, it becomes of a strong blue color. Our sample pills are shown on Fig. 4.7. Up to now in this work, several samples have been measured with different dopant concentrations, from PAni emeraldine base up to highly conducting PAni-HCl.

Figure 4.7: *Our PAni samples. Green/copper-colored corresponds to PAni-EB, while the blue colored is the highly doped PAni-HCl sample.*

All solid state NMR experiments were performed on dry powder samples by using a BRUKER AVANCE II spectrometer operating at 300.13 MHz for protons and 75.46 MHz for ^{13}C. In Fig. 4.9 ^{13}C spectra of four PAni-HCl samples are shown. Dopant concentrations and DC resistances of the samples are shown in the table of Fig. 4.8.

Hcl Concentration	DC Resistance
$3.0\text{x}10^{-3}$ M	> 2.0 MΩ
$1.0\text{x}10^{-2}$ M	> 2.0 MΩ
$2.5\text{x}10^{-2}$ M	0.3 MΩ
$5.0\text{x}10^{-2}$ M	0.6 MΩ
$7.5\text{x}10^{-2}$ M	0.5 MΩ
$1.5\text{x}10^{-1}$ M	87 Ω
1.5 M	34 Ω

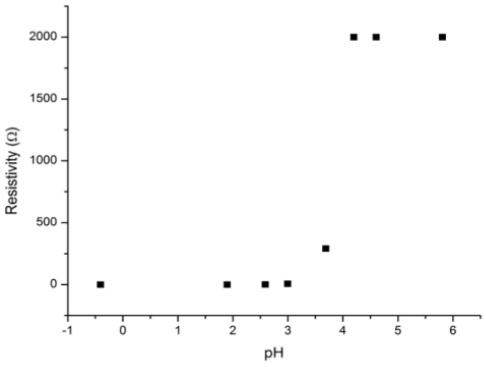

Figure 4.8: *Resistivity as a function of HCl concentration on several doped PAni samples.*

In all cases the Cross-Polarization mixing time was 2ms, the magic angle spinning speed was 8kHz and the number of scans acquired, 1600. In agreement with previously published ^{13}C measurements [KCRM88], for lower dopant concentrations the several spectra consist of three main peaks with a rich structure. In Fig. 4.9 it can be seen that there is a slight displacement of the main peak (120Hz = 1,6ppm aprox.) in the highly conducting sample. Meanwhile, the other peaks became totally broadened, losing their characteristic features. In

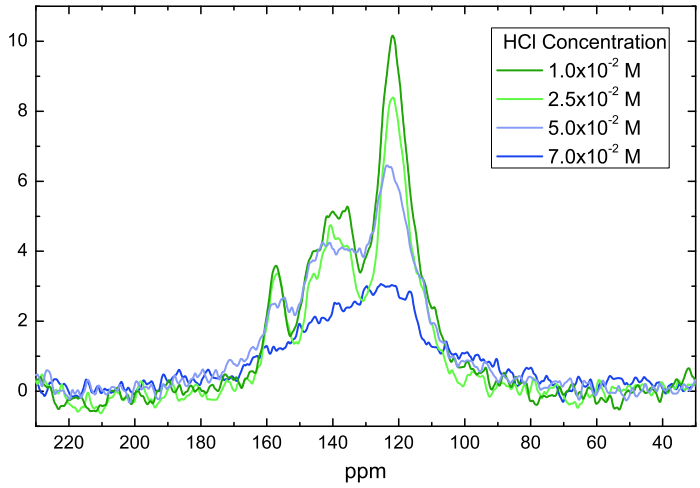

Figure 4.9: *Initial NMR experiments.* ^{13}C *measurements for PAni-HCl samples with different dopant concentrations.*

general, we are able to observe that the quality of the signal decreases with higher dopant concentrations, until a critical value is reached, where the spectrum suffers an abrupt change. This results in a single 60ppm inhomogeneously broadened unresolved resonance, in agreement with the literature.

Our goal for the next step of our research is to contribute to the development of experimental strategies that allow the identification of the processes that contribute to the decoherence in the dynamics of charge and spin excitations by means of solid state NMR techniques. This is necessary to confirm our recent theoretical results on the metal-insulator transition for conductive polymers, where we propose that decoherence mechanisms play a substantial role in the appearance of the conducting phase. This is due to charge fluctuations associated with tunneling between polymer chains and ultimately to

electron-phonon processes. In the case of PAni, charge propagation along each polymer chain, in absence of doping, is blocked by those nitrogen sites with sp3 structure (in which the non-bonded orbital contains a lone pair of electrons) connected to benzene rings. By increasing the doping, these nitrogens adopt sp2 structures with a pz orbital that participates in the band of conjugated double bonds. It is well known that the Fermi level is located in a band region of localized states of coherent interference due to the disorder. However, according to our hypothesis, decoherence mechanisms would enable charge mobility. This is discussed in the following section.

4.5 Decoherent electronic transport in PAni

In the following sections of the chapter, we attempt to elucidate in some detail the nature of conductivity of polymers by taking the PAni bipolaron lattice structure as the case study. For that purpose, we use realistic ab initio based tight-binding parameters which can be easily reduced to the minimal parametrization of the D'Amato-Pastawski model. This provides a simple solution to the otherwise complex Keldysh formulation of transport. Indeed, this strategy was applied before to PAni by Maschke [MS94] and Schreiber [HS97]. However, they focused on already conducting PAni polaronic chains that are affected by decoherence and/or inter-chain coupling. We show that quantum decoherence can lead to a dramatic change in the expected transport properties for the bipolaron lattice structure of PAni.

4.5.1 Model Hamiltonian

We consider a fully protonated BL, which we expect to correspond to the highly conducting emeraldine salt. By decimation of the benzenoid rings as it is shown in figure 4.10, we reduce the PAni emeraldine salt chain to one-dimensional effective system [LPD90]. Each ring is replaced by the proper renormalized sites at the place of the para-Carbon atoms.

The sample Hamiltonian results:

$$\hat{H}_S = \sum_{j=1}^{N} \left(E_j \hat{c}_j^+ \hat{c}_j + V_j \hat{c}_j^+ \hat{c}_{j+1} + V_j \hat{c}_{j+1}^+ \hat{c}_j \right). \tag{4.1}$$

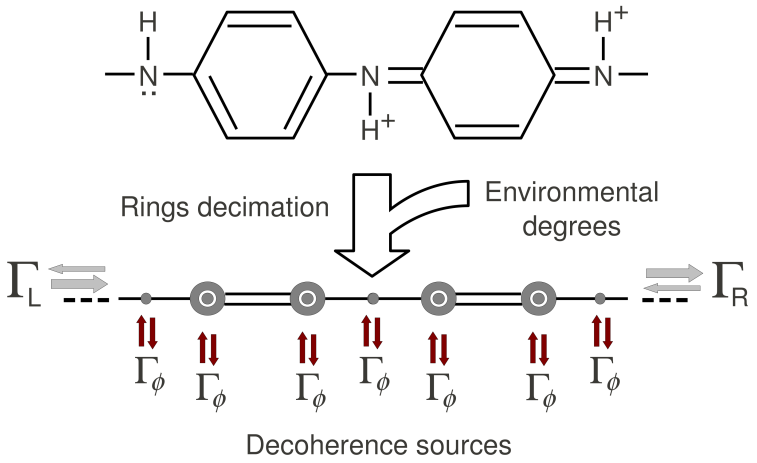

Figure 4.10: *Schematic representation of benzenoid rings decimated to obtain equivalent renormalized units in one dimension. Incoherent channels of D'Amato-Pastawski model also shown.*

When $j = 3s + 1$ with s positive integer, E_j is the Nitrogen p_z-orbital energy and V_j is the π binding energy (hopping) between the nitrogen and the para-C p_z-orbitals. When $j = 3s$ and $j = 3s - 1$ we have the renormalized parameters for para-C p_z-orbitals:

$$V_j = \frac{V_{oo}V_{po}^2}{(\varepsilon - E_o)(\varepsilon - E_o - \frac{V_{oo}^2}{\varepsilon - E_o})}, \tag{4.2}$$

and

$$E_j = E_p + \frac{V_{po}^2}{\varepsilon - E_o - \frac{V_{oo}^2}{\varepsilon - E_o}}, \tag{4.3}$$

where E_o and E_p are bare site energies for electrons in the p_z-orbitals of ortho-C and para-C respectively; V_{oo} is the hopping between ortho-C and V_{po} is the hopping between a para-C and ortho-C. In this work we use the tight binding parametrization of Vignolo *et al.* [VFG01] for the bipolaron lattice model of base-emeraldine doped with HCl.

We will consider decoherent sources on effective electron p_z-orbitals sites by including a constant imaginary correction to the site energy as in Eq. 3.15. This is the most convenient choice for computational purposes. A first principles calculation of this imaginary correction is beyond the scope of this work. Its complexity lying on the multiple effects that must be considered. In the appendix we discuss in certain detail two mechanisms: inter-chain tunneling and

the effect of torsional modes on the crucial π bonds. However, it is enough to resort to dimensional arguments based on spontaneous symmetry breaking of the quantum coherent state [SGCS97]. The reasoning takes into account that quantum bosonic modes with energies $\leq k_B T$ should be occupied by many quanta, indicating that Γ_ϕ should be of the order of $k_B T$ [Mar06]. In accordance with this general framework, Rebentrost *et al.* obtain a comparable estimation for Γ_ϕ for excitons in photosynthetic complexes interacting with a phonon bath [RMK$^+$09]. Indeed, experiments on DNA strands fits Γ_ϕ of this order using the DP model [LY01]. Thus, we fix an effective $\tilde{\Gamma}_\phi$ on each effective site such that the energy uncertainty per orbital site is $\Gamma_\phi = k_B T$. We will see in the next section that small variations of the precise value of Γ_ϕ have little impact on conductance.

Right and left leads are described by Eq. 6.8 choosing $E_0 = 0$ and $V = 5e\text{V}$ to observe the appropriate bandwidth of interest $[-10e\text{V}, 10e\text{V}]$. Furthermore, we calculated the Fermi energy by diagonalizing the exact tight-binding Hamiltonian for different configurations. For all possible chain arrangements, the Fermi level is nearly the same, around the average.

4.5.2 Sources for decoherent events in polymers

There are many sources of dephasing events for electrons in conductive polymers, from electron-electron interactions, electron-phonon couplings and interchain couplings. In this section we address two of the most representative of them, inspired in the particular problem of electronic transport in PAni. Moreover, a detailed treatment of these specific models allows us to lighten their differences and similarities with the well-known Marcus-Hush theory [Mar93] for vibration-assisted electron transfer, which is discussed in Appendix C.

4.5.2.1 Torsional Modes for p_z orbitals

Certainly, vibrational degrees of motion are natural sources of decoherence. We analyze them by introducing a simple model for electron-phonon couplings that enables the evaluation of the corresponding contribution to Γ_ϕ. From the geometrical inspection of the molecular structure, it is obvious that torsional strains on benzenoid rings disrupt π bonds between p_z orbitals of para-Carbons and Nitrogens. Their overlap depends on the angle θ between the orbital axes.

As a result, the corrected hopping energies can be written as $V = V^0 cos(\theta) \simeq V^0(1-\theta^2/2)$. The natural frequency ω_θ of this torsional motion determine the vibrational energy of benzenoid rings. A self consistent description requires that the restoring force $I\omega_\theta^2\theta$, written in terms of the moment of inertia I of the benzenoid ring, should coincide with the net change in the electronic energy described by the tight-binding model. In this case it yields

$$V^0 = I\omega_\theta^2 \tag{4.4}$$

leading to $\hbar\omega_\theta \simeq 2\times 10^{-2}\text{eV} < k_B T_R$.

In terms of the second quantization operators $\hat{b} = \sqrt{I\omega_\theta/2\hbar}(\theta + \mathrm{i}\dot{\theta}/\omega_\theta)$ and $\hat{b}^+ = \sqrt{I\omega_\theta/2\hbar}(\theta - i\dot{\theta}/\omega_{\theta\theta})$ we get the perturbation given by the coupling Hamiltonian:

$$\hat{H}_{el-ph} = -\tfrac{1}{4}\hbar\omega_\theta\left(\hat{b}^+ + \hat{b}\right)^2(\delta_{j',j} + \delta_{j',j-1}) \times \tag{4.5}$$

$$\sum_{j'}\left(\hat{c}^+_{j'}\hat{c}_{j'+1} + \hat{c}^+_{j'+1}\hat{c}_{j'}\right) \tag{4.6}$$

A Fock-space representation of this interaction Hamiltonian is represented in Fig. 4.11. Notice the similarities and differences with the representation of the linear electron-phonon interaction discussed in Ref. [PFM02, FTPM01] and the inter-chain coupling. In the present case, the effect of the perturbation on the state on a local site j can evaluated with the FGR:

$$\frac{1}{\tau_j(\epsilon)} = \sum_n P(n)\left[\frac{2\pi}{\hbar}\sum_{j',n'}\left|\langle j,n|\,\hat{H}_{el-ph}\,|j',n'\rangle\right|^2\right] \times \tag{4.7}$$

$$\delta\left[(\epsilon + n\hbar\omega_\theta) - (E_{j'} + n'\hbar\omega_\theta)\right] \tag{4.8}$$

where $|j,n\rangle = \frac{1}{\sqrt{n!}}\left(\hat{b}^+\right)^n \hat{c}^+_j\,|\emptyset\rangle$ here $|\emptyset\rangle$ is the electron and phonon vacuum and n label the number of vibrational quantums whose thermal probability is $P(n)$. In the case of interest, we consider electrons at the Fermi level, E_F. Thus, after energy integration and using the thermal average $\langle\langle n\rangle\rangle \equiv \bar{n} = \sum P(n)n$ for the expectation number of n, the decay rate becomes:

$$\frac{1}{\tau_j} = \tfrac{\pi}{16\hbar}(\hbar\omega_\theta)^2\{(\bar{n}^2 + 4\bar{n} + 2)N(E_F - 2\hbar\omega_\theta) \tag{4.9}$$

$$+2\bar{n}^2 N(E_F + 2\hbar\omega_\theta) + (8\bar{n}^2 + 8\bar{n} + 1)N(E_F)\} \tag{4.10}$$

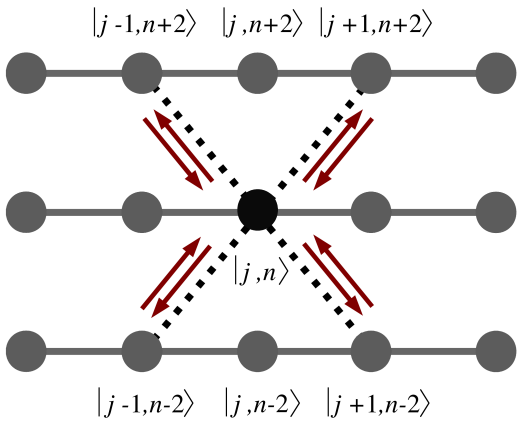

Figure 4.11: *Fock-space representation of state $|j,n\rangle$ and its surroundings. The middle row represents electronic states with n phonons in the PAni chain. Lower and upper rows represent the same chain but with different numbers of phonons. Black dotted lines are electron-phonon couplings.*

We must highlight that the quadratic dependence on displacement in the electron-phonon interaction is the responsible for the selection rules that can be appreciated in the last equation. Electrons are allowed to interact with environment only by absorbing or emitting phonon pairs. This is shown in Fig. 4.11. However, without much loss of generality that $k_BT \gg \hbar\omega_\theta$, so it is possible to approximate $E_F \approx E_F \pm 2\hbar\omega_\theta$ and $\bar{n} \approx \frac{k_BT}{\hbar\omega_\theta}$. As a result,

$$\frac{1}{\tau_j} = \frac{\pi}{8\hbar}(\hbar\omega_\theta)^2 N(E_F)\left[12\left(\frac{k_BT}{\hbar\omega_\theta}\right)^2 + 12\left(\frac{k_BT}{\hbar\omega_\theta}\right) + 3\right] \tag{4.11}$$

The evaluation of the corresponding Γ_ϕ becomes trivial in this high temperature regime,

$$\Gamma_\phi = \frac{\hbar}{2}\frac{1}{\tau_j} = \frac{3\pi}{4}N(E_F)(k_BT)^2. \tag{4.12}$$

Here, it is crucial to notice that for highly localized states the imaginary self energy results mainly from the decoherent process described above. Thus

$$N(\epsilon) \approx \frac{1}{\pi}\frac{\Gamma_\phi}{(\epsilon - E_0)^2 + \Gamma_\phi^2} \tag{4.13}$$

$$\approx 1/\pi\Gamma_\phi. \tag{4.14}$$

Therefore, from Eq. 4.12,

$$\Gamma_\phi \sim k_BT. \tag{4.15}$$

Thus, any low frequency modes yielding a quadratic dependence of the electronic energy on the displacement, which can be more general than expected, leads to an important consequence: for localized regime, it would tend to provide an energy uncertainty (decoherence) of the order of the thermal energy. A similar behavior remains valid if one relaxes the localization requirement to that of a sharply peaked resonance. A simple example is a sharp resonance in a one dimensional system [RFSO$^+$09] in which the local density of states could be written:

$$N(\epsilon) = -\mathrm{Im}\left\{\frac{1}{\pi}\frac{1}{\epsilon - E_j + \mathrm{i}\Gamma_\phi - \alpha(\Delta - \mathrm{i}\Gamma_{bulk})}\right\}, \tag{4.16}$$

where $\alpha\Gamma_{bulk}$ represent the escape to the rest of the tight-binding chain and $\alpha\Delta$ gives the energy shift due the presence of the other sites. The parameter α gives the strength of the coupling with the rest of the chain. For ϵ within the band edges, this equation results:

$$N(\epsilon) = \frac{1}{\pi\Gamma}\frac{1 + 2\alpha\Gamma_{bulk}/\Gamma}{\left(\frac{\epsilon - E_j - 2\alpha\Delta}{\Gamma}\right)^2 + (1 + 2\alpha\Gamma_{bulk}/\Gamma)^2}, \tag{4.17}$$

which in the limit of large Γ compared with $\alpha\Gamma_{bulk}$, gives $N(\epsilon) \approx 1/\pi\Gamma$. This limit is achieved at room temperature whenever $\alpha \ll 1$.

4.5.2.2 Inter-chain hopping

We start considering the effect of V_X, an inter-chain hopping at site j. Any neighboring chain can act as an "environment" for an electron at this site. This is because an electron jumping into a side chain (see Fig. 4.12) has two options: 1) to escape towards this alternative propagation channel and never return. This is obviously decoherent as it can not interfere any longer with the main pathway[FPM06, BcvT95, BcvTBac99, AMPB94]. 2) to return after having an ergodic walk on the side chain. In this case it is just the excessive amount of interferences and anti-resonances involved that leads to a decoherent description [FPM06]. Each node in the plot corresponds to a multi-chain electronic state. Notice that the interaction structure looks the same as in the local phonon picture discussed in Ref. [PFM02, FTPM01]. Using Eq. 6.8, we have for self-energy Σ_j^X describing this coupling:

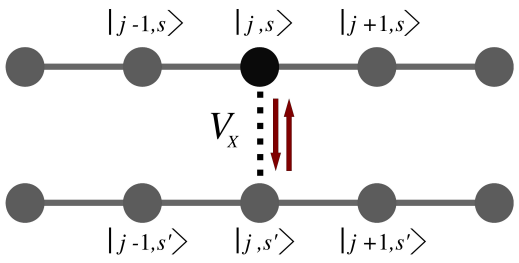

Figure 4.12: *Inter-chain hopping at site j. States are written in Dirac notation including quantum numbers s which label different PAni chains. This representation illustrates the similarity with Fock-space representation of the electron-phonon system.*

$$\Sigma_j^X = \frac{|V_X|^2}{\varepsilon - (E_j - \mathrm{i}\eta) - \Sigma_j} = \left(\frac{V_X}{V_{j,j+1}}\right)^2 \Sigma_j, \tag{4.18}$$

where E_j, $V_{j,j+1}$are site and hopping strength within the chain. As usual, η is an finitesimal imaginary part of the local energy (see section 2.2.4). Thus the inter-chain rate can be expressed as $\Gamma_\phi^X = \left(\frac{V_X}{V_{j,j+1}}\right)^2 \Gamma_j$ where Γ_j and the imaginary part of total self energies at site j. We may evaluate an estimate for the typical Γ_j by disregarding localization and considering that the side chain is an infinite PAni strand and using the representative values of $\overline{E} \simeq -0.3eV$ for and site energy and $\overline{V} \simeq -3.6eV$ for intra-chain π bonds. Thus,

$$\Gamma_j^X = \left(\frac{V_X}{\overline{V}}\right)^2 \sqrt{\overline{V}^2 - \left(\frac{\epsilon - \overline{E}}{2}\right)^2}. \tag{4.19}$$

We might wonder which range of values would be required from V_X to yield an energy uncertainty of the order $\Gamma^X \simeq k_B T_R$ where $k_B T_R$ stands for room temperature energy. The use of the discussed values yields $V_X < \overline{V}/12$. While we can not ensure that this is the case, in every site of the PAni chain, uncertainty energy associated with inter-chain coupling is not too far below thermal energy and, therefore, it is not negligible. Indeed, there could be sites in which inter-chain couplings are stronger, and they would contribute substantially to the decay of local states.

4.5.3 Numerical Results

We have performed a detailed analysis of the conductance properties of the BL model of polyaniline emeraldine salt. Due to the fact that, according to experimental data, PAni chains seem to have an average length of 400 rings [KSZ$^+$05], we have taken that number in our numerical calculations. However, it should be noted that our results do not depend critically on this parameter. We first calculated the coherent transmission probability as a function of energy for a set of chain configurations drawn from the representative ensemble. Results are in full agreement with the those of Farchioni *et al.* [VFG01, FVG99, FGP96] and evidence the mobility edges induced by correlated disorder in this 1-D system [DWP90]. While there is an appreciable density of states at the Fermi energy, it corresponds to localized states. Indeed, according to Fig. 4.13-a, the Fermi energy is far away from the extended state region. Fig. 4.13-b shows the drastic differences in conductance once that decoherent processes are taken into account. Conductance at the Fermi energy now becomes appreciable for any configuration. These results show that metallic transport is possible within a purely BL model through an environment-assisted transport [RMK$^+$09]. Even within a model of perfectly conducting PL islands bridged by BL strands, the calculated chains can be taken as representative of such transport bottleneck. One expects that small differences in quinoid ring concentrations would appear due to natural fluctuations on the oxidation degree previous to doping. In Fig. 4.14 we show the resultant conductance for various quinoid concentrations and found no significant changes in transport.

We also studied the behavior of total conductance as a function of decoherence rate. In accordance with recent works [RMK$^+$09, MRLA08], three regimes can be appreciated. Starting from T=0K, as the temperature rises dephasing events become more successful in the destruction of localization caused by coherent interference at the Fermi energy, rising the total conductance of the system. In this regime, transport rate increases as the energy uncertainty associated with temperature is increased. However, there is a Γ_ϕ value for which the conductance is maximal. If the temperature is increased further, the associated energy uncertainty becomes larger than the terms of the system Hamiltonian (characteristic hopping and site energies), and the decoherent process now are able to suppress transport. This is commonly known in the literature as the

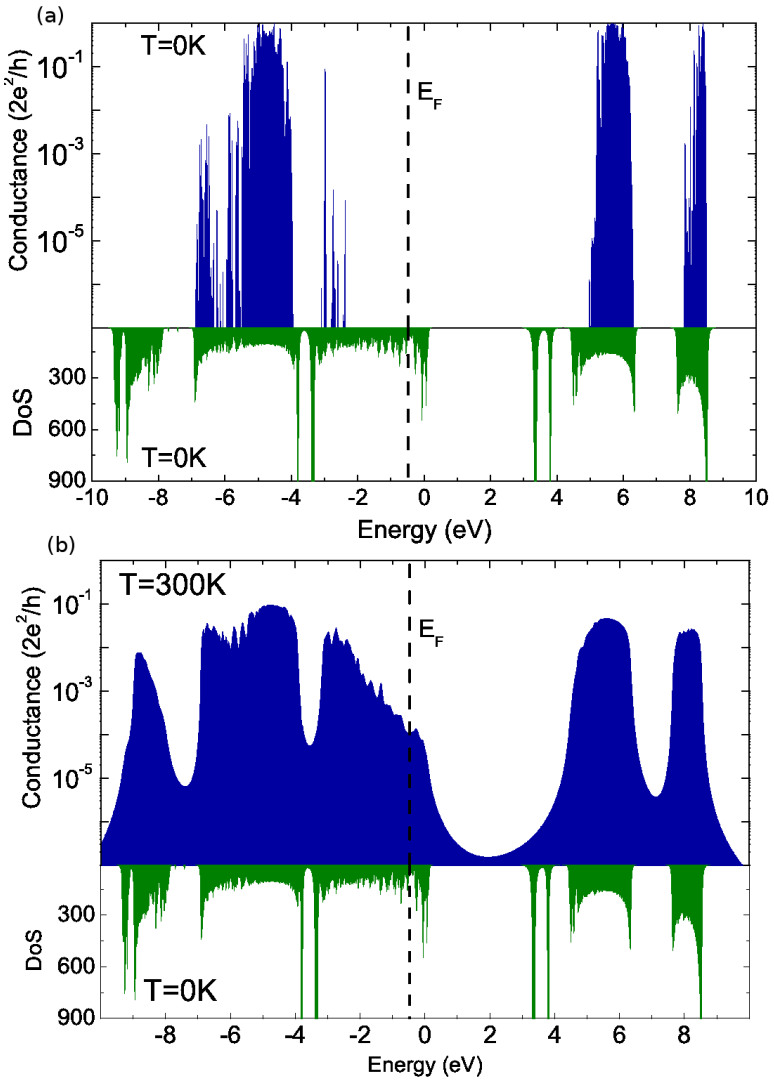

Figure 4.13: *Conductance for both: (a) T=0K, and (b) T=300K according to DP model for a 400 rings long PAni-HCl chain. We also show the T=0K Density of state for comparison purposes.*

quantum Zeno effect. In Fig. 4.15 we show our results for the dependence of total conductance with Γ_ϕ, in which the three regimes above described are clearly seen. The thermal energy, in this case, lies on an area of great influence on the total conductance of this system, and therefore decoherent processes should not be neglected. At room temperatures, the PAni BL is safely placed in the range of thermally assisted transport, and it is clear from the figure that small variations in the exact value of Γ_ϕ do not alter the outcome significantly (note the log-log scale).

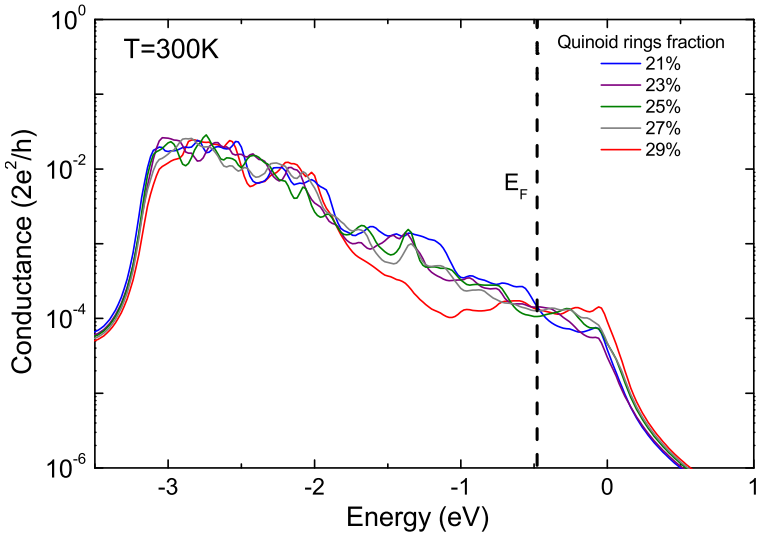

Figure 4.14: *Fluctuations in total conductance at T=300K in the main peak around the Fermi energy with the fraction of quinoid rings along the chain.*

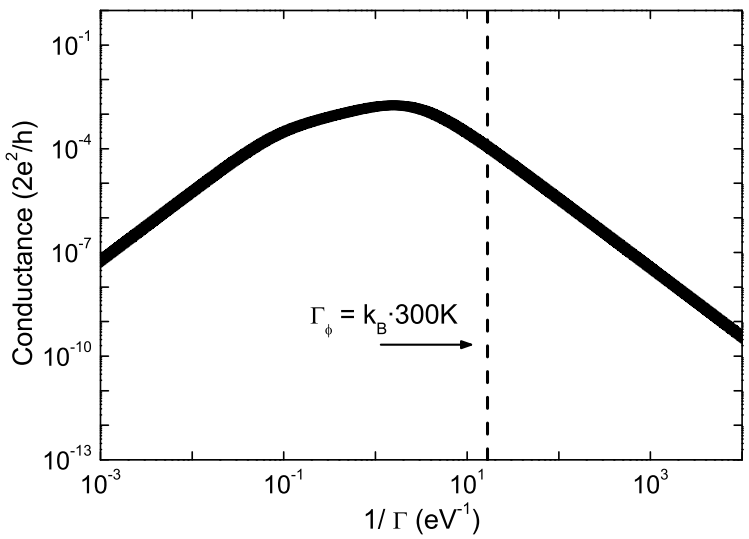

Figure 4.15: *Conductance for a 400 rings long PAni-HCl chain as a function of Γ_ϕ. The value for Γ_ϕ at $T = 300K$ also shown in dash line.*

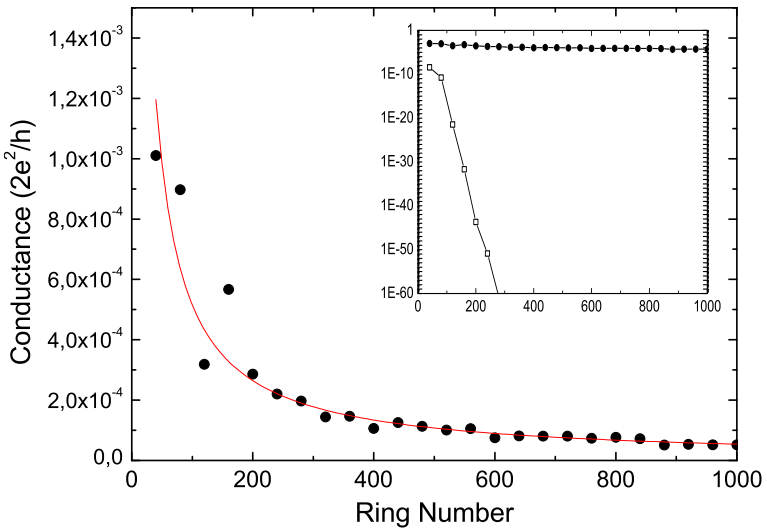

Figure 4.16: *Total conductance at T=300K as a function of the chain large. As an inset, it is shown the scale difference between coherent and total conductance.*

We studied the dependence of conductance on the chain length. The results are shown in Fig. 4.16. With the exception of some fluctuations at short lengths, conductance at T=300K decreases as the reciprocal of the chain length, as expected for an Ohmic system. The fitting gives $\mathrm{G}/\left(2e^2/h\right) = 1/\left(20,6N_R\right)$, where N_R is the number of rings of the chain. The log scale in the inset figure emphasizes the drastic difference between the full conductance and that restricted to coherent tunneling processes. The coherent conductance decays exponentially as expected for a one dimensional disordered system [MK81, PSW85]. In our case the localization length is small, $\mathrm{G}/\left(2e^2/h\right) = 22\times10^3 e^{-0.53N_R}$, which implies that even for very short disordered polymer chains, transport does not take place unless decoherence processes are involved. Indeed, conductance decays a factor 1/3 for every two rings. Therefore, in a model of islands as that mentioned in the introduction, destruction of localization by decoherence would have a fundamental role. However, our results go further and evidence that even a fully BL PAni would sustain strong electronic transport.

Fig. 4.17 shows the net current through 50 random chain configurations of bipolaronic PAni. The current was evaluated by using Eq. 3.33 for symmetric voltages at room temperature. As can be seen, the behavior of different

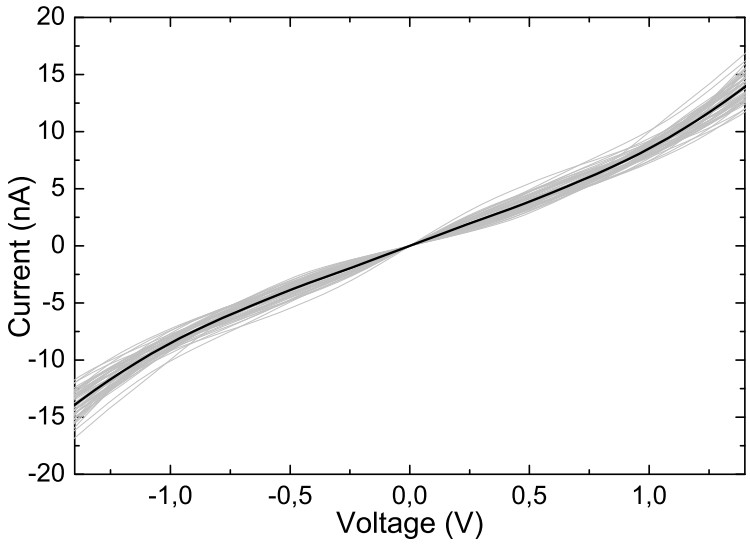

Figure 4.17: *Average current (black line) and currents for 50 different configurations (shadow lines) are shown.*

chain configurations is very similar and close to the linear regime. All chain configurations exhibit an appreciable conductance with an average value of $7,7\text{x}10^{-9}\Omega^{-1}$. Taking the PAni-HCl density as $1,329g/cm^3$ [SG02] we get a conductivity of $\sigma = 81\Omega^{-1}cm^{-1}$. This result is slightly higher than the experimental ones, $1\Omega^{-1}cm^{-1} \lesssim \sigma \lesssim 20\Omega^{-1}cm^{-1}$ [ZGW$^+$97, KC99, LCW$^+$03] which is reasonable because in the calculation of the conductivity we are considering the conductance of the ideal case of chains directly connected to the leads.

4.6 Summary

In this work we have discussed electron conductance in a doped PAni. We show that the PAni ground state configuration, the BL, has high conductance even in presence of disorder provided that decoherent processes are included. This is done without leaving the convenient *a là* Landauer approach by using the generalization introduced by D'Amato and Pastawski [DP90] where an effective transmission accounts for decoherent processes. While our formulation accepts further improvements, it provides an answer from the robust description of Keldysh formalism within a minimal parametrization. Roughly speaking, decoherent processes split each chain into a series of portions whose length

is given by the decoherence length L_ϕ [PWA95]. These define the elemental conductivities from which the sample's Ohmic transport builds on.

For many years, it has been assumed that conduction of polyanilines is inseparably linked to the existence of a polaronic crystalline structure. However, although our main intention is qualitative, we showed that decoherent processes are able to give appreciable metallic conduction in the more entropically favorable bipolaronic lattice. For this system, the uncertainty of energy associated with thermal processes cannot be neglected in the study of conductance, since k_BT falls in a region in which the interplay between incoherent and coherent dynamics results in an increased efficiency of electron transport. One might then speculate that only when the thermal energy scale becomes smaller than the Coulomb energy of the localized states, one would actually start to notice a qualitative difference with an ideal 1-D metal.

The robustness of the results obtained is evident by noting that they neither depend on variations in the oxidation degree of PAni prior to the doping process, nor on the particular arrangement of quinoid rings along the chain, or on the exact value of the energy uncertainty associated to Γ_ϕ. This justifies the fact that good conducting properties do not depend much on the purity of the emeraldine base so that small displacements toward the leucoemeraldine or pernigraniline are acceptable. The evaluation presented in the appendix show that, even when inter-chain coupling can contribute appreciably to conductivity, the coupling between the p_z bonds with torsional degrees of freedom is strong enough to provide almost all the required decoherence. This hypothesis seems consistent with the experiments that show that adding residues that restrict the torsional motion would also diminish the conductivity as compared with the unmodified bipolaronic lattice [HHY$^+$01, HLHY03, SAM$^+$04].

We do not attempt to rule out the presence of phase segregation into metallic polaronic islands and "insulating" bipolaronic domains. However, these last strands constitute the bottle-neck where thermal decoherent processes activate the conductivity. Moreover, our results go further ahead and evidence that bipolaronic chains can sustain electronic transport by themselves. In fact, based in our simulations we can estimate bulk conductivity for these chains and arrive to a remarkably good value as compared with experimental data.

5

Decoherent transport on multi-terminal devices: Efficient algorithms and applications.

Both the understanding of the effects of quantum decoherence and even its proper description in the context of transport problems are still open research subjects in modern physics. However, our expectation is that the methodology introduced in previous chapters, despite its inherent limitations, will provide simple but powerful insight into this blooming field. Perhaps one of the most important restrictions, which in turn is a desirable simplifying feature for any initial study of this subject, is the one-particle picture assumed in the model description. The underlying idea of this approach is that, in several important systems, complex many-body interactions result in the loss of the simple interferences of a one-body description.

However, in some cases there are certain many-body interactions suffered by carriers in electronic devices that can not be treated within the simple Fermi golden rule approximation, providing extra degrees of freedom that must be accounted explicitly. Fortunately many times, in some approximation, this extra degrees of freedom can be mapped into the one-electron picture as extended topological spaces, transferring the complexity of the many-body interactions to the geometry of the one-electron transport problem. The extension of the

Landauer's picture of transport for the study of decoherence effects in multi-terminal devices, in this sense, provides a starting point.

This chapter is devoted to the discussion of electronic transport on multi-terminal molecular devices, in the presence of decoherent events, in terms of a simple generalization of the D'Amato-Pastawski model. The review of the computational approach is also presented with particular emphasis on efficient recursive algorithms for solving this kind of problems. Some meaningful physical examples of its application are also presented and discussed: the case of electron-phonon interactions, Floquet theory applied to simple periodic time-dependent Hamiltonians and decoherent transport in carbon nanotubes..

5.1 Matrix continued fractions

Landauer's picture of electronic transport has almost no rival in the evaluation of quantum coherent electronic transport at the nanoscale [IL99]. As shown in section 2.1, in its simplest form conductance is determined by the coherent transmission probability between two one-dimensional electrodes acting as current source and drain. A natural extension developed by Büttiker [B̈86a], discussed in section 2.1.2, involved the application of the Kirchhoff laws, for a system composed by many channels, which can be associated not only to current leads but also to voltage probes. In the latter case, one must evaluate a self-consistent non-equilibrium chemical potential that ensures the current cancellation at the voltmeter, as explained throughout the chapter 3. Büttiker's initial observation that a voltage probe implies a classical measurement and hence could be associated to a decoherence source, was further developed into a Hamiltonian formulation by D'Amato and Pastawski [DP90] which enabled an homogeneous distribution of decoherence processes. However, its practical applications remained reduced to one-dimensional problems where it was originally formulated. This is because of the practical limitations of dealing with a great number of self-consistent reservoirs required by spatially distributed decoherent processes. Having a more efficient method would greatly improve the prospects for better simulations at the nanoscale in the presence of dephasing, a field of much current interest.

In this section we present an efficient algorithm to calculate the matrix elements of the Green's function which is very useful for wide variety of problems beyond the typical one dimensional calculations. The method is widely applicable but its efficiency is associated with block tridiagonal Hamiltonians. There are many frequent physical examples in which the Hamiltonian matrix adopts a block tridiagonal structure, specifically when interaction are truncated at a certain order. For example if hopping elements beyond first neighbors are neglected in nanowires or molecules with a single or multiple orbitals per atom. In order to obtain the Green functions matrix of the sample, the evaluation of the matrix inverse in Eq. 2.33 is needed. A way to solve this problem, based in the Matrix Continued Fractions [But73, PWA83], will prove very useful and requires to exploit iteratively the well known method of block matrix pseudo-inverses (usually referred to as "bordering"). Let us initially "partition" the matrix of the effective Hamiltonian of the system, $\hat{H}_{eff.}$, into two portions, a cluster block 1, and the rest of the system R. The Hamiltonian block subdivision may lie in geometric considerations of the tight-binding basis or can be chosen so as to take advantage of given symmetries of the Hamiltonian matrix for any given problem. In particular, if the sample Hamiltonian could be arranged in a three-diagonal block structure, much benefit can be obtained from the use of this decimation procedures. Thus, the matrix to invert in Eq. 2.33 is subdivided into four blocks, $(\epsilon\mathbb{I}-\mathbb{E}_1)$,$(\epsilon\mathbb{I}-\mathbb{E}_1)$,$-\mathbb{V}_{1R}$, and $-\mathbb{V}_{R1}$ of dimensions $N_1 \times M_1$, $N_R \times M_R$, $N_1 \times M_R$ and $N_R \times M_1$ respectively. Thus,

$$\mathbb{G}(\epsilon)^R = \begin{bmatrix} \mathbb{G}_{11} & \mathbb{G}_{1R} \\ \mathbb{G}_{R1} & \mathbb{G}_{RR} \end{bmatrix} = \begin{bmatrix} \varepsilon\mathbb{I}-\mathbb{E}_1 & -\mathbb{V}_{1R} \\ -\mathbb{V}_{R1} & \varepsilon\mathbb{I}-\mathbb{E}_R \end{bmatrix}^{-1} \tag{5.1}$$

Here it is very important to note that the Green functions matrix $\mathbb{G}(\epsilon)$ includes all corrections due to fictitious and real probes, by virtue of Eq. 3.16. In this way, the block energies denoted here by $\mathbb{E}_i$ contain the energies of the open system which are represented by complex numbers. For the two block matrix

inverse, is straightforward to show that

$$\begin{aligned}
&\left[\begin{array}{cc} \varepsilon\mathbb{I}-\mathbb{E}_1 & -\mathbb{V}_{1R} \\ -\mathbb{V}_{R1} & \varepsilon\mathbb{I}-\mathbb{E}_R \end{array}\right] = \\
&= \left[\begin{array}{cc} \mathbb{I} & 0 \\ -\mathbb{V}_{R1}(\varepsilon\mathbb{I}-\mathbb{E}_1)^{-1} & \mathbb{I} \end{array}\right] \left[\begin{array}{cc} (\varepsilon\mathbb{I}-\mathbb{E}_1) & 0 \\ 0 & \mathbb{S}_1 \end{array}\right] \left[\begin{array}{cc} \mathbb{I} & -(\varepsilon\mathbb{I}-\mathbb{E}_1)^{-1}\mathbb{V}_{1R} \\ 0 & \mathbb{I} \end{array}\right] \\
&= \left[\begin{array}{cc} \mathbb{I} & -\mathbb{V}_{1R}(\varepsilon\mathbb{I}-\mathbb{E}_R)^{-1} \\ 0 & \mathbb{I} \end{array}\right] \left[\begin{array}{cc} \mathbb{S}_R & 0 \\ 0 & (\varepsilon\mathbb{I}-\mathbb{E}_R) \end{array}\right] \left[\begin{array}{cc} \mathbb{I} & 0 \\ -(\varepsilon\mathbb{I}-\mathbb{E}_R)^{-1}\mathbb{V}_{R1} & \mathbb{I} \end{array}\right]
\end{aligned} \tag{5.2}$$

where $\mathbb{S}_{1(R)}$ is the Schur complement of $(\epsilon\mathbb{I}-\mathbb{E}_{1(R)})$, given by

$$\mathbb{S}_{1(R)} = (\epsilon\mathbb{I}-E_{1(R)}) - \mathbb{V}_{1R(R1)}(\epsilon\mathbb{I}-E_{R(1)})^{-1}\mathbb{V}_{R1(1R)}. \tag{5.3}$$

From last expressions is easy to obtain

$$\mathbb{G}_{11} = [(\epsilon\mathbb{I}-\mathbb{E}_1)-\Sigma_{1R}]^{-1} \tag{5.4}$$

$$\mathbb{G}_{RR} = [(\epsilon\mathbb{I}-\mathbb{E}_R)-\Sigma_{R1}]^{-1} \tag{5.5}$$

$$\mathbb{G}_{1R} = \mathbb{G}_{11}\mathbb{V}_{1R}(\varepsilon\mathbb{I}-\mathbb{E}_R)^{-1} \tag{5.6}$$

$$\mathbb{G}_{R1} = \mathbb{G}_{RR}\mathbb{V}_{R1}(\varepsilon\mathbb{I}-\mathbb{E}_1)^{-1} \tag{5.7}$$

where the block self-energies, Σ's, are given by:

$$\Sigma_{1R} = \mathbb{V}_{1R}(\varepsilon\mathbb{I}-\mathbb{E}_R)^{-1}\mathbb{V}_{R1} \tag{5.8}$$

$$\Sigma_{R1} = \mathbb{V}_{R1}(\varepsilon\mathbb{I}-\mathbb{E}_1)^{-1}\mathbb{V}_{1R} \tag{5.9}$$

The similarity with Eq. 2.21 allowed us to define these block self energies. Therefore the decimation of the degrees of freedom associated with the portion R of the effective Hamiltonian is implied in Eq. 5.7, where:

$$\tilde{\mathbb{E}}_1 = \mathbb{E}_1 + \Sigma_{1R} = \mathbb{E}_1 + \mathbb{V}_{1R}(\epsilon\mathbb{I}-\mathbb{E}_R)^{-1}\mathbb{V}_{R1} \tag{5.10}$$

Note that with the adopted notation for the self energies, Σ_{ij} is the correction to site i when all sites between i and j (with j included) are decimated. Once arrived to this point becomes very simple to extend the block decimation rules for an arbitrary number of clusters, by further partition of Eq. 5.10. If block R is subdivided into a cluster 2 and the rest of the system R',

$$\mathbb{G}(\epsilon) = \left(\begin{array}{c|cc} \epsilon\mathbb{I}-\mathbb{E}_1 & -\mathbb{V}_{12} & -\mathbb{V}_{1R'} \\ \hline -\mathbb{V}_{21} & \epsilon\mathbb{I}-\mathbb{E}_2 & -\mathbb{V}_{2R'} \\ -\mathbb{V}_{R'1} & -\mathbb{V}_{R'2} & \epsilon\mathbb{I}-\mathbb{E}_{R'} \end{array}\right)^{-1} \tag{5.11}$$

we can also decimate the degrees of freedom associated with block 2, taking

$$\tilde{\mathbb{E}}_1 = \mathbb{E}_1 + \Sigma_{12} \tag{5.12}$$

$$\tilde{\mathbb{E}}_{R'} = \mathbb{E}_{R'} + \Sigma_{R'2} \tag{5.13}$$

$$\tilde{\mathbb{V}}_{1R'} = \mathbb{V}_{12}(\epsilon\mathbb{I} - \mathbb{E}_{12} - \Sigma_{2R'})^{-1}\mathbb{V}_{2R'} + \mathbb{V}_{1R'} \tag{5.14}$$

which leads to an effective Eq. with the analogous to Eq. 5.1,

$$\begin{bmatrix} \mathbb{G}_{11} & \mathbb{G}_{1R'} \\ \mathbb{G}_{R'1} & \mathbb{G}_{R'R'} \end{bmatrix} = \begin{bmatrix} \varepsilon\mathbb{I} - \tilde{\mathbb{E}}_1 & -\tilde{\mathbb{V}}_{1R'} \\ -\tilde{\mathbb{V}}_{R'1} & \varepsilon\mathbb{I} - \tilde{\mathbb{E}}_{R'} \end{bmatrix}^{-1} \tag{5.15}$$

by further decimation of block R' into block 1, we have the analogous of Eq. 5.10, the decimation of blocks 2 and R' into block 1 as

$$\tilde{\mathbb{E}}_1 = \mathbb{E}_1 + \tilde{\mathbb{V}}_{1R'}(\varepsilon\mathbb{I} - \tilde{\mathbb{E}}_{R'})^{-1}\tilde{\mathbb{V}}_{R'1} \tag{5.16}$$

where $\mathbb{V}_{1R}$ is given by $[\mathbb{V}_{12}, \mathbb{V}_{1R'}]$. If the last block partition preserve a three-diagonal structure, with $\mathbb{V}_{1R'} = \mathbb{V}_{R'1} = 0$, then we have that $\tilde{\mathbb{E}}_1 = \mathbb{E}_1 + \Sigma_{1R'}$ with,

$$\Sigma_{1R'} = \mathbb{V}_{12}(\epsilon\mathbb{I} - \mathbb{E}_2 - \Sigma_{2R'})^{-1}\mathbb{V}_{21} \tag{5.17}$$

For further partition to an arbitrary number of clusters, we have:

$$\Sigma_{i,j} = \mathbb{V}_{i,i+1}\left(\epsilon\mathbb{I} - \mathbb{E}_{i+1} - \Sigma_{i+1,j}\right)^{-1}\mathbb{V}_{i,i+1}^{T} \tag{5.18}$$

$$\Sigma_{j,i} = \mathbb{V}_{j,j-1}\left(\epsilon\mathbb{I} - \mathbb{E}_{j-1} - \Sigma_{j-1,i}\right)^{-1}\mathbb{V}_{j,j-1}^{T} \tag{5.19}$$

provided that the final structure preserves a three-diagonal form and where $j > i$. We recall that corrections by the presence of the leads have been previously included in the site energies (Eq. 3.16). Leaving sites i and j,

$$\tilde{\mathbb{E}}_i = \mathbb{E}_i + \Sigma_{i,1} + \Sigma_{i,j} \tag{5.20}$$

$$\tilde{\mathbb{E}}_j = \mathbb{E}_j + \Sigma_{j,i} + \Sigma_{j,N} \tag{5.21}$$

$$\tilde{\mathbb{V}}_{i,j} = \tilde{\mathbb{V}}_{i,j-1}(\epsilon\mathbb{I} - \mathbb{E}_j - \Sigma_{j,1})^{-1}\mathbb{V}_{j-1,j} \tag{5.22}$$

With this methodology, it is straightforward to calculate *exactly* each i, j element of the complete Green's function matrix, by decimation of the entire system into sites i and j,

$$\begin{bmatrix} \mathbb{G}_{ii} & \mathbb{G}_{ij} \\ \mathbb{G}_{ij} & \mathbb{G}_{jj} \end{bmatrix} = \begin{bmatrix} \varepsilon\mathbb{I} - \tilde{\mathbb{E}}_i & -\tilde{\mathbb{V}}_{ij} \\ -\tilde{\mathbb{V}}_{ji} & \varepsilon\mathbb{I} - \tilde{\mathbb{E}}_j \end{bmatrix}^{-1} \tag{5.23}$$

and using Eq. 5.1 for the two block matrix inverse. This procedure is shown diagrammatically on 5.1 and is the analog of the method described in section 2.2.4.

Note that the diagonal elements easily calculated evaluating $\sim N$ energy corrections of the form, Σ_{i1} and Σ_{iN}, where all the sites have been decimated into site i,

$$\mathbb{G}_{ii} = \left[\epsilon\mathbb{I} - \mathbb{E}_i - \Sigma_{i1} - \Sigma_{iN}\right]^{-1} \tag{5.24}$$

and that in order to compute all the non diagonal elements of the GF matrix, we need to evaluate $\sim N^2$ energy corrections Σ_{ij}'s.

However, for tridiagonal block Hamiltonians it is possible to speed up the computation of non-diagonal Green's function elements. Non-diagonal block matrix elements of the GF could be obtained in terms of the diagonal ones, avoiding the need of the evaluation of $\sim N^2$ Σ_{ij}'s. This is the case for the trivial tridiagonal form shown in Eq. 5.7. In the extension for the general case,

$$\mathbb{G}_{i,j} = \mathbb{G}_{i,i}\prod_{k=i}^{j-1}\Sigma_{k,N}\mathbb{V}^{-1}_{k+1,k} \tag{5.25}$$

$$\mathbb{G}_{j,i} = \mathbb{G}_{j,j}\prod_{k=j}^{i-1}\mathbb{V}^{-1}_{k-1,k}\Sigma_{1,k} \tag{5.26}$$

where $i < j$. Although these expressions have been written in terms of hopping matrix inverses, $\mathbb{V}^{-1}$, Eqs. 5.25 and 5.26 are still accurate when the hopping matrices are singular. This is because the hopping matrix inverse cancels out with the hopping in the Σ definition, as it can be seen in Eqs 5.19 for example. These formulas represent the matricial formulation of those discussed in section 3.3.3, where the computational strategies of the D'Amato-Pastawski model for one-dimensional systems are reviewed.

In most cases, $\mathbb{G}^R_{ij} = \mathbb{G}^R_{ji}$, and therefore Eqs. 5.25 and 5.26 are equivalent. However, both equations were explicitly individualized for those cases in which this symmetry is broken, as in quantum pumping [Tor05].

5.2 Multiterminal D'Amato-Pastawski model

To obtain the total transmission on each channel, we can take advantage of the decimation procedures discussed above, with a simple observation. Eq. 3.18

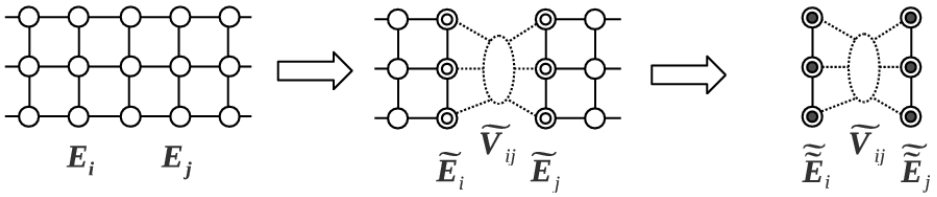

Figure 5.1: *Diagrammatic representation of the decimation scheme to calculate the elements of the Green function.*

is easily rearranged in terms of the total reflection $R_{\alpha i,\alpha,i} = 1 - \sum_{\beta,j} T_{\beta j,\alpha i}$ for process α at site i:

$$I_{\alpha i} = \frac{2e}{h} \sum_{\beta=L,\phi} \sum_{j=1}^{N} \{T_{\alpha i,\beta j}(1 - \delta_{\alpha,\beta}\delta_{i,j}) - (1 - R_{\alpha i,\alpha i})\delta_{\alpha,\beta}\delta_{i,j}\}\delta\mu_{\beta,j} \tag{5.27}$$

In a compact notation, Eq. 5.27 can be expressed in a matrix form, $\overrightarrow{I} = \frac{2e}{h}\mathbb{T}\overrightarrow{\delta\mu}$, where the transmissions matrix can be arranged in a block structure, grouping the terms that connect real or fictitious channels in the system,

$$\begin{pmatrix} I_{L1} \\ \vdots \\ I_{LN} \\ 0 \\ \vdots \\ 0 \end{pmatrix} = \frac{2e}{h} \left(\begin{array}{c|c} \mathbb{T}_{LL} & \mathbb{T}_{L\phi} \\ \hline \mathbb{T}_{\phi L} & \mathbb{T}_{\phi\phi} \end{array}\right) \begin{pmatrix} \mu_{L1} \\ \vdots \\ \mu_{LN} \\ \mu_{\phi 1} \\ \vdots \\ \mu_{\phi N} \end{pmatrix} \tag{5.28}$$

In this case, $\mathbb{T}_{\alpha\beta}$ relates transmissions of probes associated with process types $\alpha = L, \phi$ and $\beta = L, \phi$. The fact that on-site chemical potentials at incoherent channels ensure that no net current flows through them, allows us to eliminate them through a simple decimation, leading to "effective" transmissions associated with transport between channels with current flows, as shown in Eqs. 3.31-3.32.

The decimative procedure involves a simple algebraic relation between the real channels of the system and the chemical potentials associated with currents

drops or sources:

$$\mathbb{T}^{-1}\begin{bmatrix} I_1 \\ \vdots \\ I_N \\ 0 \\ \vdots \\ 0 \end{bmatrix} = \frac{2e}{h}\begin{bmatrix} \mu_1 \\ \vdots \\ \mu_N \\ \mu_{\phi 1} \\ \vdots \\ \mu_{\phi N} \end{bmatrix} \Rightarrow [\mathbb{T}^{-1}]_{LL}\begin{bmatrix} I_1 \\ \vdots \\ I_N \end{bmatrix} = \frac{2e}{h}\begin{bmatrix} \mu_1 \\ \vdots \\ \mu_N \end{bmatrix} \tag{5.29}$$

which implies $\overrightarrow{I} = \frac{2e}{h}\tilde{\mathbb{T}}\overrightarrow{\delta\mu}$, where $\tilde{\mathbb{T}} = [[\mathbb{T}^{-1}]_{LL}]^{-1}$ contains the effective transmissions between real channels in the system. Using Eqs. 5.3 and 5.7, we have:

$$\tilde{\mathbb{T}} = \mathbb{T}_{LL} - \mathbb{T}_{L\phi}[\mathbb{T}_{\phi\phi}]^{-1}\mathbb{T}_{\phi L} \tag{5.30}$$

and for the matrix elements of $\tilde{\mathbb{T}}$, this implies a recursive scheme,

$$\tilde{\mathbb{T}}_{ij}^{(k)} = \tilde{\mathbb{T}}_{ij}^{(k-1)} - \frac{\tilde{\mathbb{T}}_{i,k}^{(k-1)}\tilde{\mathbb{T}}_{k,j}^{(k-1)}}{\tilde{\mathbb{T}}_{k,k}^{(k-1)}} \tag{5.31}$$

where $k \,\epsilon\, \{\phi 1 ... \phi N\}$ and $\tilde{\mathbb{T}}_{ij}^{(k)}$ stands for the matrix element $i, j \,\epsilon\, \{L1 ... LN\}$ of matrix $\mathbb{T}$ after the decimation of k incoherent channels. Once that all incoherent channels were decimated, we have an effective transmission matrix $\tilde{\mathbb{T}}$ given by:

$$\tilde{\mathbb{T}} = \begin{bmatrix} (\tilde{R}_{L1,L1} - 1) & \tilde{T}_{L1,L2} & \cdots & \tilde{T}_{L1,LN} \\ \vdots & \vdots & \ddots & \vdots \\ \tilde{T}_{LN,L1} & \tilde{T}_{LN,L2} & \cdots & (\tilde{R}_{LN,LN} - 1) \end{bmatrix} \tag{5.32}$$

which accounts for decoherent transmission through different paths of the system. This effective transmission matrix relates real currents on each site of the sample with the voltage drops associated with each electron reservoir. It should by noticed that by the Kirchhoff law, rows and columns sums over $\mathbb{T}$ and $\tilde{\mathbb{T}}$ must be zero.

Although this is the most general problem, in most cases one deals with the situation in which there is an unique voltage drop across every possible real system channels. On this cases, there is one chemical potential associated with electron injection and the others electrodes present in the sample are connected with chemical potentials with (particle) populations at the same lower reference energy. We will label "L" (or "Left") the lead associated with electron source and "R" (or "Right") those associated with electron sinks,

because of the similarity with the simplest case of transmittance between two electrodes. Assuming, for the sake of simplicity, that the left lead is only connected to site 1, and requiring a unique voltage drop with $\delta\mu_i \equiv 0 \ \forall_{i\neq 1}$, we summarized the formulation of the problem after the incoherent channels decimation as:

$$I_i = \frac{2e}{h}\tilde{T}_{Ri,L1}\mu_{L1} = GV \tag{5.33}$$

where G is the associated conductance and V is the voltage drop in volts. In the simplest case of single channel transport, the effective matrix $\tilde{\mathbb{T}}$ has dimension 2×2.

5.3 Application examples

As a corollary of the recipes presented so far, we state that environment interactions that could be approximated within a FGR, are treated as decoherence sources by DP model. However, stronger interactions must be explicitly incorporated into the description, providing extra available degrees of freedom. An extended tight-binding Hamiltonian, generally in the form of a multi-terminal system, can be use to treat these problems in some approximation. The multi-channel formulation allows to distinguish between independent contributions to the total decoherent transmission.

In fact, electronic nanodevices are intrinsically multi-channel systems. Polarons and time-dependent interactions are examples in which some degrees of freedom, as some phonon-electron couplings, must be treated explicitly while others could be question-less sources of decoherent processes. To illustrate the methodology presented in the previous sections, we present simple examples of multi-terminal transport in which the scheme of the DP model is applied to account for decoherence.

5.3.1 Decoherent polaronic model

We start considering a simple model which provides an explicit description of a single vibrational mode coupled to a "local" electronic state of a particular site i of the sample Hamiltonian. Although this problem is discussed extensively in Ref. [PFM02], here we are interested in taking into account decoherence effects

on the one-electron transmission probability. The system Hamiltonian is

$$H_S = \hbar\omega_0 \hat{b}^+ \hat{b} + \sum_{\alpha=1}^{N} E_\alpha \hat{c}_\alpha^+ \hat{c}_\alpha + \sum_{\alpha=1}^{N} V_g \hat{c}_\alpha^+ \hat{c}_\alpha (\hat{b}^+ + \hat{b}) \tag{5.34}$$

where the first and second term represents the phonon and electron degrees of freedom respectively and the last term is the coupling between them. The eigenstates of this Hamiltonian are analogous to the polaron states of the Holstein's local polaron model [AMPB94, WJW88]. The eigenvalues are given by,

$$E_{\alpha,n} = E_\alpha + \hbar\omega_0 \left(n + \frac{1}{2} \right) - \frac{|V_g|^2}{\hbar\omega_0} \tag{5.35}$$

As discussed in Ref. [PFM02], it is clear that the phonon absorption / emission process can be viewed as a "vertical" hopping in a two-dimensional network. The Fock space is equivalent to the electron tight-binding model with an expanded dimensionality [AMPB94]. For simplicity it is considered the case of a single state, or "resonant" state, of energy E_0 in the region of interest. The problem for an electron that tunnels trough the system can be mapped to the one-body problem showed in Fig. 5.2.

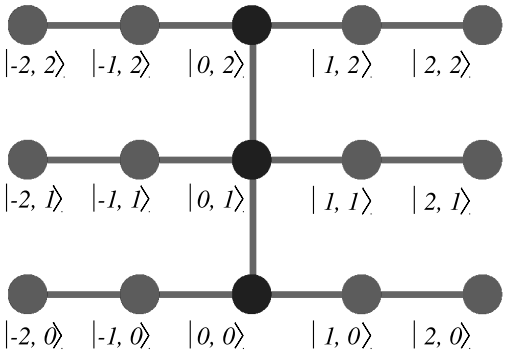

Figure 5.2: *Fock space representation of the system Hamiltonian.*

When an electron comes from the left while there are n_0 phonons in the well, it arrives at the resonant site where it couples to the phonon field, and it can either keep the available energy E as kinetic energy or change it by emitting or absorbing n phonons. Each of this processes contributes to the

total "multichannel" *coherent* transmission which is given by,

$$T = \sum_n T_{n_0+n,n_0} \tag{5.36}$$

It must be stressed that, in this over-simplified example, there is no proper treatment of Pauli exclusion principle. Prima facie, "vertical" hoppings could be blocked by the presence of other electrons and the exclusion principle might play a crucial role. However, with a little more attention, a simple model can be constructed in which vertical process are properly included, consistently transformed into a total energy conserving flow where the Pauli blocking factors do not appear at all. The insight is given in section 3.2.2, where the problem of the exclusion principle is discussed. A simplified picture with the basic ingredients is shown on Fig. 5.3 The key is that the initial "phonon" populations

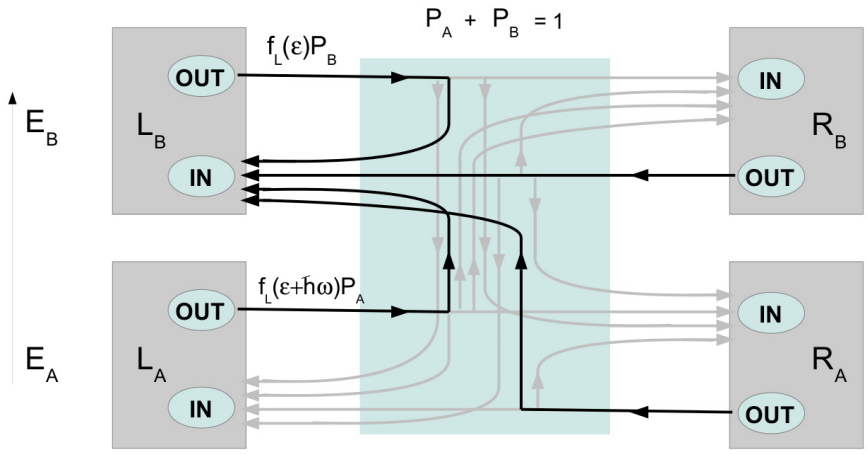

Figure 5.3: *A construction for a simple model in which electronic vertical process are consistently transformed into an total energy conserving flow. The initial "phonon" populations are transformed into quantum channel probabilities. Scattering states that contribute to a single incoming channel are highlighted with bold lines. Notice that unitary of scattering matrix imposes that total incoming probability is always smaller than one. Thus, the Pauli blocking factor is not required.*

are transformed into probabilities associated with each channel. The linear response conductance is obtained from the static expressions. In this simple model, the Pauli principle is circumvented, since the absence of overflow everywhere is guaranteed. Note that a treatment beyond the linear response is possible, with a self-consistent evaluation of the phonon populations. However,

this interesting treatment involves little more complex expressions and exceeds the purpose of this brief section. We presented it outlined to state that the one-electron picture for this polaronic systems is valid, but needs a little more attention than the one given in the following discussions: the underlying idea is that the transport problem in Landauer's picture is builded in terms of scattering states that can not be blocked by Pauli factors. Although the range validity of the following results might be narrow, the example remains sufficiently rough to illustrate in simple terms the methodology of the DP model for multi-terminal transport.

In order to include the effects of decoherence in the transport properties of this system, we need to introduce a finite time-life to the polaron states through an imaginary correction to the resonant energies, given by Eq. 3.15. The available "direct" channels are associated with the transmission probabilities, $T_{Rn',Ln}$, $T_{Ln',Ln}$ and the available incoherent channels, are those related to $T_{Ln,\phi n}$, $T_{Ln,\phi n'}$, $T_{\phi n,\phi n'}$. If we assume that electrons are injected with $n_0 = 0$ phonons in the well, then the total transmission is simply,

$$\tilde{T} = \sum_{i=1}^{N} \tilde{T}_{Rn,L0} \tag{5.37}$$

where each $\tilde{T}_{L0,Rn}$ includes the decimation of the incoherent channel, just as in Eq. 3.31. The results for different processes and for total transmission are shown in Fig. 5.4. As it can be seen in the figures, in general the effect of decoherence on transmission is to broaden the resonances, lowering the peaks, and lifting the tails. Note also the coherent nature of the anti-resonances, that are destroyed after decoherent processes.

On Fig. 5.5, a color map for the transmission probability as a function of dephasing strength and incident energy is shown.

5.3.2 Time-dependent problems

The last section of the introductory chapter is devoted to the transport properties of time-periodic dependent Hamiltonians. As shown there, the extra degree of freedom that appeared due to the interaction of the electrons with a photon field can be mapped into a one-particle Floquet Hamiltonian in an extended Hilbert space, that satisfies an eigenvalue equation similar to the

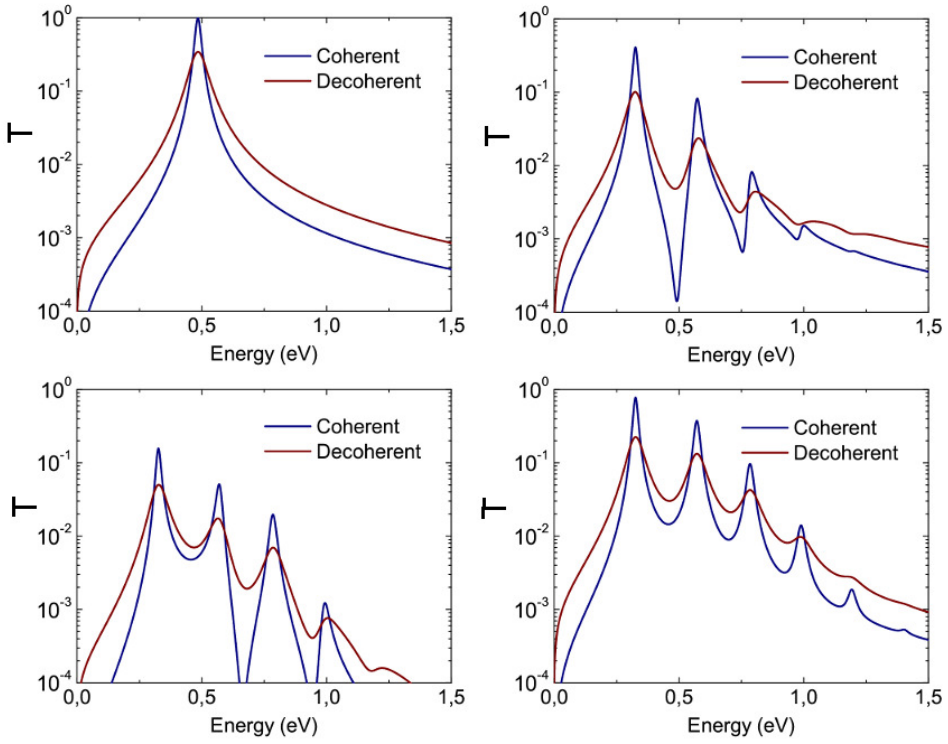

Figure 5.4: *Adimensional conductance for $\hbar\omega_0 = 0.2eV$, $E_0 = 0.5eV$ and $V_g = 0.1eV$ (a) without electron-phonon interaction; (b) an electron leaving the sample without extra phonons; (c) an electron leaving the sample with one extra phonon; (d) Total conductance.*

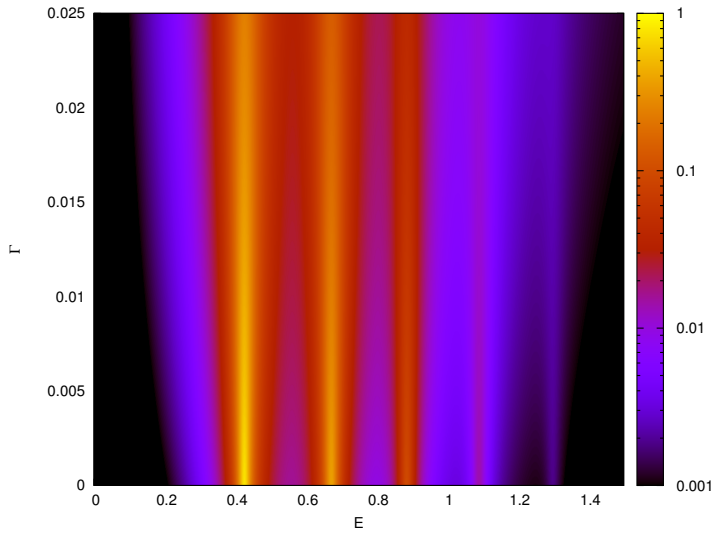

Figure 5.5: *Color map for the total transmission probability of the polaronic system as a function of the energy and Γ.*

time-independent Schrödinger equation. This extended space is the analog of the Fock space of the previous section. The advantage in this case is that, under wide applicable assumptions, the one-electron Landauer's picture of transport is a good approximation, at least for average DC currents. As a consequence, the results of the DP model are more representative.

Therefore, here we consider a time-dependent quantum system whose dynamics is governed by a Schrödinger equation given by:

$$i\hbar\frac{d}{dt}|\psi(t)\rangle = \left[\hat{H}(t) + \hat{\Sigma}\right]|\psi(t)\rangle \tag{5.38}$$

where the Hamiltonian of the system depends explicitly on time. The self-energy $\hat{\Sigma}$ comes, as before, after a decimation of the environmental degrees of freedom, and implies a no-unitary time evolution,

$$\hat{\Sigma} = \hat{\Sigma}_L + \hat{\Sigma}_\phi \tag{5.39}$$

where $\hat{\Sigma}_L$ is the self-energy associated with the leads and $\hat{\Sigma}_\phi$ accounts for dephasing processes. Electrons interacting with a time dependent potential can gain or loss energy. If the potential is periodic in time, $\hat{H}(t) = \hat{H}(t+\tau)$ with period τ, we can describe the state of the system using the Floquet theory [KLH05a]. We consider the system Hamiltonian given by,

$$\hat{H}_S = \sum_{i=1}^{N}\left\{E_i(t)\hat{c}_i^+\hat{c}_i + \sum_{j=1 j\neq i}^{N} V_{ij}\left[\hat{c}_i^+\hat{c}_j + \hat{c}_j^+\hat{c}_i\right]\right\}, \tag{5.40}$$

for the special case in which the electron-photon interaction is only possible at site with α,

$$E_i(t) = E_i + V_0\cos(\omega_0 t)\delta_{i,\alpha} \tag{5.41}$$

In this simple case, electrons arriving at site α are able to absorb or emit photons and leave the site with energies $\epsilon' = \epsilon + n\hbar\omega_0$. As discussed before, the absorption/emission process can be viewed as a "vertical" hopping in a two-dimensional network [Tor05].

For simplicity it is considered the case of a single state, or "resonant" state, of energy E_α in the region of interest. The problem for an electron that tunnels trough the system can be mapped to the one-body problem in the same way as in the case showed in Fig. 5.2. However, in the floquet system the vertical hopping does not depend on the channel label n.

When an electron comes from the left, it arrives at the resonant site where it couples to the photon field, and it can either keep the available energy E as kinetic energy or change it by emitting or absorbing n photons. Each of this processes contributes to the total "multichannel" *coherent* transmission which, as in the phonon example, is given by,

$$T = \sum_{n\sim-\infty}^{\infty} T_{n_0+n,n_0} \tag{5.42}$$

Note that in the interaction with the photon field there is yet another difference with the phonon example. The amount of available channels is no limited for photon absorption nor for emission. However, again only a limited range of channels, $|n| < N_{max}$ would lead to finite transmission amplitudes [Tor05], and only within this range are the real channels that need to be considered.

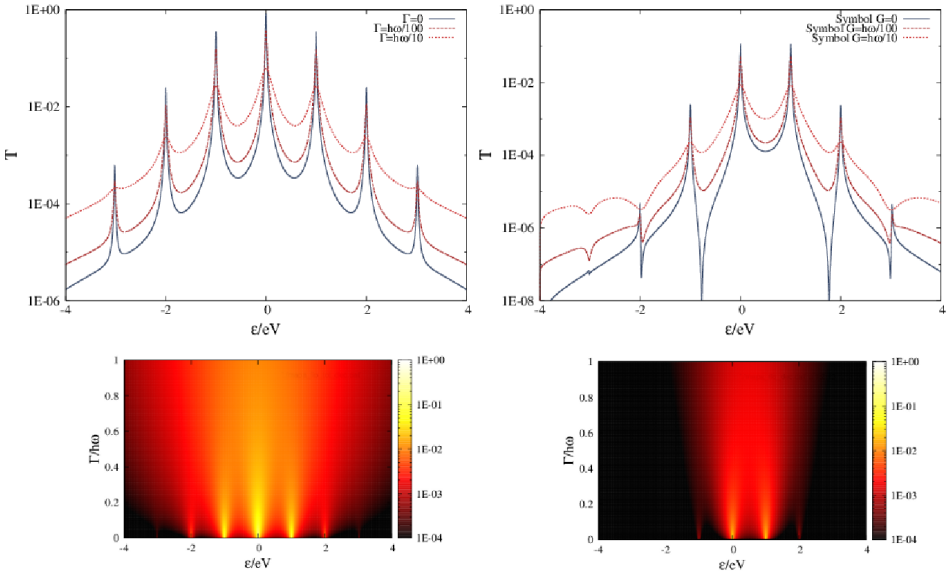

Figure 5.6: *Multichannel decoherent transmission for the periodic time-dependent model. On the left, total conductance. On the right hand side, an electron leaving the sample emitting one photon. In this example,* $\hbar\omega = 1eV$*,* $E_F = 0eV$ *and* $V_g = 0.5eV$*.*

In order to include the effects of decoherence in the transport properties of this system, we need to introduce a finite time-life to the electron states through an imaginary correction to the resonant energies, given by Eq. 3.15. The available "direct" channels are associated with the transmission probabilities,

$T_{Rn',Ln}$,$T_{Ln',Ln}$ and the available incoherent channels, are those related to $T_{Ln,\phi n}$, $T_{Ln,\phi n'}$, $T_{\phi n,\phi n'}$,

$$\tilde{T} = \sum_n \tilde{T}_{Rn,Ln'} \tag{5.43}$$

where each $\tilde{T}_{L0,Rn}$ includes the decimation of the incoherent channel, just as in Eq. 3.31. The results for total transmission with different values of Γ are shown in Fig. 5.6.

5.3.3 Carbon nanotubes

Allotrops of carbon with cylindrical structure are usually called *carbon nanotubes* (CNTs). In particular, single-walled CNTs are formed by only one sheet of hexagonally arranged carbon atoms. In multi-walled CNTs, individual nanotubes align themselves into ropes in a pi-stacking. Since their discovery, they have attracted considerable scientific and engineering attention due to their outstanding mechanical and electrical properties. Depending on their helicity, CNTs exhibit either semi-conducting or metallic behavior, and, for low resistance contacts, ballistic transport is observed in the low bias regime. In particular, this section is devoted to the study of decoherent transport in

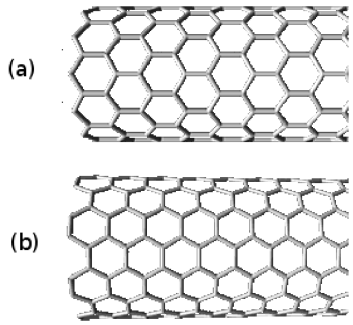

Figure 5.7: *Single-walled carbon nanotubes corresponding to the structures: (a) zigzag, and (b) armchair.*

single-walled carbon nanotubes corresponding to zigzag and armchair structures, illustrated in Fig. 5.7. The structure symmetry of a nanotube strongly affects its electrical properties. In ideal zigzag CNTs, transport is nearly metallic, with a very small band gap, if the number of carbon atoms in its diameter is a multiple of 3. All armchair CNTs do not have gaps and behave as metals.

A nearest neighbors tight-binding description for the π Hamiltonian matrix of CNTs has a tridiagonal block structure. The block dimension is given by the number of carbon atoms that defines the width of the nanotube. In the armchair (n, n) structure, the block dimension is $2n \times 2n$. Diagonal blocks are given in the form

$$\mathbb{E} = \begin{pmatrix} \ddots & & & & & \\ & E & V & 0 & 0 & \\ & V & E & 0 & 0 & \\ & 0 & 0 & E & V & \\ & 0 & 0 & V & E & \\ & & & & & \ddots \end{pmatrix} \quad \textit{(Armchair)} \tag{5.44}$$

where E are the site energies and V the hoppings. The hopping blocks have the form

$$\mathbb{V} = \begin{pmatrix} \ddots & & & & & V \\ & 0 & 0 & 0 & 0 & \\ & V & 0 & 0 & 0 & \\ & 0 & V & 0 & 0 & \\ & 0 & 0 & V & 0 & \\ 0 & & & & & \ddots \end{pmatrix} \quad \textit{(Armchair)} \tag{5.45}$$

the block hopping sequence is $..., \mathbb{V}, \mathbb{V}^T, \mathbb{V}, \mathbb{V}^T ....$, and the tridiagonal block Hamiltonian is

$$\mathbb{H} = \begin{pmatrix} \ddots & & & & & \\ & \mathbb{E} & \mathbb{V} & 0 & 0 & \\ & \mathbb{V}^T & \mathbb{E} & \mathbb{V}^T & 0 & \\ & 0 & \mathbb{V} & \mathbb{E} & \mathbb{V} & \\ & 0 & 0 & \mathbb{V}^T & \mathbb{E} & \\ & & & & & \ddots \end{pmatrix} \quad \textit{(Armchair)} \tag{5.46}$$

In the zigzag $(m, 0)$ structure, blocks have dimension $m \times m$, $\mathbb{E}$'s are diagonal, and is straightforward to show that the hopping block sequence has the form $..., \mathbb{V}_1, \mathbb{V}_2, \mathbb{V}_1^T, \mathbb{V}_2, ...$

Coherent and decoherent transmission probabilities as a function of the (incident) Fermi energy for zigzag CNTs are shown of Fig. 5.8. Decoherent degrades and smooths the transmission function across the CNT.

One of the most remarkable results, however, is the recovering of the Ohm's law for decoherent transmission. The results for T^{-1} as a function of the nanotube length, for different values of Γ_ϕ, are shown in Fig. 5.9. These qualita-

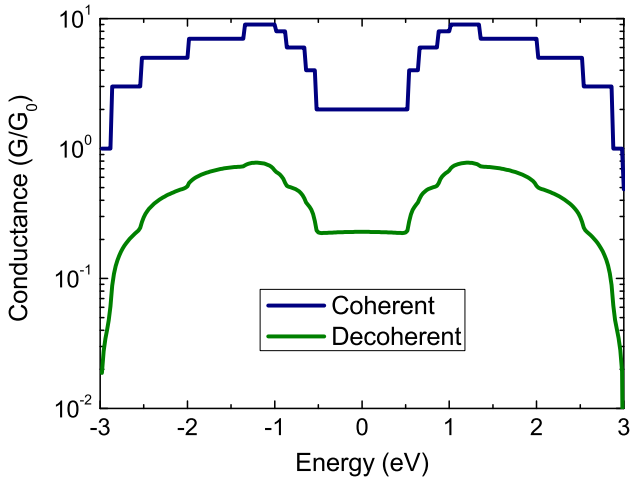

Figure 5.8: *Coherent and decoherent transmission probabilities as a function of the Fermi energy for zigzag CNTs of 9 atom width.*

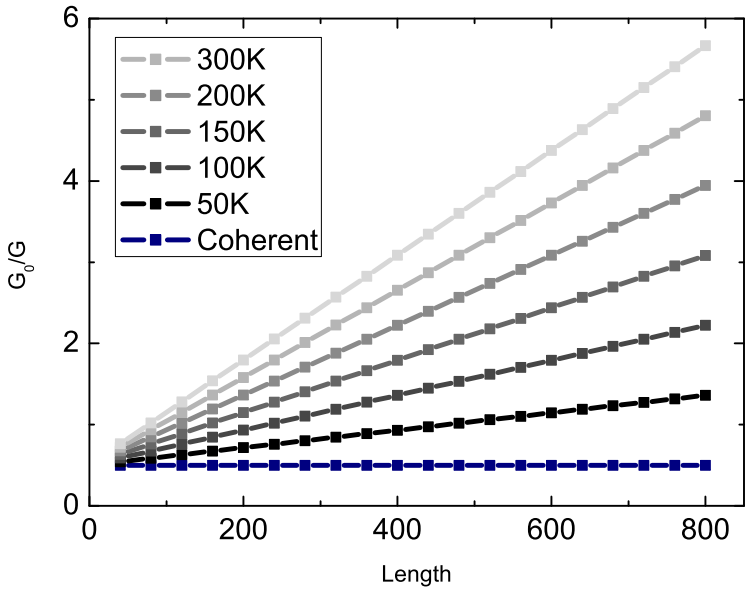

Figure 5.9: $\left(\frac{G}{G_0}\right)^{-1}$ *as a function of the length for armchair (5,5) CNTs. Coherent transport is ballistic, as expected. Remarkably, the Ohm's law is recovered for decoherent transport.*

tive results are in agreement with recent four-point measurements of resistance in single-walled nanotubes, where the Ohm's law is observed experimentally [GCF+05].

5.4 Summary

Many-body interactions suffered by carriers in electronic devices that can not be treated within the simple Fermi golden rule approximation, provide extra degrees of freedom that must be accounted explicitly in the transport description. This situation, in some approximation, can be mapped into the one-electron picture as a multi-terminal setup, transferring the complexity of the many-body interactions to the geometry of the one-electron transport problem. On the other hand, system-environment interactions that can be approximated within a FGR, are treated as decoherence sources with the insight of the DP model.

In fact, electronic nanodevices are intrinsically multi-channel systems. Polarons and time-dependent interactions are examples in which some degrees of freedom, as some phonon-electron couplings, must be treated explicitly while others could be question-less sources of decoherent processes. To this end, exact and computational efficient methods to analyze decoherent transport on intrinsically multi-terminal setups were presented. The matrix continued fractions approach, as an extension of the continued fractions methods discussed in the introductory chapter, constitutes the strategy to obtain the overall Green function matrix of the system. For tridiagonal block Hamiltonians, a generalization of the "Thouless-Kirkpatrick" formula, that relates non diagonal with diagonal elements of the Green's function, was presented. The Kirchhoff law expressions for the D'Amato-Pastawski model on multichannel systems were derived. In this way, we obtained an efficient method to introduce decoherence in the study of electronic transport in real situations, where the complexity of the system in study prevents the usual approach in which only a single channel is present.

Although in the simple examples considered the effect of decoherence is not highly surprising, compared with the case of polyanilines were its effects produces a dramatic change in the transport properties, the purpose was the

clearest introduction of the methodology involved, and the possibilities for the study of more complex situations, such as quantum pumping, biological systems, etc remains basically with exactly the same approach. Both the understanding of the effects of quantum decoherence and even its proper description in the context of transport problems are still open research subjects in modern physics. However, our expectation is that the methodology introduced, despite its inherent limitations, will provide simple but powerful insight into this blooming field.

6

Magneto-transport in nanowires

The phenomenon in which the electrical resistance of a conductor is affected under the influence of an external magnetic field is known as magnetoresistance. Of substantial importance, this property was discovered by Lord Kelvin and for the next century there was hardly any improvement of the performance of magnetoresistive materials since his work [Fer08]. By the year 1988, two research groups independently discovered materials showing a very large magnetoresistance, now known as giant magnetoresistance (GMR). These materials are also called magnetic multilayers, since the effect is observed in thin-film structures composed of alternating ferromagnetic and non-magnetic layers. The 2007 Nobel Prize in physics was awarded to Albert Fert and Peter Grünberg for the discovery of GMR. The effect is observed as a significant change in the electrical resistance depending on whether the magnetization of adjacent ferromagnetic layers are in a parallel or an anti-parallel alignment. The overall resistance is relatively low for parallel alignment and relatively high for anti-parallel alignment.

The phenomenon of GMR has had a growing interest in last decades. Since its discovery by Albert Fert's and Peter Gründberg's groups, GMR has driven the development of the field of spintronics, with immediate applications in electronic devices [Fer08]. This effect is commonly explained by means of a

simple classical picture that involves important conceptual simplifications based on the so called *sd* model and the two resistors model.

6.1 Mott's *sd* model

The *sd* model was introduced long time ago by Mott [Mot35, Mot36] as a useful simplification of the band structure of transition metals to explain their electronic resistance. Its use is still wide extended for the study of transport properties in ferromagnetic materials. In this simple model, the rather complicated band structure of ferromagnets is assumed to be comprised by only two bands, of s and d type. The electrons of the d band do not contribute directly to the conductance, since their effective mass is large and have poor mobility. Electrons in the s band are nearly free. In presence of a magnetic field, these bands suffer a splitting. The sub-bands of electrons with up and down spin orientations have a different number of occupied states: this defines a majority spin direction. The s band is parabolic, with a spin-split potential energy Δ resulting from the *sd* exchange interaction. The d band is very narrow, with a significant difference in the number of up and down states at the Fermi energy [Fal06]. This is depicted on Fig. 6.1.

The exchange interaction between electrons in s and d bands has a characteristic rate which can be determined by the Fermi Golden Rule (FGR):

$$\frac{1}{\tau_{\phi,\sigma}} = \frac{2\pi}{\hbar} |V_\phi|^2 N_{d,\sigma}(\varepsilon_F) \tag{6.1}$$

where σ accounts for the orientation of the electron spin in the conduction band, V_ϕ is the strength of the exchange coupling and $N_{d,\sigma}$ is the density of states of the sub-band for the spin σ in the band d. Since this rate is spin-dependent, electrons with their spin aligned to the field suffer more scattering events than the others, because of the relation $N_{d,\downarrow}(\varepsilon_F) > N_{d,\uparrow}(\varepsilon_F)$.

In a Drude description, $\tau_{\phi,\sigma}$ represents the time between collisions and determines the mean free path of the electrons. This rate is associated with a relaxation that, although conserving spin, leads to quantum decoherence of the conduction electrons.

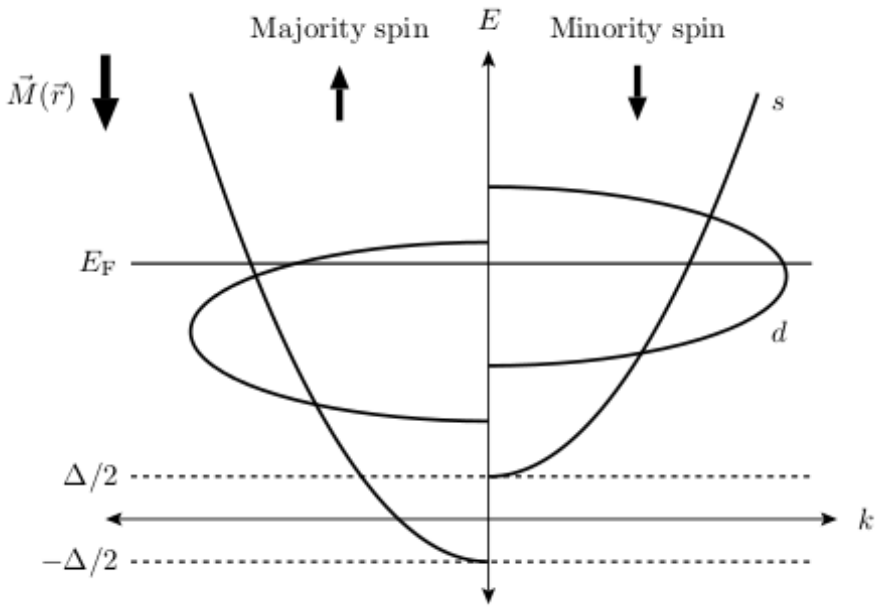

Figure 6.1: *Sketch of the simplified band structure in the sd model. The arrows denote the electron spin direction in each sub-band with respect to the magnetization direction [Fal06].*

6.2 Two-resistor model

If the system temperature is low compared with the Curie's temperature, most scattering events will conserve the spin direction. The length scale for spin-reversing scattering (spin diffusion length) ℓ_{sf}, is generally much larger than the spin-dependent mean free paths ℓ_σ. Therefore, in transport over distances less that ℓ_{sf}, spin-up and spin-down electrons can be considered as almost independent and they will represent two parallel contributions to the net current. Each of these contributions can be characterized by a Drude resistance:

$$R_\sigma = \frac{\hbar}{e^2}\frac{L}{\ell_\sigma} \tag{6.2}$$

where L is the system length. Note that in this one-dimensional case, there is no cross-section factor. The quantity ℓ_σ is related the rate defined in Eq. 6.1 by $\ell_\sigma = v_F \tau_{\phi,\sigma}$, where v_F is the Fermi velocity. Inserting this into Eq. 6.2, one obtains:

$$R_\sigma = \frac{\hbar}{2\pi e^2}\frac{L}{v_F}\left|V_\phi\right|^2 N_{d,\sigma}(\varepsilon) \tag{6.3}$$

Notice that the resistance for the current of electrons with spin σ is proportional to the density of states of the d electrons with the same spin orientation. Hence, electrons with its spins parallel to the magnetic field have higher mean free path and lower resistance.

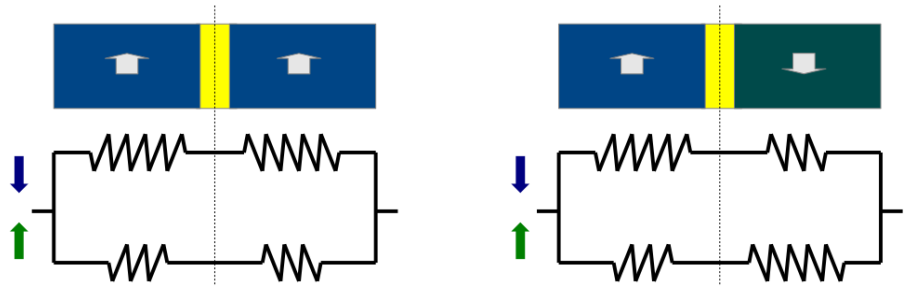

Figure 6.2: *Magnetic configuration and corresponding two-resistor model representation for a GMR bilayer, for (a) parallel configuration and (b) anti-parallel configuration.*

The basic GMR effect can be represented in a ferromagnetic bilayer structure comprising two layers in which the magnetization is either parallel or anti-parallel. This is illustrated on Fig. 6.2, and constitutes the conceptual simplification of trilayer structures known as spin valves [MLPD95], in which two ferromagnetic layers are separated by a non-magnetic metallic layer [Fal06]. The resistance on each configuration can be easily calculated in this simple two-resistor model, using the simplifications introduced above with the *sd* model. In the parallel configuration,

$$R_P = 2R_\downarrow R_\uparrow / \left(R_\downarrow + R_\uparrow\right), \tag{6.4}$$

while on the other,

$$R_A = \frac{1}{2}\left(R_\downarrow + R_\uparrow\right). \tag{6.5}$$

The GMR effect is commonly explained by these different resistances associated with each setup. The classical nature of this description is usually justified assuming that the phase-coherence length, L_ϕ, is significantly smaller than the spin diffusion length, ℓ_{sf}. The simple two-resistor model, hence, contains the essence of the physics involved in the GMR. However, in a more detailed description, based in the Boltzmann equation, ℓ_{sf} must be explicitly included

in order to describe spin-relaxation processes. On intrinsically quantum treatments to this (and related) problems, there is a persistent difficulty in describing relaxation processes that do not occur in the particle reservoirs. Therefore, all quantum approaches are commonly restricted to the case $L \ll \ell_{sf}$.

In a Boltzmann description allowing spin-flip processes, it has been shown [VF93] that, in the anti-parallel configuration, the relaxation of spin on either side of the interface takes the form of an exponential decay. The characteristic length of this decay is ℓ_{sf}. The qualitative results of this description are reproduced on Fig. 6.3 (extracted from Ref. [Fal06]). A very important conjecture

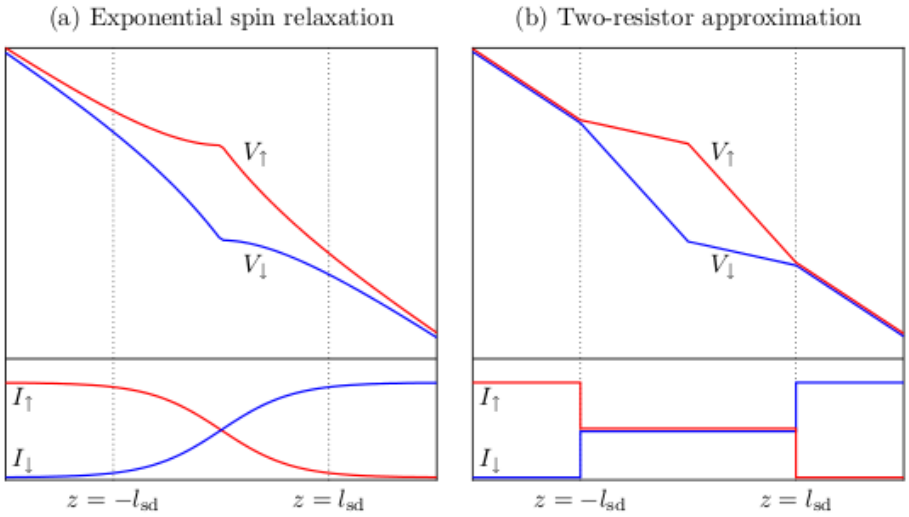

Figure 6.3: *Qualitative diagrams comparing the spin-dependent voltages and currents for the bilayer with anti-parallel configuration in the case of (a) a realistic exponential relaxation of electron spin between up and down channels, and (b) the approximation represented by the corresponding two-resistor model. Extracted from Ref. [Fal06].*

is that each spin channel can be approximately considered to be in local equilibrium, and therefore local spin-dependent electrochemical potentials exists at each point in space [Fal06]. Notice that this is explicitly assumed in the D'Amato-Pastawski model, where the local chemical potentials on each tight-binding site are associated with local interactions of the carriers which have the effect of phase-breaking processes. These interactions are provided by the *sd* exchange. In the following section we show that the DP model provides all the ingredients for a generalized Landauer-Büttiker approach of magnetotransport.

6.3 Generalized Landauer-Büttiker approach

The key insight to go from a purely quantum to a classical description is the proper introduction of the quantum decoherence into the analytical treatment of the problem. This is precisely the insight of the D'Amato-Pastawski DP model [DP90] for decoherent transport. A generalized version of this model that can be fairly applied to account for all the basic characteristics involved in GMR is proposed [FCP]. Its computational power and its robustness becomes evident when the regime $\ell_{sf} \leq L$ is considered.

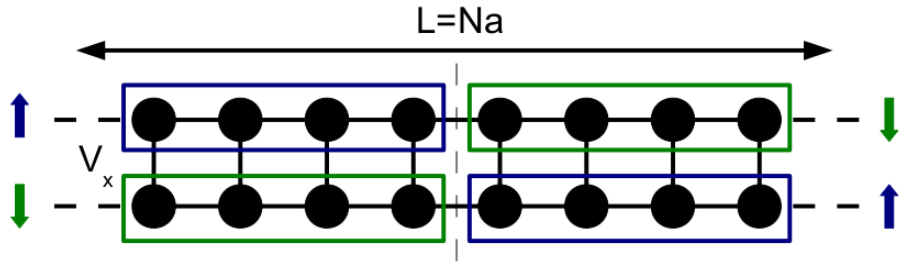

Figure 6.4: *Tight-binding model for magneto-transport in a bilayer structure. Each chain is associated with a spin current. The interface is illustrated with a dashed line.*

We deal with a quantum approach to a generalized two-resistor model. The problem of electron transport across bilayer structures can be addressed drawing on the Landauer-Büttiker picture [IL99] generalized [Pas91, Pas92] to include spin-conserving and spin-reversing processes. The latter can be modeled by a direct coupling between the electrons in the s band. However, spin-conserving processes are the consequence of the interaction of the electrons in the s band with the environmental degrees of freedom provided by the electrons in the d band, which do not contribute directly to the conductance. Spin-conserving processes, thus, can be regarded as decoherent events. Therefore, the quantum mechanical description of this problem can be simplified by a single particle tight-binding Hamiltonian for electrons in the s band that includes the system-environment interactions properly. A sketch is illustrated on Fig. 6.4.

The DP model refers to a simple way to account for the infinite degrees of freedom of the thermal bath and the particle reservoirs. In this case, the

sample's Hamiltonian is described in a nearest neighbor tight-binding approach, with local spin-reversing interactions

$$\hat{H}_S = \sum_{n=1}^{N} \sum_{\sigma=\uparrow,\downarrow} [E_{n,\sigma}\hat{c}^{\dagger}_{n,\sigma}\hat{c}_{n,\sigma} + \sum_{m} V_{n\sigma,m\sigma}\hat{c}^{\dagger}_{n\sigma}\hat{c}_{m\sigma}\delta_{n,m\pm1} + V_x\hat{c}^{\dagger}_{n,\sigma}\hat{c}_{n,\sigma'}\,(1-\delta_{\sigma,\sigma'})] \tag{6.6}$$

where the labels n and m indicate sites on a lattice, N is the total number of sites, and σ denotes the spin direction. An *effective* Hamiltonian incorporates the leads and the interactions with the environment:

$$\hat{H}_{\text{eff.}} = \left(\hat{H}_S - \mathrm{i}\eta\ \hat{I}\right) + \hat{\Sigma}_L + \hat{\Sigma}_R + \hat{\Sigma}_\phi, \tag{6.7}$$

where $\hat{\Sigma}_L = \Sigma_L(\hat{c}^{\dagger}_{1\uparrow}\hat{c}_{1\uparrow}+\hat{c}^{\dagger}_{1\downarrow}\hat{c}_{1\downarrow})$ and $\hat{\Sigma}_R = \Sigma_R(\hat{c}^{\dagger}_{N\uparrow}\hat{c}_{N\uparrow}+\hat{c}^{\dagger}_{N\downarrow}\hat{c}_{N\downarrow})$ are, respectively, the self-energies operators describing the escape to the left and the right leads obtained through a Dyson equation,

$$\Sigma_{L(R)} = \frac{V^2}{\varepsilon - (E_0 - \mathrm{i}\eta) - \Sigma_{L(R)}} \tag{6.8}$$

$$= \Delta_{L(R)}(\varepsilon) - \mathrm{i}\Gamma_{L(R)}(\varepsilon), \tag{6.9}$$

where $\Gamma_{L(R)}$ results proportional to the escape rate, and hence to the Fermi velocity, at the $L(R)$ lead.

The spin-conserving scatterings are regarded as decoherent events characterized by a spin-dependent rate $\tau_{\phi,\sigma}$, given by Eq. 6.1. Therefore, as suggested in the DP model [PM01], theses processes can be included in the Hamiltonian description simply through local imaginary correction to the site energies

$$\hat{\Sigma}_\phi = \sum_{\sigma=\uparrow,\downarrow} \sum_{l} -\mathrm{i}\Gamma_{\phi,\sigma}\hat{c}^{\dagger}_{l,\sigma}\hat{c}_{l,\sigma}. \tag{6.10}$$

where $\Gamma_{\phi,\sigma}$ is obtained from Eq. 6.1 as $2\Gamma_{\phi,\sigma} = \hbar/\tau_{\phi,\sigma}$. These imaginary shifts result from the renormalization of the site energies due to the decimation of environmental degrees of freedom. In this way, $\Gamma_{\phi,\sigma}$ can be regarded as an energy uncertainty associated to a decay rate of the local state at site l,σ described by the FGR. We drop any possible dependence on l simplifying the description. Since $\hat{I}$ is the identity operator, η can be taken as an infinitesimal imaginary part of the local energy, $E_{n,\sigma} \to E_{n,\sigma} - \mathrm{i}\eta$, resulting in a decay to the environment in the same sense as the Γ's above.

As usual, given the effective Hamiltonian we have the retarded and advanced Green's functions in terms of the real energy variable ε:

$$\mathbb{G}^R(\varepsilon) = [\varepsilon\mathbb{I} - \mathbb{H}_{\text{eff.}}]^{-1} \tag{6.11}$$

$$= \mathbb{G}^{A\dagger}(\varepsilon), \tag{6.12}$$

where $\mathbb{H}_{\text{eff.}}$ may be non-linear in ε and non-hermitian for $\eta \neq 0$.

To simplify the notation for the following expressions, we first note that in the resulting model setup, every state can be subject to two types of decay Γ_α. Decays toward the leads, via Γ_L and Γ_R, or decays due to spin-conserving events, via $\Gamma_{\phi,\sigma}$. Second, sites on the tight-binding Hamiltonian were labeled by two indices, *real* site i index and spin σ index. We group site indices in the form $(n, \sigma) \to i$. With this notation, latin letters represent sites in the two-dimensional tight-binding Hamiltonian, while Greek letters label decay processes $\alpha = L, R, \phi$. The complete setup for the tight-binding model is shown on Fig. 6.5

With this notation the generalized Fisher-Lee transmission probability between a process α on site i and a process β on site j results [PM01]:

$$T_{\alpha i,\beta j}(\varepsilon) = 2\Gamma_{\beta j}(\varepsilon)G^R_{j,i}(\varepsilon)2\Gamma_{\alpha i}(\varepsilon)G^A_{i,j}(\varepsilon). \tag{6.13}$$

Within the DP model, each decay process α on a site i is associated with a particle reservoir characterized by a chemical potential $\delta\mu_{\alpha i}$ [PM01]. This on-site chemical potentials can be regarded as local voltage probes, that allow keeping track on the total voltage drop across the sample, site by site. With the transmission probabilities given by the generalized Fisher-Lee formula, and invoking linear response, it is possible to compute the net current associated with each process [PM01]:

$$I_{\alpha i} = \frac{e}{h}\sum_{\beta j}\left(T_{\alpha i,\beta j}\delta\mu_{\beta j} - T_{\beta j,\alpha i}\delta\mu_{\alpha i}\right) \tag{6.14}$$

and zero net current is imposed for decoherent processes at each site and energy ε, $I_{\phi i} = 0$. This accounts for an incoherent re-injection of every particle that has decayed through the $\Gamma_{\phi i}$ terms. Eq. 6.14 can be expressed in a compact matrix notation, separating the conceptually different decoherent processes from those associated with the leads:

$$\begin{pmatrix} \overrightarrow{I}_\ell \\ 0 \end{pmatrix} = \frac{e}{h}\mathbb{T}\begin{pmatrix} \delta\overrightarrow{\mu_\ell} \\ \delta\overrightarrow{\mu}_\phi \end{pmatrix} \tag{6.15}$$

where $\mathbb{T}$ is the array of transmission probabilities defined by Eq. 6.14 and can also be subdivided in the same block structure:

$$\mathbb{T} = \begin{pmatrix} \mathbb{T}_{\ell\ell} & \mathbb{T}_{\ell\phi} \\ \mathbb{T}_{\phi\ell} & \mathbb{T}_{\phi\phi} \end{pmatrix} \tag{6.16}$$

With this notation it is stressed that $\mathbb{T}_{\ell\ell}$ only involves terms that connect leads ($\ell = L, R$), $\mathbb{T}_{\phi\phi}$ only involves transmissions between decoherent processes and the blocks $\mathbb{T}_{\ell\phi}$ and $\mathbb{T}_{\phi\ell}$ connect leads with decoherent processes. The local voltage at each site, given by the elements of the vector $\delta\overrightarrow{\mu}_\phi$, can be tracked, after Eq. 6.15, as:

$$\delta\overrightarrow{\mu}_\phi = \mathbb{T}_{\phi\phi}^{-1}\mathbb{T}_{\phi\ell}\delta\overrightarrow{\mu}_\ell \tag{6.17}$$

where the chemical potentials at the leads $\delta\overrightarrow{\mu}_\ell$ are given. Another quantity of interest, is the local current between every pair of sites, and can be computed according to [KW08]:

$$I_{\phi i,\phi j} = \int_{-\infty}^{\infty} d\varepsilon \left[V_{ij}G_{ij}^{<}(\varepsilon) - V_{ji}G_{ji}^{<}(\varepsilon)\right] \tag{6.18}$$

where $\mathbb{G}^{<} = \mathbb{G}^{R}\Sigma^{<}\mathbb{G}^{A}$ and,

$$\Sigma^{<}(\varepsilon) = \sum_{\ell} \delta\mu_\ell \left[\Sigma_\ell^{\dagger}(\varepsilon) - \Sigma_\ell(\varepsilon)\right] \tag{6.19}$$

This approach provides all the basic ingredients to understand the basic properties of magnetotransport in bilayer structures from a quantitative Hamiltonian description. The results obtained with this scheme are shown in the next section.

6.4 Numerical results

We consider a tight-binding representation of spin-up and spin-down electrons of the *s*-band for the anti-parallel bilayer configuration, with 1000 pair of sites. The domain wall is placed exactly on the middle, and is represented by the crossing of the chains. On each site, the *sd* exchange interaction is modeled by a phase-breaking probe acting as a particle reservoir, introducing a spin-dependent local imaginary energy shift Γ_ϕ. This is sketched on Fig. 6.5. In this way, each spin channel can be approximately considered to be in *local*

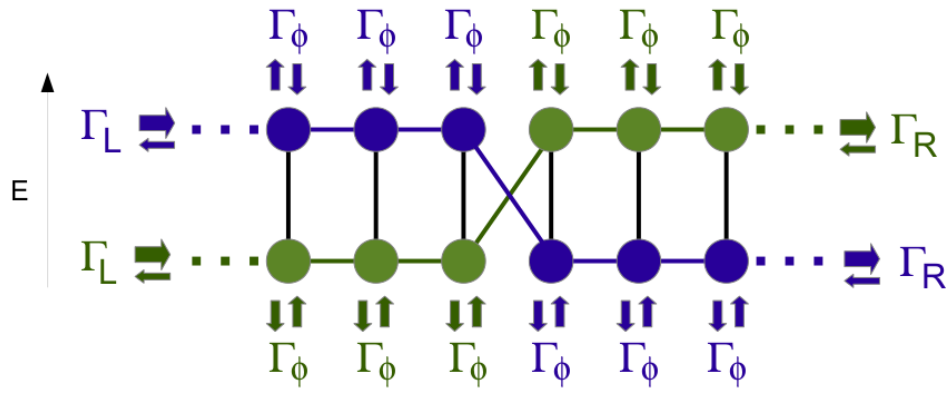

Figure 6.5: *Sketch of the effective tight-binding Hamiltonian in the anti-parallel configuration of the bilayer structure. The sd exchange interaction is modeled by phase-breaking probes acting as a particle reservoirs, introducing a spin-dependent local imaginary energy shift* Γ_ϕ.

equilibrium, and therefore local spin-dependent chemical potentials exists at each site.

First, we neglect spin-flips taking $V_x = 0$ in Eq. 6.7. The results for this case are shown on Fig. 6.6. Trivially, when spin-flip interactions are not allowed the two current contributions are totally independent, and the results of the two-resistor model are obtained. The overall voltage drop is equal for the two

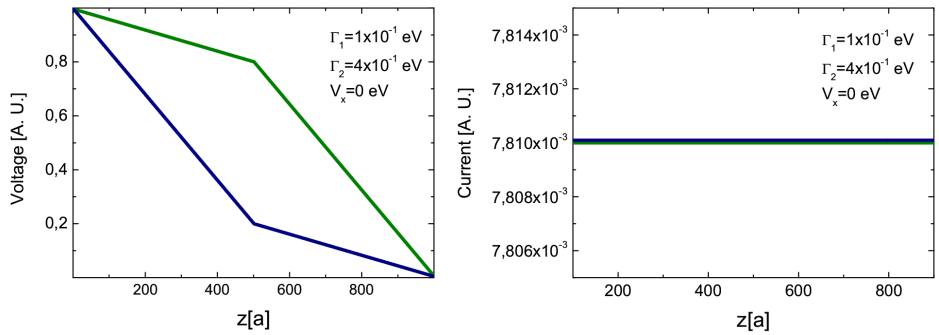

Figure 6.6: *Results of the DP model for the anti-parallel configuration in the bilayer structure, when spin-flips are not allowed. The same results as in the two-resistor model are obtained. On the left hand side, voltage drop. On the right, the associated currents.*

spin directions and since $V_x = 0$, there is no "vertical" flow. As a consequence both currents are equal, as shown on the left hand side in Fig. 6.6.

The results for the most important case, when $V_x \neq 0$, are shown in Fig.

6.7. In this case the powerful insight of the DP model for magnetotransport is appreciated. The exponential relaxation of spins is clearly observed. Currents start in equilibrium with each other and there is a splitting at the interface, as expected [VF93]. At the interface, the external magnetic field is inverted.

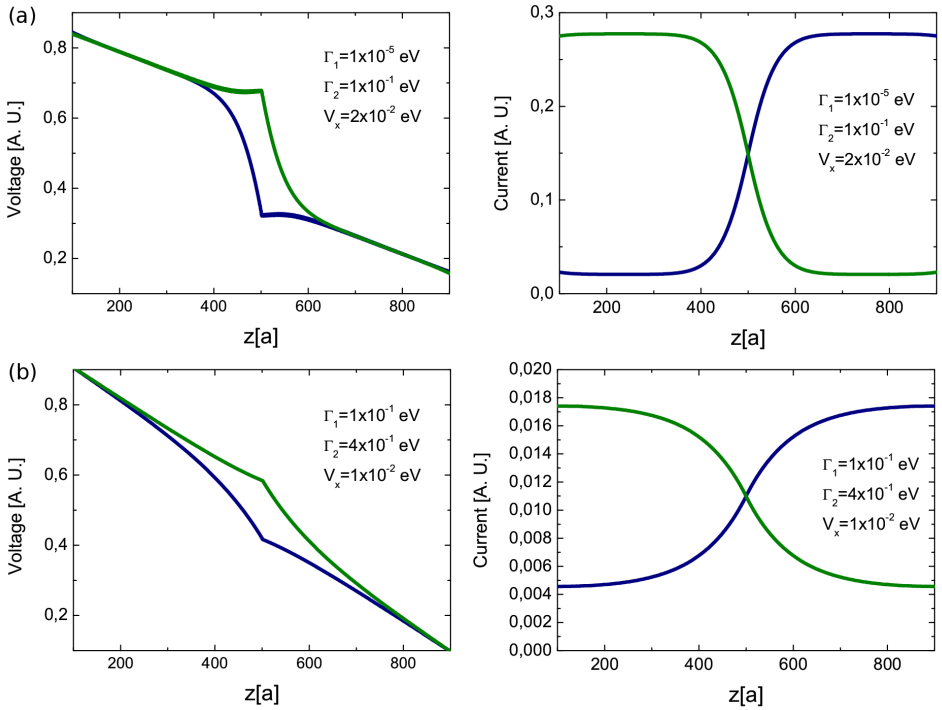

Figure 6.7: *Results of the DP model for the anti-parallel configuration in the bilayer structure, when spin-flips are allowed. In (a) the strength of the dephasing is smaller than in (b). The exponential relaxation of spins is observed.*

The currents associated with each spin direction try to accommodate to the new configuration, reversing their magnitudes. There is a net flow between up and down spins. The equilibrium at each site with a local chemical potential is reflected as a smooth behavior, with an exponential decay. This results are compared with Fig. 6.3 on section 6.2 of this chapter.

For a similar system, in the anti-parallel bilayer structure with $N = 600$, we computed local chemical potential difference between both spin directions, $\Delta\mu$, as a function of the site position, z. As before, the interface is located at the center. When $\ell_{sf} \gg L$, the two-resistor model is recovered. However, when ℓ_{sf} is comparable with L the spin-diffusion is important and allows a relaxation of the current at the interface. Note that the width is given by $2\ell_{sf}$.

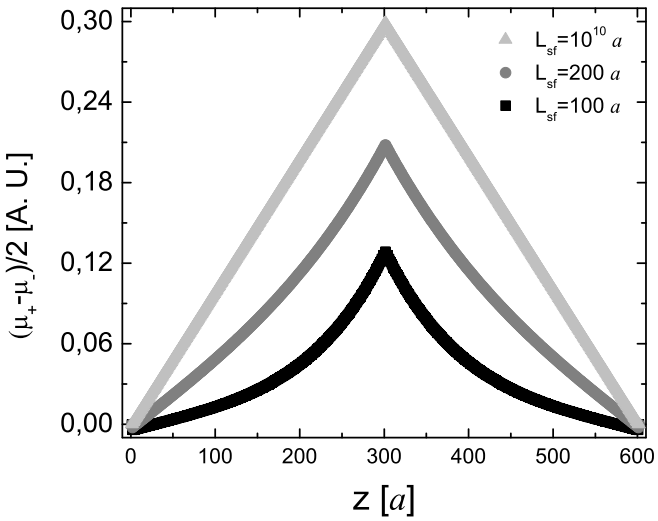

Figure 6.8: *Local chemical potential difference at each site in the anti-parallel bilayer structure. When $\ell_{sf} \gg L$, the two-resistor model is recovered. Otherwise, currents show an exponential relaxation. The width of the $\Delta\mu$ distribution is given by $2\ell_{sf}$.*

6.5 Summary

Mott's *sd* model provides a useful and wide extended simplification of the band structure of ferromagnets. Electrons in the *s* band are nearly free while electrons in the *d* band have poor mobility and are not *directly* relevant for the transport mechanism. However, the exchange interaction between electrons in *s* and *d* bands provides a phase-breaking mechanism for conduction electrons. The sub-bands of electrons with up and down spin orientations have a different number of occupied states, and this defines a majority spin direction. In this way, the strength of the exchange interaction is different for each spin orientation and as a result, the mean free path is not the same for up and down spins.

If the spin-diffusion length is greater than the spin-dependent mean free path, up and down spin orientations provide nearly independent contributions to the overall current and the giant magnetoresistance effect can be understood in simple terms, with a two-resistor model. The classical approach to the problem is justified because the phase-coherence length is expected to be

significantly smaller than the spin-diffusion length in most cases. However, introducing spin-flip processes within this classical approach constitutes a very difficult task. In a Boltzmann description allowing spin-flip processes, it has been shown that, in the anti-parallel configuration, the relaxation of spin on either side of the interface takes the form of an exponential decay and the characteristic length of this decay is ℓ_{sf}. A very important conjecture is that each spin channel can be approximately considered to be in local equilibrium, and therefore local spin-dependent electrochemical potentials exists at each point in space.

On intrinsically quantum treatments to this (and related) problems, there is a persistent difficulty in describing relaxation processes that do not occur in the particle reservoirs. Therefore, all quantum approaches are commonly restricted to the case $L \ll \ell_{sf}$. The key insight to go from a purely quantum to a classical description is the proper introduction of the quantum decoherence into the analytical treatment of the problem and this is precisely the insight of the D'Amato-Pastawski model for decoherent transport. A generalized version of this model that can be fairly apply to account for all the basic characteristics involved in GMR were proposed and its computational power and robustness becomes evident. The GMR phenomenon was previously described in terms of the self-consistent solutions of the phenomenological Boltzmann equation. As we have proved, the implementation suggested by the DP model undoubtedly opens the possibility to evaluate more complex quantum interference effects at the magnetic interface, which have not been addressed yet in enough detail [Fer08].

7
Conclusion

By now, it is a general wisdom that quantum ballistic transport can be experimentally observed in metallic molecular wires of nanometer lengths at low temperatures. Landauer's picture of electronic transport provides an elegant and accurate framework to understand and predict the nature of this behavior. However, there are important departures from these predictions which are the natural consequences of the limits of the coherent description. For example, for a long time, and in spite of an apparent initial success, a description of transport in conducting polymers at low temperatures has been lacking. In the meanwhile, the fundamentals of decoherent processes in transport and their consequences are currently of intense activity in various contexts, from quantum optics and quantum information to molecular electronics. In particular, researchers in this last field have become aware that environmental degrees of freedom might play a crucial role since, as we also showed in various cases, destruction of quantum coherence due to the dephasing effect of system-environment interactions lead to an enhancement of transport.

A simple computational model for decoherence in one-electron transport problems is not only desirable, but also strongly required, since in several important systems, complex many-body interactions result in the loss of the simple interferences of a one-body description. In this work, this is done without

leaving the convenient *a là* Landauer approach by using the generalization introduced by D'Amato and Pastawski where an effective transmission accounts for decoherent processes. Our formulation accepts further improvements as it is just a form of the robust Keldysh formalism within a minimal parametrization. In Chapter 3 we provided computational strategies for the implementation of the DP model, with strong emphasis on the description of our efficient algorithm. Our purpose is that the methodology described could enable the widespread implementation of the DP model in the great variety of systems where it is required.

In Chapter 4 we have discussed electron conductance in a doped PAni. We showed that the PAni ground state configuration, the BL, has high conductance even in presence of disorder, provided that decoherent processes are included. Roughly speaking, decoherent processes split each chain into a series of portions whose length is given by the decoherence length L_ϕ [PWA95]. These define the elemental conductivities from which the sample's Ohmic transport builds on.

For many years, it has been assumed that conduction of polyanilines is inseparably linked to the existence of a polaronic crystalline structure, which is incompatible with thermodynamics. However, we showed that decoherent processes are able to give appreciable metallic conduction in the more entropically favorable bipolaronic lattice. For this system, the uncertainty of energy associated with thermal processes cannot be neglected in the study of conductance, since k_BT falls in a region in which the interplay between incoherent and coherent dynamics results in an increased efficiency of electron transport. One might then speculate that only when the thermal energy scale becomes smaller than the Coulomb energy of the localized states, one would actually start to notice a qualitative difference with an ideal 1-D metal.

The robustness of our results is evident by noting that, in contrast with a coherent transport, they neither depend on variations in the oxidation degree of PAni prior to the doping process, nor on the particular arrangement of quinoid rings along the chain, or on the exact value of the energy uncertainty associated to Γ_ϕ. This justifies the fact that good conducting properties do not depend much on the purity of the emeraldine base so that small displacements toward the leucoemeraldine or pernigraniline are acceptable. We showed that, even when inter-chain coupling can contribute appreciably to conductivity, the

coupling between the p_z bonds with torsional degrees of freedom is strong enough to provide almost all the required decoherence. This hypothesis seems consistent with the experiments that show that adding residues that restrict the torsional motion would also diminish the conductivity as compared with the unmodified bipolaronic lattice [HHY$^+$01, HLHY03, SAM$^+$04].

We do not attempt to rule out the presence of phase segregation into metallic polaronic islands and "insulating" bipolaronic domains. However, these last strands constitute the bottle-neck where thermal decoherent processes activate the conductivity. Moreover, our results go further ahead and evidence that bipolaronic chains can sustain electronic transport by themselves. In fact, based in our simulations we can estimate bulk conductivity for these chains and arrive to a remarkably good value as compared with experimental data.

In Chapter 5 we showed that many-body interactions suffered by carriers in electronic devices that can not be treated within the simple Fermi golden rule approximation, provide extra degrees of freedom that must be accounted explicitly in the transport description. This situation, in some approximation, can be mapped into the one-electron picture as a multi-terminal setup, transferring the complexity of the many-body interactions to the geometry of a fictitious one-electron transport problem. On the other hand, system-environment interactions that can be approximated within a FGR, are treated as decoherence sources with the insight of the DP model. In fact, electronic nanodevices are intrinsically multi-channel systems. As we clarified, "polarons" and time-dependent interactions are examples in which some degrees of freedom, as some phonon-electron couplings must be solved explicitly, while others can be included as sources of decoherence through the FGR. To this end, we developed exact and computational efficient methods to analyze decoherent transport on intrinsically multi-terminal setups. The matrix continued fractions approach, as an extension of the continued fractions methods discussed in the introductory chapter, constitutes the strategy to obtain the overall Green's function matrix of the system. For tridiagonal block Hamiltonians, a generalization of the "Thouless-Kirkpatrick" formula, that relates non diagonal with diagonal elements of the Green's function, was presented. The Kirchhoff law expressions for the DP model on multichannel systems were established. In this way, we obtained an efficient method to introduce decoherence in the study of electronic

transport in realistic situations, where the complexity of the system prevents the usual approach in which only a single channel is present.

In Chapter 6 we prove that the DP model provides all the ingredients for a generalized Landauer-Büttiker approach of magneto-transport in nanowires. On intrinsically quantum treatments to this (and related) problems, there is a persistent difficulty in describing relaxation processes that do not occur in the particle reservoirs [GWJS04]. However, with the insight of the DP model, we accounted for all the basic characteristics involved in giant magnetoresistance effect, a phenomenon that was previously described in terms of the self-consistent solutions of the phenomenological Boltzmann equation. Our perspective is that this model will open the possibility to evaluate more complex quantum interference effects at the interface which have not been addressed yet in enough detail [Fer08].

Both the understanding of the effects of quantum decoherence and even its proper description in the context of transport problems are still open research subjects in modern physics. However, our expectation is that the methodology introduced, despite its inherent limitations, will provide simple but powerful insight into this blooming field.

Appendices

A

Diagonal elements of the transmission matrix

In this section we show that the diagonal elements of $\mathbb{T}$, that involve reflexion probabilities, can be written in the form:

$$(1/g_{\alpha i}) = \sum_{\beta=L,R,\phi} \sum_{j=1}^{N} T_{\alpha i,\beta j} = 4\pi N_i \Gamma_{\alpha i} \tag{A.1}$$

where N_i is the local density of states at the site i, and $\Gamma_{\alpha i}$ is the imaginary shift introduced in the local site energy E_i due to the local escape associated with the process α. This demonstration is very simple and relies on the formulation of the *optical theorem* for the Green's function, which can be found on Ref. [PM01] and we reproduce here with little more detail.

After the decimation of the environmental degrees of freedom, the effective Hamiltonian of the system has the form:

$$\hat{H}_S \longrightarrow \hat{H}_{\text{ef}} = \hat{H}_S + \hat{\Sigma} \tag{A.2}$$

where H_S is the Hamiltonian operator of the isolated sample and $\hat{\Sigma}$ accounts for the self-energies of the environment. In terms of the Green's function matrix, this can be expressed as a Dyson equation,

$$\mathbb{G}^R = \mathbb{G}^{(0)R} + \mathbb{G}^{(0)R}\Sigma^R\mathbb{G}^R \tag{A.3}$$

where $\mathbb{G}^{(0)R}$ is the retarded Green's function associated with H_S and $\mathbb{G}^R$ is associated with the entire effective Hamiltonian. From the Dyson equation, we can isolate Σ^R,

$$\begin{aligned}[\mathbb{G}^{(0)R}]\mathbb{G}^R[\mathbb{G}^R]^{-1} - [\mathbb{G}^{(0)R}]^{-1}\mathbb{G}^{(0)R}[\mathbb{G}^R]^{-1} &= \Sigma^R \\ [\mathbb{G}^{(0)R}]^{-1} - [\mathbb{G}^R]^{-1} &= \Sigma^R\end{aligned} \tag{A.4}$$

In the same way of Eq. A.3, we can write a Dyson equation for the advanced Green's function to obtain an expression of the form given by Eq. A.4. Subtracting Σ^A from Σ^R the terms $\mathbb{G}^{(0)R}$ cancel and,

$$\begin{aligned}\Sigma^R - \Sigma^A &= [\mathbb{G}^A]^{-1} - [\mathbb{G}^R]^{-1} \\ &= [\mathbb{G}^R]^{-1}\{\mathbb{G}^R[\mathbb{G}^A]^{-1} - 1\} \\ &= [\mathbb{G}^R]^{-1}[\mathbb{G}^R - \mathbb{G}^A][\mathbb{G}^A]^{-1}\end{aligned} \tag{A.5}$$

which finally leads to:

$$\mathbb{G}^R - \mathbb{G}^A = \mathbb{G}^R[\Sigma^R - \Sigma^A]\mathbb{G}^A \tag{A.6}$$

This is the result that is known as the *optical theorem*, which relates local densities of states (associated with the imaginary parts of the Green's function, as in Eq. 2.36) and decay rates (associated with imaginary shifts to local site energies). As defined by Eq. 3.19, total transmission probabilities *from* each site i and process α is:

$$\frac{1}{g_i} \equiv \sum_{j=1} \sum_{\beta=L,R,\phi}^{N} T_{j\beta,i\alpha} \tag{A.7}$$

and the total reflexion probability on site i and process α is given by:

$$R_{\alpha i,\alpha i} = 1 - \sum_{j=1} \sum_{\beta=L,R,\phi\neq\alpha,i}^{N} T_{\beta j,\alpha i} \tag{A.8}$$

With the help of the optical theorem (Eq. A.6) we can write,

$$\begin{aligned}\mathrm{Im}\{\mathbb{G}^R\} &= \mathbb{G}^R\Gamma\mathbb{G}^A \\ \mathrm{Im}\{G^R_{i,j}\} &= \sum_{j=1} \sum_{\beta=L,R,\phi}^{N} G^R_{i,j}\Gamma_{\beta j}G^A_{j,i}\end{aligned} \tag{A.9}$$

and then,

$$\begin{aligned} 1/g_i &= 4\sum_{j=1}\sum_{\beta=L,R,\phi}^{N}\Gamma_{\alpha i}G^R_{i,j}\Gamma_{\beta j}G^A_{j,i} \\ &= 4\Gamma_{\alpha i}\sum_{j=1}\sum \beta = L,R,\phi^N\{G^R_{i,j}\Gamma_{\beta,j}G^A_{j,i}\} \\ &= 4\Gamma_{\alpha i}\mathrm{Im}\{G^R_{ii}\} \end{aligned} \tag{A.10}$$

and the last expression is simply,

$$1/g_i = 4\pi N_i\Gamma_{\alpha i} \tag{A.11}$$

With this expression it is possible to express diagonal terms of the matrix $\mathbb{T}$ in terms of diagonal elements of the Green's function matrix, as shown in Eq. 3.39, in section 3.3.3.

B

Nuclear Magnetic Resonance

Nuclear Magnetic Resonance (NMR) spectroscopy is a research technique that relies in the magnetic nature of certain atomic nuclei. Immersed in a static magnetic field and exposed to a second pulsed radio-frequency (RF) field, the response of the nuclei provide detailed information about the structure, dynamics, reaction state, and chemical environment of molecules. The term *resonance* implies the tuning with a natural frequency of the magnetic system [Sli90]. This appendix covers the basic theory behind this technique.

B.1 Basics aspects

Many atomic nuclei, in their ground state, have non zero spin angular momentum $\overrightarrow{\mathbf{J}}_i$, and an associated magnetic moment given by:

$$\overrightarrow{\mu}_i = \gamma \overrightarrow{\mathbf{J}}_i \tag{B.1}$$

where γ is the gyromagnetic factor and is a constant value, characteristic of each type of nucleus. With a few exceptions, the order of magnitude of these magnetic moments is in the range 10^{-3}-10^{-4} Bohr magnetons. Most of the basic concepts involved in NMR experiments can be understood in terms of the *vector model*. In the presence of an applied magnetic field $\overrightarrow{\mathbf{B}}_0$, the bulk

nuclear magnetization, $\overrightarrow{\mathbf{M}}$, is given by the sum of individual magnetizations of nuclei,

$$\overrightarrow{\mathbf{M}} = \sum_i \overrightarrow{\mu}_i \tag{B.2}$$

therefore, bulk magnetization can be expressed as,

$$\overrightarrow{\mathbf{M}} = \gamma \overrightarrow{\mathbf{J}} \tag{B.3}$$

where $\overrightarrow{\mathbf{J}}$ represents the sum of the individual angular moments of nuclei. The influence of an applied uniform magnetic field $\overrightarrow{\mathbf{B}}_0$, manifests as a torque on the magnetization vector, $\overrightarrow{T} = d\overrightarrow{\mathbf{J}}/dt$ which in this case is:

$$\overrightarrow{T} = \overrightarrow{\mathbf{M}} \times \overrightarrow{\mathbf{B}}_0 \tag{B.4}$$

that leads to,

$$\frac{d\overrightarrow{\mathbf{M}}}{dt} = \gamma \overrightarrow{\mathbf{M}} \times \overrightarrow{\mathbf{B}}_0 \tag{B.5}$$

This equation describes the motion of the vector $\overrightarrow{\mathbf{M}}$ in the applied field $\overrightarrow{\mathbf{B}}_0$. The magnetization precesses around $\overrightarrow{\mathbf{B}}_0$ with a constant angle, as shown in Fig. B.1. The frequency of this precession is known as the *Larmor frequency*. Since the standard practice in NMR is to consider the field $\overrightarrow{\mathbf{B}}_0$ in the z axis,

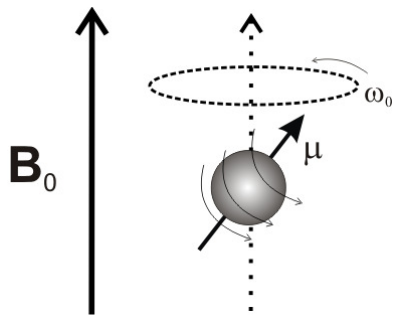

Figure B.1: *Larmor frequency.*

the Larmor frequency results,

$$\omega_0 = \gamma B_0 \tag{B.6}$$

Now we consider the effect of the radio-frequency (RF) field. This field is usually represented by the vector $\overrightarrow{\mathbf{B}}_1$ and is applied perpendicular to the static field $\overrightarrow{\mathbf{B}}_0$. The RF field is composed by two components with circular polarization, both with amplitude B_1 and frequency ω_{rf}. One of this components

rotates in the same direction of the spin precession and is the responsible for the *resonance* phenomenon when $\omega_{rf} = \omega_0$. The other component is usually neglected since $B_1 \ll B_0$.

Therefore, from a classical point of view, consider the magnetization initially parallel to the field $\overrightarrow{\mathbf{B}}_0$. Then, the RF field is applied in resonance for a time t_p. This is known as a θ_p pulse, where $\gamma B_1 \equiv \omega_1 t_p \equiv \theta_p$. This pulse produces a rotation of the magnetization $\overrightarrow{\mathbf{M}}$ in an angle θ_p from the z axis. The standard notation for the NMR pulses is $(\theta_p)_\varphi$, where φ refers to the direction of the RF field and is called *phase* of the pulse. In particular, if $\theta_p = \pi/2$, the magnetization precesses in the $x - y$ plane. If we perform a coordinate transformation to a *rotating frame* which rotates with frequency ω_{rf} around $\overrightarrow{\mathbf{B}}_0$, then the field $\overrightarrow{\mathbf{B}}_1$ is static in this frame. Hence, the time-dependence of the RF field is removed in the rotating frame.

In a typical experiment, the application of RF fields produce transitions that modify the equilibrium population of the nuclei spin system. How the system recovers the termodinamic equilibrium state is precisely what provides the information.

B.2 Experiments

The basic arrangement of an NMR spectrometer is shown on Fig. B.2. The sample is positioned in the magnetic field and excited via pulsations in the radio frequency input circuit. The realigned magnetic fields induce a radio signal in the output circuit which is used to generate the output signal. Fourier analysis of the complex output produces the actual spectrum. The pulse is repeated as many times as necessary to allow the signals to be identified from the background noise.

The chemical shift in absolute terms is defined by the frequency of the resonance expressed with reference to a standard compound which is defined to be at 0 ppm. The scale is made more manageable by expressing it in parts per million (ppm) and is independent of the spectrometer frequency.

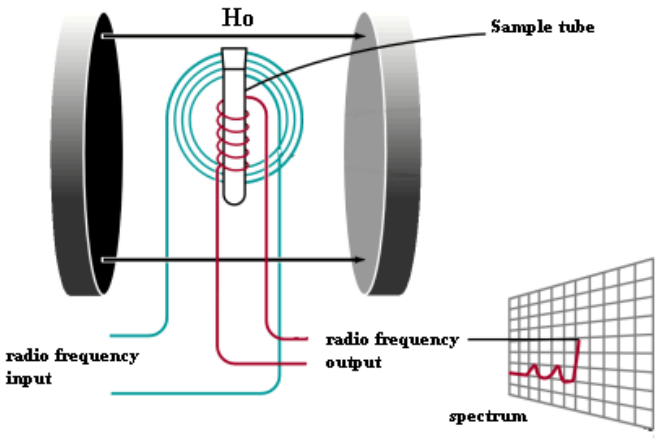

Figure B.2: *NMR setup.*

B.2.1 1 Pulse experiment

The simplest NMR experiment involve only one pulse. The diagram of pulse sequence is illustrated on Fig. B.3.

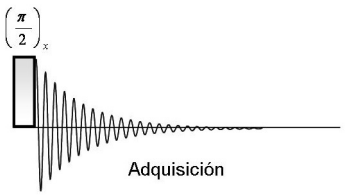

Figure B.3: *One pulse NMR experiment.*

When a pulse $(\frac{\pi}{2})_{\varphi}$ is applied, the magnetization, initially in equilibrium, $(\hat{I}_z)$ is flipped to the plane $x - y$, where precesses around the axis z. over time relaxation will cause this magnetization to decay away to zero. The free induction decay (FID) signal, which results from the magnetization precessing in the x y plane will therefore decay away in amplitude. This loss of x- and y-magnetization is called transverse relaxation. Fourier transformation of the free induction signal will produce a spectrum with lines at the characteristic frequencies of the signal. The width of each peak is related with the decay time of the FID.

B.2.2 Magic Angle Spinning

Magic angle spinning (MAS) is a technique in which the sample is rotated very fast, averaging out the solid-state dipolar interaction. The angle of spinning to the magnetic field is chosen so that $3\cos\theta - 1$ is equal to zero. NMR spectra in solid state are usually very broad for materials. When spinning the sample at low speed the chemical shift anisotropy will result in spinning sidebands. These spinning sidebands appear at distances to the main signal which are multiples of the spinning frequency. At high enough speed the spinning sidebands get smaller.

B.2.3 Heteronuclear decoupling

Couplings between nuclear spins generate substantial broadening of the spectral lines of solid state NMR experiments. Dipolar interaction can be responsible for hundreds of kHz in magnitude, while the indirect coupling (or J interaction) is weaker and requires the nuclei to be chemically bound. To obtain high-resolution spectra in solid state NMR, it is necessary to eliminate this interactions, specially dipolar couplings. Prima facie, this could be accomplished with the help of MAS techniques. However, often is not possible to reach the spin velocities needed.

Natural abundance of ^{13}C nuclei is very low. Then, dipolar interactions between identical ^{13}C nuclei is weaker and can be eliminated from the NMR spectra with MAS. However, the number of ^{1}H atoms in organic compounds is usually large and the *heteronuclear* dipolar interaction ^{1}H-^{13}C is strong. The simplest example of heteronuclear decoupling is the *continuous wave* decoupling, which involve the application of a continuous RF pulse during the entire FID acquisition. Within the theory of average Hamiltonians, is possible to show that during the irradiation period, the operator $\hat{I}_z$ precesses in a way such that the dipolar Hamiltonian vanishes in a complete precession period and tends to zero for long irradiation times.

B.2.4 Cross Polarization

In this example the abundant nucleus was chosen to be ^{1}H and the observed nucleus is ^{13}C. The abundant nucleus is excited, and its energy is then trans-

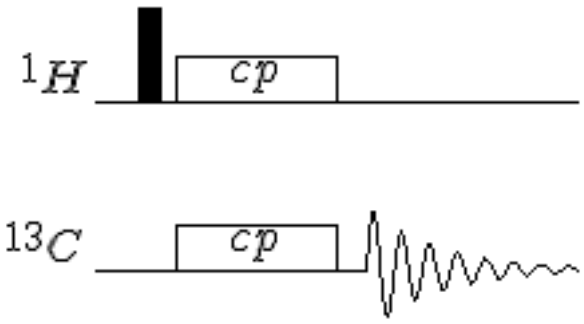

Figure B.4: *Cross-polarization technique.*

fered to the observed nucleus by using a long low power pulse on both channels. The RF power ratio of these pulses needs to be tuned so that the transition energy for both nuclei is the same. So that for instance for the polarization transfer from a ^{1}H to a ^{13}C, the rotating field B1 must be 4 times weaker for the proton channel than for the carbon channel.

This method often gives a much stronger signal than direct excitation, allow faster repetition rate (it now depends on the T1 of the proton instead the one of lower gyromagnetic ratio nuclei). The major limitation of CP method is the requirement of high power irradiation, that could deteriorate the sample or the probe.

C

Comparison to Marcus-Hush theory

Electron couplings with Torsional degrees of freedom involved the physically relevant situation of a quadratic interaction with the vibrational coordinate. This is not conceptually different with the standard linear electron-phonon coupling used to describe the Franck-Condon effect [Mar00] and the electron-transfer process [Nit06]. All these physical processes are contained in a simple Hamiltonian

$$\hat{H} = \sum_{j=A,B} E_j \hat{c}_j^+ \hat{c}_j + \hbar\omega_0 \left(\hat{b}^+\hat{b} + \tfrac{1}{2}\right) - V_g \left(\hat{b}^+ + \hat{b}\right) \hat{c}_B^+ \hat{c}_B \tag{C.1}$$

$$+V_{AB}(\hat{c}_A^+ \hat{c}_B + \hat{c}_B^+ \hat{c}_A), \tag{C.2}$$

whose interactions in the Fock space are represented in Fig. C.1. The electron transfer problem is best represented resorting to the polaronic transformation which would diagonalize the Hamiltonian but for the tunneling described by V_{AB}. The essence of an estimation of the electron transfer rate is a FGR evaluation of the tunneling between the electronic states A and B in the regime of weak coupling non-adiabatic limit $\hbar\omega_0 \ll k_B T, |V_{AB}| \ll |V_g|$.

$$k_{A\longrightarrow B} = \frac{1}{\tau_{A\longrightarrow B}} = \frac{2\pi}{\hbar} |V_{AB}|^2 [F(\Delta E)] \tag{C.3}$$

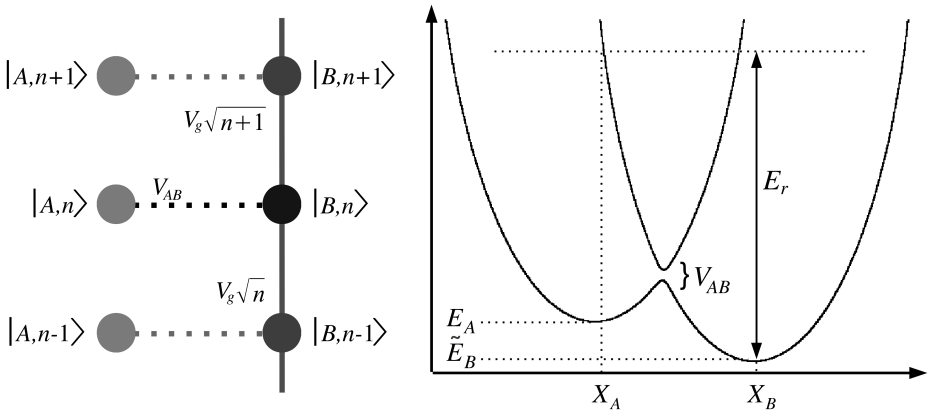

Figure C.1: *Fock-space representation of Eq. C.2 and its corresponding semiclassical picture in terms of vibronic degree of freedom X as used in the Marcus-Hush model for electron transfer reactions. The potential surface at the right becomes shifted when represented in the polaronic basis allowing to define the reorganization energy E_r. In this model, the electronic coupling V_{AB} must be small enough to remain perturbative. Left panel is also used to represent the decoherence by electron-phonon coupling when $V_g \ll V_{AB}$.*

where $\Delta E = E_A - \tilde{E}_B$, $\tilde{E}_B = E_B - V_g^2/\hbar\omega_0$ and $F(\Delta E)$ is a density of directly connected states denominated Franck-Condon factor. Thus it satisfies

$$\int_{-\infty}^{\infty} F(\Delta E)\mathrm{d}\Delta E = 1. \tag{C.4}$$

$F(\Delta E)$ is estimated resorting to a thermal average and following the Marcus original treatment which interprets the transition probability according to a Landau-Zener formula. Thus

$$F(\Delta E) = \frac{1}{\sqrt{4\pi E_r k_B T}} \exp\left[-\frac{(\Delta E - E_r)^2}{4E_r k_B T}\right] \tag{C.5}$$

where the reorganization energy E_r is indicated in the plot.

In contrast to this treatment, in a decoherence problem one focus on estimating how the electron-phonon interaction degrades the standard coherent Rabi oscillation [Pas07]. This describes an electron jumping forth and back between states B and A and attenuates within a decoherence time τ_ϕ. Similarly to Eq. (3.14) of Ref. [Pas92] a FGR evaluation gives:

$$\frac{1}{\tau_\phi} = \frac{2\pi}{\hbar}|V_g|^2 \langle\langle (n+1)N(E_B+\hbar\omega_0) + nN(E_B-\hbar\omega_0)\rangle\rangle \tag{C.6}$$

$$\simeq \frac{4\pi}{\hbar}|V_g|^2 \left[\frac{k_B T}{\hbar\omega_0} N(E_B)\right]. \tag{C.7}$$

where $\langle\langle\rangle\rangle$ stands for thermal average. The approximation involves a high temperature limit and again, the square brackets indicate a density of directly connected states. As in previous section, the assumption that phonon induced electron energy uncertainty leads to the self-consistent condition of Eq. 4.14:

$$\Gamma_\phi = \frac{\hbar}{2\tau_B} = |V_g| \sqrt{\frac{2\pi k_B T}{\hbar\omega_0}}, \tag{C.8}$$

which is valid provided that $\hbar\omega_0 \ll k_B T, |V_g| \ll V_{AB}$. Notice that in an ab-intio parametrization of the tight-binding Hamiltonian, the coupling constant results from evaluating the dependence of the parameter on the appropriate generalized coordinate, e.g. $V_g = \partial E_B/\partial\theta$.

Thus, in both problems, electron transfer in presence of a some reorganization energy and electron transport with decoherence from a phonon bath, the Hamiltonian is the same. However, since the calculated observables are different, the term used as perturbation in the FGR differ. In the first case the perturbation is the electron jump V_{AB}, while in the decoherent situation the perturbation is the electron-phonon coupling constant V_g.

List of Figures

References

[AALR79] E. Abrahams, P. W. Anderson, D. C. Licciardello, and T. V. Ramakrishnan. Scaling theory of localization: Absence of quantum diffusion in two dimensions. *Phys. Rev. Lett.*, 42:673–676, Mar 1979.

[AMPB94] E. V. Anda, S. S. Makler, H. M. Pastawski, and R. G. Barrera. Electron-phonon effects on transport in mesoscopic heterostructures. *Braz. J. Phys.*, 24:330, 1994.

[And58] P. W. Anderson. Absence of diffusion in certain random lattices. *Phys. Rev.*, 109:1492–1505, Mar 1958.

[And78] P. W. Anderson. Local moments and localized states. *Rev. Mod. Phys.*, 50(2):191–201, Apr 1978.

[B̈86a] M. Büttiker. Four-terminal phase-coherent conductance. *Phys. Rev. Lett.*, 57:1761–1764, Oct 1986.

[B̈86b] M. Büttiker. Role of quantum coherence in series resistors. *Phys. Rev. B*, 33:3020–3026, Mar 1986.

[B̈88] M. Büttiker. Symmetry of electrical conduction. *IBM J. Res. Dev.*, 32:317–334, May 1988.

[BAA06] D.M. Basko, I.L. Aleiner, and B.L. Altshuler. Metalinsulator transition in a weakly interacting many-electron system with localized single-particle states. *Annals of Physics*, 321(5):1126 – 1205, 2006.

[BcvT95] Janez Bonča and S. A. Trugman. Effect of inelastic processes on tunneling. *Phys. Rev. Lett.*, 75(13):2566–2569, Sep 1995.

[BcvTBac99] J. Bonča, S. A. Trugman, and I. Batistić. Holstein polaron. *Phys. Rev. B*, 60(3):1633–1642, Jul 1999.

[BS85] J. L. Bredas and G. B. Street. Polarons, bipolarons, and solitons in conducting polymers. *Accounts of Chemical Research*, 18(10):309–315, 1985.

[But73] W. H. Butler. Self-consistent cluster theory of disordered alloys. *Phys. Rev. B*, 8(10):4499–4510, Nov 1973.

[CBMP10] C. J. Cattena, R. A. Bustos-Marún, and H. M. Pastawski. Crucial role of decoherence for electronic transport in molecular wires: Polyaniline as a case study. *Phys. Rev. B*, 82:144201, Oct 2010.

[CCFG02] Carlo Cavazzoni, Renato Colle, Riccardo Farchioni, and Giuseppe Grosso. Car - parrinello molecular dynamics study of electronic and structural properties of neutral polyanilines. *Phys. Rev. B*, 66(16):165110, Oct 2002.

[Con85] E. M. Conwell. The differences between one-dimensional and three-dimensional semiconductors. *Physics Today*, 38:46–59, June 1985.

[DÁLP07] E. P. Danieli, G. A. Álvarez, P. R. Levstein, and H. M. Pastawski. Quantum dynamical phase transition in a system with many-body interactions. *Solid State Communications*, 141:422–426, February 2007.

[Dat97] S. Datta. *Electronic transport in mesoscopic systems*. Cambridge studies in semiconductor physics and microelectronic engineering. Cambridge University Press, 1997.

[DAWJ88] R. Newbury M. Pepper H. Ahmed J. E. F. Frost D. G. Hasko D. C Peacock D. A. Ritchie D. A. Wharam, T. J. Thornton and G. A. C. Jones. One-dimensional transport and the quantisation of the ballistic resistance. *Journal of Physics C: Solid State Physics*, 21(8):L209, 1988.

[DP90] J. L. D'Amato and H. M. Pastawski. Conductance of a disordered linear chain including inelastic scattering events. *Phys. Rev. B*, 41(11):7411–7420, Apr 1990.

[DT74] D.J. and Thouless. Electrons in disordered systems and the theory of localization. *Physics Reports*, 13(3):93 – 142, 1974.

[DWP90] David H. Dunlap, H-L. Wu, and Philip W. Phillips. Absence of localization in a random-dimer model. *Phys. Rev. Lett.*, 65(1):88–91, Jul 1990.

[EGZ+87] A. J. Epstein, J. M. Ginder, F. Zuo, R. W. Bigelow, H. . Woo, D. B. Tanner, A. F. Richter, W. . Huang, and A. G. MacDiarmid. Insulator-to-metal transition in polyaniline. *Synthetic Metals*, 18(1-3):303–309, 1987.

[EK00] Eldon G. Emberly and George Kirczenow. Landauer theory, inelastic scattering, and electron transport in molecular wires. *Phys. Rev. B*, 61:5740–5750, Feb 2000.

[Fal06] P. E. Falloon. *Electron Transport through Domain Walls in Ferromagnetic Nanowires.* Thèses de doctorat, Universit Louis Pasteur. June 2006. URL: http://scd-theses.u-strasbg.fr/1135/01/FALLOON2006.pdf.

[FCP] L. J. Fernandez, C. J. Cattena, and H. M. Pastawski. Generalized landauer-büttiker equations in multiprobe conductors: Application to magneto-transport in magnetic nanowires. *To be published.*

[Fer08] A. Fert. Nobel lecture: Origin, development, and future of spintronics. *Rev. Mod. Phys.*, 80:1517–1530, Dec 2008.

[FGP96] Riccardo Farchioni, Giuseppe Grosso, and Giuseppe Pastori Parravicini. Renormalization approach for transport and electronic properties of conducting polymers. *Phys. Rev. B*, 53(8):4294–4299, Feb 1996.

[FL81] D. S. Fisher and P. A. Lee. Relation between conductivity and transmission matrix. *Phys. Rev. B*, 23:6851–6854, Jun 1981.

[FPM06] L. E. F. Foa Torres, H. M. Pastawski, and E. Medina. Antiresonances as precursors of decoherence. *Europhysics Letters*, 73:164–170, January 2006.

[Fre30] J. Frenkel. On the electrical resistance of contacts between solid conductors. *Phys. Rev.*, 36:1604–1618, Dec 1930.

[FSWL07] K. Fehse, G. Schwartz, K. Walzer, and K. Leo. Combination of a polyaniline anode and doped charge transport layers for high-efficiency organic light emitting diodes. *Journal of Applied Physics*, 101(12):124509–+, June 2007.

[FTPM01] L. E. F. Foa Torres, H. M. Pastawski, and S. S. Makler. Tuning a resonance in fock space: Optimization of phonon emission in a resonant-tunneling device. *Phys. Rev. B*, 64(19):193304, Oct 2001.

[FVG99] Riccardo Farchioni, Patrizia Vignolo, and Giuseppe Grosso. Transport properties of emeraldine salts: The nature of the metallic state. *Phys. Rev. B*, 60(23):15705–15713, Dec 1999.

[GCF+05] B. Gao, Y. F. Chen, M. S. Fuhrer, D. C. Glattli, and A. Bachtold. Four-point resistance of individual single-wall carbon nanotubes. *Phys. Rev. Lett.*, 95:196802, Oct 2005.

[GdSL+89] D. S. Galvo, D. A. dos Santos, B. Laks, C. P. de Melo, and M. J. Caldas. Role of disorder in the conduction mechanism in polyanilines. *Phys. Rev. Lett.*, 63(7):786–789, Aug 1989.

[GH98] Milena Grifoni and Peter Hnggi. Driven quantum tunneling. *Physics Reports*, 304(56):229 – 354, 1998.

[GRME87] J. M. Ginder, A. F. Richter, A. G. MacDiarmid, and A. J. Epstein. Insulator-to-metal transition in polyaniline. *Solid State Communications*, 63(2):97–101, 1987.

[GWJS04] Victor A. Gopar, Dietmar Weinmann, Rodolfo A. Jalabert, and Robert L. Stamps. Electronic transport through domain walls in ferromagnetic nanowires: coexistence of adiabatic and nonadiabatic spin dynamics. *Phys. Rev. B*, 69:014426, Jan 2004.

[Hee01a] A. J. Heeger. Nobel lecture: Semiconducting and metallic polymers: The fourth generation of polymeric materials. *Rev. Mod. Phys.*, 73(3):681–700, Sep 2001.

[Hee01b] A. J. Heeger. Semiconducting and metallic polymers: The fourth generation of polymeric materials. *Journal of Physical Chemistry B*, 105(36):8475–8491, 2001.

[HHY+01] C. . Han, S. . Hong, K. . Yang, M. . Bai, C. . Lu, and C. . Huang. Highly conductive new aniline copolymers containing butylthio substituent. *Macromolecules*, 34(3):587–591, 2001.

[HKSS88] A. J. Heeger, S. Kivelson, J. R. Schrieffer, and W. P. Su. Solitons in conducting polymers. *Rev. Mod. Phys.*, 60(3):781–850, Jul 1988.

[HLHY03] C. . Han, C. . Lu, S. . Hong, and K. . Yang. Highly conductive and thermally stable self-doping propylthiosulfonated polyanilines. *Macromolecules*, 36(21):7908–7915, 2003.

[HR03] James R. Heath and Mark A. Ratner. Molecular electronics. *Physics Today*, 56(5):43–49, 2003.

[HS97] R. Hey and M. Schreiber. Temperature-dependent dc transport in polyaniline chains. *Phys. Rev. B*, 56:1854–1863, Jul 1997.

[IL99] Y. Imry and R. Landauer. Conductance viewed as transmission. *Rev. Mod. Phys.*, 71(2):S306–S312, Mar 1999.

[JGA00] C. Joachim, J. K. Gimzewski, and A. Aviram. Electronics using hybrid-molecular and mono-molecular devices. *Nature*, 408:541–548, November 2000.

[KC99] C. . Kuo and C. . Chen. Characterization of polyaniline doped with diphenyl phosphate. *Synthetic Metals*, 99(2):163–167, 1999.

[KCRM88] S. Kaplan, E. M. Conwell, A. F. Richter, and A. G. MacDiarmid. Solid-state carbon-13 nmr characterization of polyanilines. *Journal of the American Chemical Society*, 110(23):7647–7651, 1988.

[KGH+67] L. P. Kadanoff, W. Götze, D. Hamblen, R. Hecht, E. A. S. Lewis, V. V. Palciauskas, M. Rayl, J. Swift, D. Aspnes, and J. Kane. Static phenomena near critical points: Theory and experiment. *Rev. Mod. Phys.*, 39:395–431, Apr 1967.

[KLH05a] S. Kohler, J. Lehmann, and P. Hänggi. Driven quantum transport on the nanoscale. *J. Phys. Rep.*, 406:379–443, February 2005.

[KLH05b] S. Kohler, J. Lehmann, and P. Hnggi. Driven quantum transport on the nanoscale. *Physics Reports*, 406(6):379 – 443, 2005.

[KM93] B. Kramer and A. MacKinnon. Localization: theory and experiment. *Reports on Progress in Physics*, 56:1469–1564, December 1993.

[KSZ+05] H. S. Kolla, S. P. Surwade, X. Zhang, A. G. MacDiarmid, and S. K. Manohar. Absolute molecular weight of polyaniline. *Journal of the American Chemical Society*, 127(48):16770–16771, 2005.

[KW08] K. Kazymyrenko and X. Waintal. Knitting algorithm for calculating green functions in quantum systems. *Phys. Rev. B*, 77:115119, Mar 2008.

[Lan88] R. Landauer. Spatial variation of currents and fields due to localized scatterers in metallic conduction. *IBM J. Res. Dev.*, 32:306–316, May 1988.

[Lan92] Rolf Landauer. Conductance from transmission: common sense points. *Physica Scripta*, 1992(T42):110, 1992.

[LCW+03] Y. Long, Z. Chen, N. Wang, Z. Zhang, and M. Wan. Resistivity study of polyaniline doped with protonic acids. *Physica B: Condensed Matter*, 325:208–213, 2003.

[LPD90] P. R. Levstein, H. M. Pastawski, and J. L. D'Amato. Tuning the through-bond interaction in a two-centre problem. *Journal of Physics Condensed Matter*, 2:1781–1794, February 1990.

[LY01] X.-Q. Li and Y. Yan. Electrical transport through individual DNA molecules. *Applied Physics Letters*, 79:2190–+, October 2001.

[Mac01] A. G. MacDiarmid. Nobel lecture: "synthetic metals": a novel role for organic polymers. *Rev. Mod. Phys.*, 73:701–712, Sep 2001.

[Mad96] O. Madelung. *Introduction to solid-state theory*. Springer series in solid-state sciences. Springer, 1996.

[Mar93] Rudolph A. Marcus. Electron transfer reactions in chemistry. theory and experiment. *Rev. Mod. Phys.*, 65:599–610, Jul 1993.

[Mar00] M.P. Marder. *Condensed matter physics*. Wiley-Interscience. John Wiley, 2000.

[Mar06] H. C. F. Martens. Delocalization in weakly coupled disordered wires: Application to conjugated polymers. *Phys. Rev. Lett.*, 96(7):076603, Feb 2006.

[MB04] H. C. F. Martens and H. B. Brom. A quantitative evaluation of metallic conduction in conjugated polymers. *Phys. Rev. B*, 70(24):241201, Dec 2004.

[MGM86] S. Ma, G. Grinstein, and G. Mazenko. *Directions in condensed matter physics: Memorial volume in honor of Prof. S. K. Ma*. World Scientific series on directions in condensed matter physics. World Scientific, 1986.

[MK81] A. MacKinnon and B. Kramer. One-parameter scaling of localization length and conductance in disordered systems. *Phys. Rev. Lett.*, 47(21):1546–1549, Nov 1981.

[MLPD95] D. J. Monsma, J. C. Lodder, Th. J. A. Popma, and B. Dieny. Perpendicular hot electron spin-valve effect in a new magnetic field sensor: The spin-valve transistor. *Phys. Rev. Lett.*, 74:5260–5263, Jun 1995.

[Mot35] N. F. Mott. A discussion of the transition metals on the basis of quantum mechanics. *Proceedings of the Physical Society*, 47(4):571, 1935.

[Mot36] N. F. Mott. The electrical conductivity of transition metals. *Proc. R. Soc. Lond. A.*, 153:699–717, February 1936.

[Mot69] N. F. Mott. Conduction in non-crystalline materials. *Philosophical Magazine*, 19(160):835–852, 1969.

[MRLA08] M. Mohseni, P. Rebentrost, S. Lloyd, and A. Aspuru-Guzik. Environment-assisted quantum walks in photosynthetic energy transfer. *J. Chem. Phys.*, 129(17):174106–+, November 2008.

[MRSU00] F. Milde, R. A. Römer, M. Schreiber, and V. Uski. Critical properties of the metal-insulator transition in anisotropic systems. *European Physical Journal B*, 15:685–690, June 2000.

[MS94] Klaus Maschke and Michael Schreiber. Electron transport along a spatially disordered chain in the presence of dissipation. *Phys. Rev. B*, 49:2295–2305, Jan 1994.

[Nac01] Branislav K. Nikolić. Deconstructing kubo formula usage: Exact conductance of a mesoscopic system from weak to strong disorder limit. *Phys. Rev. B*, 64:165303, Oct 2001.

[NBMC+] D. Nozaki, R. Bustos-Marún, C. J. Cattena, G. Cuniberti, and H. M. Pastawski. Efficient coarse-grained model for electron transport through large molecular systems under dephasing environment. *To be published.*

[Ngu07] M. T. Nguyen. *General and theoretical aspects of anilines*, pages 75–162. Number v. 1 in Patai series: the chemistry of functional groups. Wiley, 2007.

[Nit06] A. Nitzan. *Chemical dynamics in condensed phases: relaxation, transfer and reactions in condensed molecular systems*. Oxford graduate texts in mathematics. Oxford University Press, 2006.

[NR03] A. Nitzan and M. A. Ratner. Electron Transport in Molecular Wire Junctions. *Science*, 300:1384–1389, May 2003.

[Pas86] H. M. Pastawski. *Propiedades electrónicas de sólidos amorfos*. PhD Thesis. Instituto Balseiro, Universidad Nacional de Cuyo, 1986.

[Pas91] H. M. Pastawski. Classical and quantum transport from generalized Landauer-Büttiker equations. *Phys. Rev. B*, 44:6329–6339, Sep 1991.

[Pas92] H. M. Pastawski. Classical and quantum transport from generalized Landauer-Büttiker equations. II. Time-dependent resonant tunneling. *Phys. Rev. B*, 46:4053–4070, August 1992.

[Pas07] H. M. Pastawski. Revisiting the Fermi Golden Rule: Quantum dynamical phase transition as a paradigm shift. *Physica B Condensed Matter*, 398:278–286, September 2007.

[Pas10] H. M. Pastawski. *Quantum theory of solids. Curse notes*. 2010. URL: http://www.lanais.famaf.unc.edu.ar/cursos/qts/index.php?sec=notas.

[PE01] V.N. Prigodin and A.J. Epstein. Nature of insulatormetal transition and novel mechanism of charge transport in the metallic state of highly doped electronic polymers. *Synthetic Metals*, 125(1):43 – 53, 2001. Celebrating the year 2000 Nobel prize in Chemistry for the discovery and development of conducting polymers.

[PE03] V. N. Prigodin and A. J. Epstein. Quantum hopping in metallic polymers. *Physica B Condensed Matter*, 338:310–317, October 2003.

[Pei55] R.E. Peierls. *Quantum theory of solids*. International series of monographs on physics. Clarendon Press, 1955.

[PFM02] H. M. Pastawski, L. E. F. Foa Torres, and E. Medina. Electron phonon interaction and electronic decoherence in molecular conductors. *Chemical Physics*, 281:257–278, August 2002.

[PH08] M. B. Plenio and S. F. Huelga. Dephasing-assisted transport: quantum networks and biomolecules. *New Journal of Physics*, 10(11):113019–+, November 2008.

[Phi03] P.W. Phillips. *Advanced solid state physics*. Frontiers in Physics Series. Westview Press, 2003.

[PM01] H. M. Pastawski and E. Medina. 'tight binding' methods in quantum transport through molecules and small devices: From the coherent to the decoherent description. *Revista Mexicana de Fisica*, 47(SUPPL. 1):1–23, 2001.

[PND05] A. Petr, A. Neudeck, and L. Dunsch. On the magnetic susceptibility of polyaniline - an alternative approach. *Chemical Physics Letters*, 401:130–134, January 2005.

[PSW85] H. M. Pastawski, C. M. Slutzky, and J. F. Weisz. Localization as a breakdown of extended states. *Phys. Rev. B*, 32(6):3642–3653, Sep 1985.

[PU98] H. M. Pastawski and G. Usaj. Dimensional crossover in spin diffusion: A manifestation of the quantum zeno effect. *Phys. Rev. B*, 57(9):5017–5020, Mar 1998.

[PWA83] H. M. Pastawski, J. F. Weisz, and S. Albornoz. Matrix continued-fraction calculation of localization length. *Phys. Rev. B*, 28:6896–6903, December 1983.

[PWA95] H. M. Pastawski, J. F. Weisz, and E. A. Albanesi. Transport properties of organic conductors: Influence of the statistics of distances between charged centers. *Phys. Rev. B*, 52(15):10665–10668, Oct 1995.

[RFSO+09] E. Rufeil-Fiori, C. M. Sánchez, F. Y. Oliva, H. M. Pastawski, and P. R. Levstein. Effective one-body dynamics in multiple-quantum nmr experiments. *Phys. Rev. A*, 79(3):032324, Mar 2009.

[Ric79] Michael J. Rice. Charged [pi]-phase kinks in lightly doped polyacetylene. *Physics Letters A*, 71(1):152 – 154, 1979.

[RMK+09] P. Rebentrost, M. Mohseni, I. Kassal, S. Lloyd, and A. Aspuru-Guzik. Environment-assisted quantum transport. *New J. Phys.*, 11(033003), 2009.

[Sam73] H. Sambe. Steady states and quasienergies of a quantum-mechanical system in an oscillating field. *Phys. Rev. A*, 7:2203–2213, Jun 1973.

[SAM+04] H. J. Salavagione, D. F. Acevedo, M. C. Miras, A. J. Motheo, and C. A. Barbero. Comparative study of 2-amino and 3-aminobenzoic acid copolymerization with aniline synthesis and copolymer properties. *Journal of Polymer Science, Part A: Polymer Chemistry*, 42(22):5587–5599, 2004.

[SBE+87] S. Stafström, J. L. Brédas, A. J. Epstein, H. S. Woo, D. B. Tanner, W. S. Huang, and A. G. MacDiarmid. Polaron lattice in highly conducting polyaniline: Theoretical and optical studies. *Phys. Rev. Lett.*, 59(13):1464–1467, Sep 1987.

[Sch05] Maximilian Schlosshauer. Decoherence, the measurement problem, and interpretations of quantum mechanics. *Rev. Mod. Phys.*, 76:1267–1305, Feb 2005.

[Sco10] J. Campbell Scott. *History of Conductive Polymers*, pages 1–17. John Wiley and Sons, Ltd, 2010.

[SG02] J. Stejskal and R. G. Gilbert. Polyaniline. preparation of a conducting polymer (iupac technical report). *Pure and Applied Chemistry*, 74(5):857–867, 2002.

[SGC91] P. A. Schulz, D. S. Galvo, and M. J. Caldas. Conductivity of polymer chains: A tunneling approach. *Phys. Rev. B*, 44(12):6073–6077, Sep 1991.

[SGCS97] S. L. Sondhi, S. M. Girvin, J. P. Carini, and D. Shahar. Continuous quantum phase transitions. *Rev. Mod. Phys.*, 69(1):315–333, Jan 1997.

[SHC94] N. S. Sariciftci, A. J. Heeger, and Y. Cao. Paramagnetic susceptibility of highly conducting polyaniline: Disordered metal with weak electron-electron interactions (fermi glass). *Phys. Rev. B*, 49(9):5988–5992, Mar 1994.

[Shi65] J. H. Shirley. Solution of the schrödinger equation with a hamiltonian periodic in time. *Phys. Rev.*, 138:B979–B987, May 1965.

[SK54] J. C. Slater and G. F. Koster. Simplified lcao method for the periodic potential problem. *Phys. Rev.*, 94:1498–1524, Jun 1954.

[Sla75] J.C. Slater. *Solid-state and molecular theory: a scientific biography.* A Wiley-Interscience publication. Wiley, 1975.

[Sli90] C.P. Slichter. *Principles of magnetic resonance.* Springer series in solid-state sciences. Springer, 1990.

[SSH79] W. P. Su, J. R. Schrieffer, and A. J. Heeger. Solitons in polyacetylene. *Phys. Rev. Lett.*, 42(25):1698–1701, Jun 1979.

[Sta95] S. Stafström. Conductance and localization in a system of coupled conjugated polymer chains. *Phys. Rev. B*, 51(7):4137–4142, Feb 1995.

[TK81] D. J. Thouless and S. Kirkpatrick. Conductivity of the disordered linear chain. *Journal of Physics C: Solid State Physics*, 14(3):235, 1981.

[Tor05] L. E. F. Foa Torres. Mono-parametric quantum charge pumping: Interplay between spatial interference and photon-assisted tunneling. *Phys. Rev. B*, 72:245339, 2005.

[VF93] T. Valet and A. Fert. Theory of the perpendicular magnetoresistance in magnetic multilayers. *Phys. Rev. B*, 48:7099–7113, Sep 1993.

[VFG01] P. Vignolo, R. Farchioni, and G. Grosso. Tight-Binding Effective Hamiltonians for the Electronic States of Polyaniline Chains. *Physica Status Solidi B Basic Research*, 223:853–866, February 2001.

[VS08] A. Varela-Álvarez and J. A. Sordo. A suitable model for emeraldine salt. *Journal of Chemical Physics*, 128(17):174706–+, May 2008.

[vWvHB+88] B. J. van Wees, H. van Houten, C. W. J. Beenakker, J. G. Williamson, L. P. Kouwenhoven, D. van der Marel, and C. T. Foxon. Quantized conductance of point contacts in a two-dimensional electron gas. *Phys. Rev. Lett.*, 60:848–850, Feb 1988.

[Wil79] Kenneth G. Wilson. Problems in physics with many scales of length. *Scientific American*, 241:158–179, 1979.

[Wil83] Kenneth G. Wilson. The renormalization group and critical phenomena. *Rev. Mod. Phys.*, 55:583–600, Jul 1983.

[WJW88] Ned S. Wingreen, Karsten W. Jacobsen, and John W. Wilkins. Resonant tunneling with electron-phonon interaction: An exactly solvable model. *Phys. Rev. Lett.*, 61(12):1396–1399, Sep 1988.

[WP84] J.F. Weisz and H.M. Pastawski. Critical strength for ideal incommensurate structures. *Physics Letters A*, 105(8):421 – 424, 1984.

[WP91] H.-L. Wu and Philip Phillips. Polyaniline is a random-dimer model: A new transport mechanism for conducting polymers. *Phys. Rev. Lett.*, 66(10):1366–1369, Mar 1991.

[ZGW+97] X. . Zeng, K. . Gong, K. . Weng, W. . Xiao, W. . Gan, and T. . Ko. Effects of ultra-high pressures on the electrical resistance of polyaniline by in situ ft-ir studies. *Chemical Physics Letters*, 280(5-6):469–474, 1997.

[Zur03] W. H. Zurek. Decoherence and the transition from quantum to classical – Revisited. *eprint arXiv:quant-ph/0306072*, June 2003. URL: http://arxiv.org/pdf/quant-ph/0306072v1.